This document contains:

1) a supplement to our online response to Professor Genthon (https://www.atmos-meas-tech-discuss.net/amt-2017-234/amt-2017-234-AC2-supplement.pdf),

2) our response to Dr. Kochendorfer, and

3) the marked-up revised manuscript.

1) The introduction (lines 33 – 37) states that 2 types of instrumentations to measure precipitation have been developed: the capture and optical gauges. This ignores radars which are powerful tools to measure and even profile precipitation. Because of ground clutter and vertical resolution, radars do admittedly not measure precipitation right at the very surface but because they can profile vertically it may be checked whether precipitation rates vary or not as it reaches closer to the surface. Radars do not “obstruct the wind and deflects falling particles in the measurement zone” (line 38). There is no “clogging with snow” with radars (line 47).

In the US National Weather Service (NWS) network, a radar-derived snow amount is dependent on gauge measurements made simultaneous with the radar measurements. A published example of this is the NWS gauge-radar network data analyzed by Martinaitis et al. (2015). In that network, and presumably others, the gauge-calibrated radar-derived estimates of snow can be significantly biased. Factors contributing to this are gauge clogging by snowfall, postevent thaw of snow, and underestimation of snow because wind speed is either not used to correct for gauge undercatch or it is unavailable. Martinaitis et al. (2015) state that “..The accuracy of hourly radar-derived QPE values of winter precipitation is unknown..”. Given this caveat, the dependence of radar precipitation estimates on gauge measurements, and the factors you mention (vertical structure, Earth curvature, ray ducting, ground clutter, and etc.), we have opted to not mention that radars can be used to derive snowfall amounts.

The first sentence of the introduction was revised to this:

Two types of instrumentation are available for making point measurements of liquid-equivalent snowfall rates and liquid-equivalent snow accumulations: 1) Weighing gauges and related devices that measure snowfall as it collects in a container or on a surface (Brock and

Richardson, 2001; Chapter 9), and 2) optical gauges that measure the concentration and size of snow particles either in free fall or within a wind tunnel (Loffler-Mang and Joss, 2000; Deshler, 1988).

Martinaitis, S.M., S.B.Cocks, Y.Qi, B.T.Kaney, J.Zhang, and K.Howard, Understanding winter precipitation impacts on automated gauge observations within a real-time system, J. Hydrometeor., 16, 2345-2363, https://doi.org/10.1175/JHM-D-15-0020.1, 2015

We thank Dr. Kochendorfer for reviewing the manuscript.

"Hotplate precipitation gauge calibrations and field measurements" describes theoretical and observational work focused on a novel precipitation gauge. The hotplate precipitation gauge measures precipitation by recording the amount of energy that is consumed by heating, melting, and evaporating precipitation captured on an upward-facing heated plate. The manuscript includes improvements to algorithms used to estimate the wind-induced undercatch of the hotplate, the conversion of energy to evaporation, and the effects of radiation, temperature, and wind on the energy balance and precipitation rate of the sensor. These algorithms are developed and tested using field and laboratory measurements.

Although the hotplate is not widely used, it is a unique, low-maintenance sensor capable of measuring all forms of precipitation in areas where power is available. Based on the hotplate's good performance in SPICE, there may be renewed interest in this technology when the SPICE results become widely available. The refinements and testing of the hotplate described in the present manuscript are therefore both valuable and timely.

SPICE this is the World Meteorological Organization Solid Precipitation Intercomparison Experiment (e.g., Kochendorfer et al. 2017b).

Some general comments below indicate areas where there is room for improvement. The manuscript is generally well written, but typos and other more specific suggestions are documented in the specific comments.

General Comments

The description of the hotplates and algorithms discussed in the Introduction and Methods sections should be augmented to clearly state how the R11, YES, Boudala et al. (2010), and UW algorithms differ from each other. As currently written, it is difficult for a reader unfamiliar with this sensor to understand the relationship between the R11 and YES algorithms. The manuscript is focused mainly on improving the R11 algorithm, but the connection between the R11 algorithm and the YES algorithm should be described more clearly. This will help establish the relevance of the manuscript to uninformed hotplate users, who will presumably rely upon the YES algorithm.

On L268-L274, we **assumed** that the YES algorithm had incorporated R11's surface area and R11's distinction between the theoretical and actual conversion factors. We don't know for certain if these effects are incorporated into the YES algorithm. Until there is more input on this, it will be impossible to establish the "connection" you are requesting. Professor Rasmussen (https://www.atmos-meas-tech-discuss.net/amt-2017-234/#discussion) speculated that YES had *not* incorporated the energy conversion factor that R11 recommended, however, he was not categorical on this.

The algorithms presented in R11 and the present manuscript were adjusted for wind speed losses. There were also differences in the way the wind speed was estimated, and in how the conversion from power to latent energy (*f2*) was estimated. With such possibly competing or self-compensating differences, a good reference precipitation measurement is necessary to properly evaluate the different algorithms.

The reviewer is neglecting the fact that we showed that a reference precipitation rate, produced by the Ismatec pump, is consistent with rates derived using data from the two hotplates, provided the data from those hotplates were processed using the UW algorithm. This tests the f_2 in a controlled setting.

The present manuscript would be strengthened significantly if instead of adjusted single-Alter shielded weighing gauge precipitation measurements, reference precipitation measurements shielded by a double fence were used to validate the improved algorithm and compare it to the R11 and YES-derived precipitation. Particularly at windy sites, wind speed adjustments introduce significant uncertainty in the resultant precipitation measurements (Kochendorfer et al., 2017a; Fortin et al., 2008). The hotplate-derived wind speeds shown in the present manuscript were fairly low, and many of the E98 values were greater than 0.5 (Table 5). This is good, but the manuscript should still include some discussion or quantification of the uncertainty introduced by the adjustment of the single-Altar shielded weighing gauge measurements.

What we did discuss was this: In Fig. 12b there is agreement (statistically) when we compare UW-algorithm-derived precipitation (based on U adjusted to 10 m for evaluating E) vs NOAH-II precipitation. Also, in Fig. 12c there is agreement (statistically) when we compare UW-algorithm-derived precipitation (based on U from the anemometer for evaluating E) vs NOAH-II precipitation. In both of these comparisons the NOAH-II values are wind-corrected. We did not state that the agreement in Fig. 12b and Fig. 12c is relative to measurements that may be subject to bias (NOAH-II wind-corrected accumulations).

We will modify by finishing the paragraph with this:

Since there is error in the NOAH-II values used in this comparison, there is also need for characterization of that uncertainty (random and systematic). Error can propagate from the NOAH-II measurements themselves and from the catch efficiency function we applied to those data (section 3.8).

WMO-SPICE included three hotplates, tested for two winter seasons at three separate sites with Double Fence Automated Reference (DFAR) measurements. I will try to help the authors obtain these data if they are interested in expanding the scope of the manuscript. I haven't looked at all of the WMO-SPICE hotplate data, but at the US (Marshall) site at least, the SHP values appear to be available. Feel free to contact me directly to discuss this at john.kochendorfer@noaa.gov.

We feel this should be done, but not in this paper. Also, we thank you for your offer to share data. If we do decide to do the analysis, we would want access to the hotplate gauge that was used to acquire those measurements. This would enable us to do the hot/cold test, and thus derive the surface temperature. The other ingredient of the analysis would be the calibration of α, β, and γ. This requires a period of recorded SPICE data with varying wind, no precipitation, and preferably at night.

Why were event totals used instead of higher frequency measurements? 30 or 60 minute rate/accumulation comparisons would provide many more points (or 'events') for evaluation, and would be accompanied with the added benefit of more stationary meteorological conditions and representative averages for wind speed, precipitation type, etc.

Our focus is on precipitation events lasting, on average, ~ 12 hours (Table 5). This provides useful comparison of the two algorithms, and of the two gauges (hotplate and weighing). Also, it is conjectural that precipitation is stationary on 30 minute time intervals. In our opinion, analysis of higher frequency measurements is beyond the scope of the manuscript; hence we plan to stick with our event-based comparison.

I didn’t notice any mention of the hotplate power consumption. This should be added to the manuscript, assuming that I did not overlook it. In the Introduction the advantages of the hotplate are carefully documented, but this significant limitation appears to be omitted.

Given that many weighing gauges have openings that are electrically heated, we are of the opinion that this is not a serious limitation for a hotplate. We added this to the end of L53:

In some applications a disadvantage of the hotplate, relative to a weighing gauge, is its electrical power consumption. This is ~ 200 W in Wyoming during winter.

How much testing of this sensor has been performed in rain? I would expect there to be a significant amount of splash out in heavy rain.

We do not have any information on this. Rain rates in our four rain cases from OWL were ≤ 20 mm/hr.

Ln 61. Did YES produce more than one type of hotplate during the history of this product? The version of the hotplate firmware used should be included in the manuscript, if this relevant and available.

L109. We revised the sentence to say this:

Consequently, our hotplate (Wolfe and Snider, 2012) was upgraded to firmware version 3.1.2 in 2011.

Specific Comments:

Ln 33 – 37. Heated tipping buckets are also used to measure snowfall (eg. Buisán et al., 2017).

L34-35. Because the following reference provides a general overview of many different devices, including tipping buckets, we revised the sentence to say this:

1) Weighing gauges and related devices that measure snowfall as it collects in a container or on a surface (Brock and Richardson, 2001; Chapter 9),

Brock, F.V., and S.J. Richardson, Meteorological Measurement Systems, Oxford University Press, New York, 304 pp., 2001

Ln 56. Reference Fig. 1, which includes the radiation sensors. Also specify that only downwelling/incoming radiation was measured (and used to estimate net radiation). Or alternatively specify that the radiation sensors only faced upward, and upwelling/outgoing radiation was not measured.

This was remedied in the following ways:

Changed L142 to “a measured downwelling shortwave flux (SW; Table 1)”

Changed entry in Table 1 to “Downwelling Shortwave Flux”

Changed entry in Table 1 to “Longwave Radiation”

Removed two occurrences of “net” in the text

Ln 71. Here and elsewhere in the manuscript, the term “latent” should be replaced with “latent energy” or “latent heat”. Likewise “sensible” (Ln 70) should be replaced with “sensible heat” throughout the manuscript.

We reserved “latent heat” for the quantity of energy absorbed during a phase transition. This is consistent with the definition in the American Meteorological Society Glossary: “The specific enthalpy difference between two phases of a substance at the same temperature.”

In the revision, L71 and L215, and throughout, we changed “latent energy” to “latent power output.” It’s dorky, but necessary because the budget equation is an energy-rate equation.

Electrical power supplied to the top plate (Q_{top}) compensates for power lost via sensible energy, radiative, and vapor mass transfer. Henceforth, we refer to the latter process as latent power output.

In Eq. 3 we have “power”, not “energy”, so in L440 to L444 we modified the text to this:

Fig. 8 shows budget terms (Eq. 3) for one of the four rainfall events in our dataset (OWL-15). The three power output terms (sensible, longwave, and latent), and three power input terms (top plate, longwave, and shortwave) are shown in Fig. 8a - b. In this section we begin with the sequence of latent power output ($P{\cdot}E/f_2$ in Fig. 8a) and explain how we calculate the sequence of rainfall rate.

And the caption to Fig. 8 was changed to this:

Figure 8 – Hotplate properties during rain (event = OWL-15). Because this event classifies as rain, E = 1 was applied in the UW algorithm. a) Power output terms in the Eq. 3; i.e., the sensible, latent, and longwave output terms. b) Power input terms in the Eq. 3; i.e., the top plate, longwave, and shortwave input terms. The shortwave term is zero for this nighttime example, but is set to 0.1 W in the plot. c) Thresholded precipitation rate. d) Unthresholded precipitation rate.

Ln 72. State explicitly that the effects of radiation on the energy balance of the bottom plate are assumed to be negligible.

L71 to L73. We revised this text to say this:

The hotplate-derived wind speed, evaluated at gauge height via the "factory calibration" discussed in R11, is used in this analysis. The bottom plate power (Q_{bot}) is likely a measurement used in the calculation of that wind speed, but this is speculative because the factory wind speed algorithm is proprietary. We symbolize this wind speed as U and use it to evaluate a Reynolds number (Re), and use the latter to parameterize sensible heat transfer from the ventilated surface of the top plate. R11 also derived wind speeds by fitting Q_{bot}, ambient temperature, and a wind speed measured at 10 m above ground level (AGL). This wind speed is not used in this analysis. The hotplate ambient temperature (T) measurement comes from the sensor seen below the radiation instruments (Fig. 1), the relative humidity (RH) measurement comes from a sensor that protrudes below the electronics box (Fig. 1), and the hotplate pressure sensor is contained within the electronics box. A complete description of our nomenclature is provided in the Appendix.

Ln 74. Change "evaluate at Reynolds number" to "estimate a Reynolds number".

Are you commenting on this because we held properties of the film constant in the calculation of the Reynolds and Nusselt numbers (section 3.6), in the fitting (section 5.2), and in the application of the fitted relationship within the UW algorithm (section 5.3)? In our opinion, constant film properties is an appropriate assumption provided the assumption made in the fitting and is also made in the application of the fit. No change was made.

Figure 1. I had a hard time identifying the air temperature sensor. I initially assumed that an independent measurement was used. This is in part because I am accustomed to seeing air temperature measurements within larger fan-aspirated or louvered radiation shields, but it would help if the labels on the right side of Fig. 1 were more clearly

associated with their appropriate component. Also add RH and pressure to the appropriate labels.

Please see above, and also, see that we added this section to the Methods:

3.1 - Temperature Measurements

Ice bulb temperatures at OWL were calculated using temperature, RH, and pressure measurements made within a fully shielded housing (Steenburgh et al., 2014). At GLE and BTL ice bulb temperatures were calculated using the hotplate-derived temperature, RH, and pressure values (Table 1). Because the hotplate temperature sensor is incompletely shielded (Fig. 1), there is concern that its measurement is positively biased by solar heating. We investigated this by differencing hotplate-derived temperatures, acquired during precipitation events at OWL, and values acquired by the fully shielded temperature sensor operated at OWL. On average, the hotplate values were larger (0.4 ± 0.4 ºC). We did not attempt to correct for this bias.

Ln. 97 – 98. Please summarize the formulation of the R11 conversion factors. Explain how they were different.

The requested information is presented in a subsequent section.

Ln. 110. Specify “downwelling longwave and shortwave fluxes”.

Yes.

Ln. 116 - 119. Radiative output and input haven’t been defined. Also it needs to be made clear that radiative energy budget terms are only for the top plate.

The sentence introducing Eq. 3 is changed to this:

We used the following equation to analyze the top plate’s power budget.

Also, in our opinion, L117, L118, and L119, are self-explanatory.

The sensible power output term is for both plates?

This is clarified in the revision.

Th is assumed equal for the top and bottom plate, even when precipitation is occurring?

We evaluated the surface temperature of the top plate in the “Warm-cold Ambient Temperature Tests” section. We did not model the *bottom* plate power budget, or derive the bottom plate temperature. We presume the bottom plate temperature is a parameter in the “factory calibration” discussed previously. However, the factory calibration is proprietary, so this is just speculation.

Has this been confirmed with actual measurements of the plate temperatures?

Not that we are aware of. Please see previous response.

Ln. 133 – 134. “In the infrared… is the relevant property” is awkward as written.

Revised.

Ln. 136. “The value we picked is…” is awkward as written.

Revised.

Ln. 137. Specify that this is only for the top plate.

We changed the sentence on L133 to read as this:

Two radiative properties are applied in our analysis of the top plate’s power budget (Eq. 3). In the infrared, or longwave, the emissivity of the top plate is the key property.

Ln. 141. “the hotplate’s reflectance is the relevant property” is awkward as written.

Revised.

Ln. 142. Specify that the shortwave flux was downwelling.

Yes.

Ln. 164- 165. Add the word “accurate” and replace “whether the sensed hydrometeors are rain or snow” with, “precipitation type”: Rewrite as, “rate is dependent on the *accurate* assessment of *precipitation type*.”

Thanks for the suggestion. In our view, “precipitation type” is too vague. The text was changed to this:

The accuracy of a hotplate-estimated precipitation rate depends on whether the sensed hydrometeors are rain or snow (R11 and Fig. 3a).

Ln. 168. After “pressure” specify that these measurements were all recorded by the hotplate system.

Since this is explained in the added section 3.1, the sentence was changed to this:

Measurements used to derive the ice bulb temperature are described in section 3.1.

Ln. 182. Please explain/explore why the calibration changed after servicing.

YES told us that electrical components were replaced, however, we feel that this is too much detail to present. Adam Wettlaufer did state that calibration changes “..were likely a consequence of the servicing provided by YES..” Interested readers can look at his analysis. In the revision we will revise this sentence to this:

Wettlaufer (2013) demonstrates that calibration constants did change over the 2011 to

2015 interval, and likely in response to servicing conducted twice at YES.

Ln. 188. Delete the word, “vertically” or rewrite. I understand what you are saying (after looking at Fig. 2), but is confusing because the plates are oriented horizontally.

Yes.

Ln. 194 - 207. I worked it out eventually, but I found most of this section quite confusing. It should be made clear that this entire discussion is focused only on the top plate.

In the revision, we have made it clear that Eq.1 and Eq. 3 are power budgets for the top plate.

It sounds like YES assumed that the source of upwelling longwave radiation (the ground) was the same temperature as the air. This is not a good assumption, as the surface temperature of the earth often differs significantly from the air.

A fair criticism, but we compensate for this in Eq. 5. Also, the L193 to L195 sentence was revised to this:

In response to that finding, newer versions of the hotplate have a device that measures longwave radiation (pyrgeometer, e.g., Albrecht et al., 1974) (Fig. 1 and Table 1).

It would be worth comparing the resultant downwelling infrared radiation with a measurement recorded using a normal pyrgeometer, from which the incoming longwave flux is typically calculated using the radiation measurement and the body temperature of the sensor. It also begs the question of why YES took this extra step. Was it because they were interested in the net IR flux, or because the use the outgoing longwave flux in their assessment of the bottom plate energy balance? Also the “downward” in “net downward” (Ln. 194) should be deleted. Strictly speaking, “net downward” is an oxymoron. This may have contributed to my confusion. Because an upward facing pyrgeometer is not typically used to estimate net radiation without another downward facing pyrgeometer, I initially assumed that the "net" was incorrect, as opposed to the "downward".

Sorry for the confusion. The word "net" is removed from the revision.

Ln. 197. Add "net" – "Eq. 4 represents the *net* longwave radiant measurement…".

We are not interested in the "net" longwave. So, rather than explain Eq. 4 as a "net", we explained the two quantities that contribute to M_{IR}. Also, please see above; the word "net" is removed from the revised manuscript.

Ln. 207. Clarify that eq. 6 was only for use in the indoor experiment, where the temperature of the metal plate was estimated using the air temperature.

This is explained later in the text; in our opinion this is not the place for that explanation.

Ln. 212. Change the word, "settings" to something more appropriate like "variables".

In the revision, we use "calibration parameters." Later in the discussion, these become a "T_h/γ pair."

Ln 214. Change the word, "with" to "using" or "from" – "IR_d *was* calculated *using* Eq. 6".

Yes.

Ln. 229. Rewrite as, "that relationship *was* applied…".

Yes.

Ln. 230. Rewrite, "dimensionless representation of the sensible power output" - describe the Nusselt number more accurately.

This was revised for clarity.

Ln 251 – 252. Treating all precipitation above 0 °C as liquid is a little worrying. There are many examples of solid precipitation occurring above 0 °C (and liquid precipitation occurring below 0 °C) (eg. Kochendorfer et al., 2017b; Wolff et al., 2015). A third conversion factor for mixed (or ambiguous) precipitation would be more defensible. It could be some combination of 9a and 9b, or a transition between the two.

In our opinion, the cases we analyze are clear cut. That is, four have ice bulb temperatures larger than 0 ^{o}C, and thus the particles are either melted or melting as they approach the hotplate surface. Hence, for our cases we do not think we need to justify the "combination" you are recommending.

Ln 268 and 271. Is it realistic to assume that the hotplate temperature (Th) is equal to 0 °C?

We **assumed** Th = 0 ^{o}C (see L255) to be consistent with R11. We did this so we could compare to the f2 reported in R11. We concluded that our calculation of f2, and R11's calculation of f2, are consistent. In both cases there is the assumption T_h = 0 °C; however, we feel the proper way to do this is to account the warming terms involving heat capacities. These issues are discussed in section 3.8 (revision), and in section 3.7 (reviewed manuscript).

Is the bottom plate also 0 °C when precipitation is occurring?

We did not model the *bottom* plate power budget, or derive the bottom plate temperature.

I thought that the temperature of both plates was nominally 75 °C.

This is a simplification introduced by R11. But it is restricted to their formulation of f2, which we mimicked (see above).

Ln 282. “This is accounting” is awkward as written.

We revised the sentence to this:

This is due to the warming discussed in section 2.

Ln 286. “catch efficiency is accounting” is awkward as written. Ln. 287. “accounts for the fact” is awkward as written.

The two sentences were rewritten to this:

In this section, we evaluate a wind speed-dependent function and use it to account for the top plate’s snow particle catch efficiency (*E*; section 2). The physical processes this function accounts for are, 1) snow particle bouncing subsequent to collision with the top plate, followed by transfer away from the top plate by wind, and 2) shearing off of a snow particle after it has landed on the top plate (R11).

Ln. 300. I understand that this is being done for the sake of comparison with R11, but it should be pointed out that there is no good reason to adjust the hotplate derived wind speed to another height. The manuscript should note that it is preferable to apply a catch efficiency function using the wind speed at the sensor’s location.

This is later in manuscript. Please see L514.

Ln. 336. Why were only the hangar data used?

We changed this text to the following:

In our analysis of the warm-cold measurements we only used data acquired in the hangar. As we describe below, this may have improved the accuracy of the resultant T_h/γ pairs. This is because all data needed to derive a T_h/γ pair can be obtained without turning off the hotplate. Wettlaufer (2013) analyzed both hanger and lab data. Both in his work and in ours, the relevant hotplate properties were derived by averaging over a 5 minute warm interval and a 5 minute cold interval, and applying these averages in Eq. 7a – 7b.

The temperature range used in the different warm-cold tests varies significantly. In some cases it is quite narrow, and in others quite warm.

We did not have control over how cold the hanger gets, at night, or how warm it gets, during the day. The warm-cold temperature pairings (hangar) came from measurements made in the middle of the afternoon and early in the morning, respectively.

Ln. 328 – 338, and Table 3. The derived hotplate temperature is quite variable.

We did discuss the servicing done at YES (L178 to L184). This may be the source of the variability. Also, some of the variability may stem from the ± 0.5 W error. The latter is the basis for the error limits we placed on the T_h and γ values presented in Table 3. For these error limits, please see Table 3 and the discussion on L349 to L353.

There appears to be some cross- correlation between gamma and the hotplate temperature (Table 3), with larger values of gamma associated with smaller hotplate temperatures. These values also appear to be correlated with the warm-cold temperatures of the indoor experiments they were derived from, which suggests that they may not be constant even for the same sensor. A comparison of measured hotplate temperatures (a small thermocouple or an IR could be used) and derived temperatures would help determine if the actual hotplate temperature varies as much as the derived temperature.

Note that the second term in Eq. 7a or Eq. 7b scales with the product of T_h and γ; hence, the correlation you mention is a consequence of the mathematical form of the Equations 7a and 7b. We do not think it is important to go into that issue.

We have not attempted to measure the surface temperature using the methods you recommend.

Ln. 361 – 362. This is awkward as written. Remove extraneous text. If there is no reason to question the fact that all of the water made it to the hotplate, there is no reason to bring it up.

Yes.

Ln 371. UW is used to describe *PUW*, the UW algorithm, and the UW hotplate. A different designation/abbreviation should be used to differentiate between sensor and algorithm. For example, *PUW* could easily be mistaken for *P* from the UW hotplate, rather than *P* from the UW algorithm. One solution would be to rename the UW hotplate.

In the revision, we clarify this earlier in the manuscript. This revised text and footnote are near L58:

These are a hotplate gauge owned by the University of Wyoming (UW) and by the National Center for Atmospheric Research (NCAR; Boulder, CO).

When a distinction is needed, we indicate the hotplate, followed by a forward slash, and the location of the deployment. For example, the UW hotplate, deployed at the OWL site, is designated UW/OWL.

Ln 374 and Fig. 4. R11 should be included in the drip test, and added to Fig. 4 and Fig. 5. Or the omission should be justified in the text.

First, the setting $E = 1$ is applied here. That is definitely true for the P_{UW} and presumably true for the P_{YES}. Hence, a difference cannot arise from different catch efficiencies. Second, the f_2 we apply in the new algorithm is the solid line in Fig. 3a (2.92×10^{-8} m/J), and we are assuming that the f_2 applied in the YES algorithm is the dashed line (3.38×10^{-8} m/J). We evaluated both of these f2 values at the right-hand margin of Fig. 3a (T = 5 ^{o}C). Based on the f_2 discussed in the previous two sentences, we expect the P_{REF}/P_{YES} ratio to be ~ 16% smaller than the P_{REF}/P_{UW} ratio. This is what we see in Fig. 5, so we conclude as described on L392 to L399. Adding what you are proposing will not change these conclusions, but it will complicate interpretation of Fig. 4 and Fig. 5. We prefer to avoid inserting information you are requesting, both in the figure and in the discussion of the figure.

Ln 382 – 384 and Fig. 4. Augment the figure with cross-hatching or something similar to better illustrate the 1 min averaging periods.

The abscissa is ticked in minutes. Perhaps that was missed. Adding hatching, or similar, complicates the figure.

We will revise the caption of Fig. 5 to this:

Figure 4 – Precipitation rates, derived using the UW and YES algorithms, plotted vs time. Dashed vertical lines illustrate nondrip-to-drip transitions, drip-to-nondrip transitions, and one-minute precipitation averaging intervals. In this figure, the one-minute averaging intervals are ~ 16:08 to ~ 16:09 UTC and ~ 16:17 to ~ 16:18 UTC. Measurements are from the UW hotplate operating indoors on 20120229. The UW/GLE calibration constants (Table 3) and an f_2 derived with the second of two methods (section 3.7) were applied in the UW algorithm.

Also clarify that these 1-min periods were used for the regressions in Fig. 5, assuming that is what was done.

Yes, here is how we changed L382 to L383:

We set the end of these at the drip-to-nondrip transitions and symbolize the averages as $\langle P_{UW} \rangle$ and $\langle P_{YES} \rangle$.

Fig. 5 and Ln 385 – 390. More detail is needed on how these values were obtained (see above).

This is addressed (see above).

Also why were 0 mm hr^{-1} precipitation periods excluded? An evaluation of the total accumulation should also be included. It is hard to tell from Fig. 4, but it seems possible that the 'overestimated' YES algorithm might be just as accurate as the UW algorithm after including the 0 precipitation periods and the period after the nondrip-to-drip transition.

The Fig. 4 shows, based on one-minute averaging, that YES is larger than UW. If an integral from the nondrip-to-drip transition to the drip-to-nondrip transition is performed, it seems, from Fig. 4, that the YES/UW difference will enhance further. Yet, because of the possibility of a violation of the steady-state assumption (L376), and because of the minimum (L377), we discourage such a YES/UW comparison.

Careful here with "accuracy." We have a reference, P_{ref}. We use the latter for the determination of accurate vs inaccurate. Fig. 5 shows inaccuracy for YES, and accuracy for UW. Table 4 summarizes the accuracy/inaccuracy of two hotplate gauges.

About the "zeros." The graphs on the next page have the result presented in Fig. 5, but with UW algorithm in top left, the YES algorithm in the bottom left, the UW algorithm with zeros included (top right), and the YES algorithm with zeros included (bottom right). Clearly, the effect you are speculating about ("…seems possible…") is negligible. Finally, because we take P_{ref} to be a standard, the curve fitting is based on minimization of the sum of the squares of the *x* deviations (horizontal departures of data from the regression line). This is stated in the Fig. 5 caption.

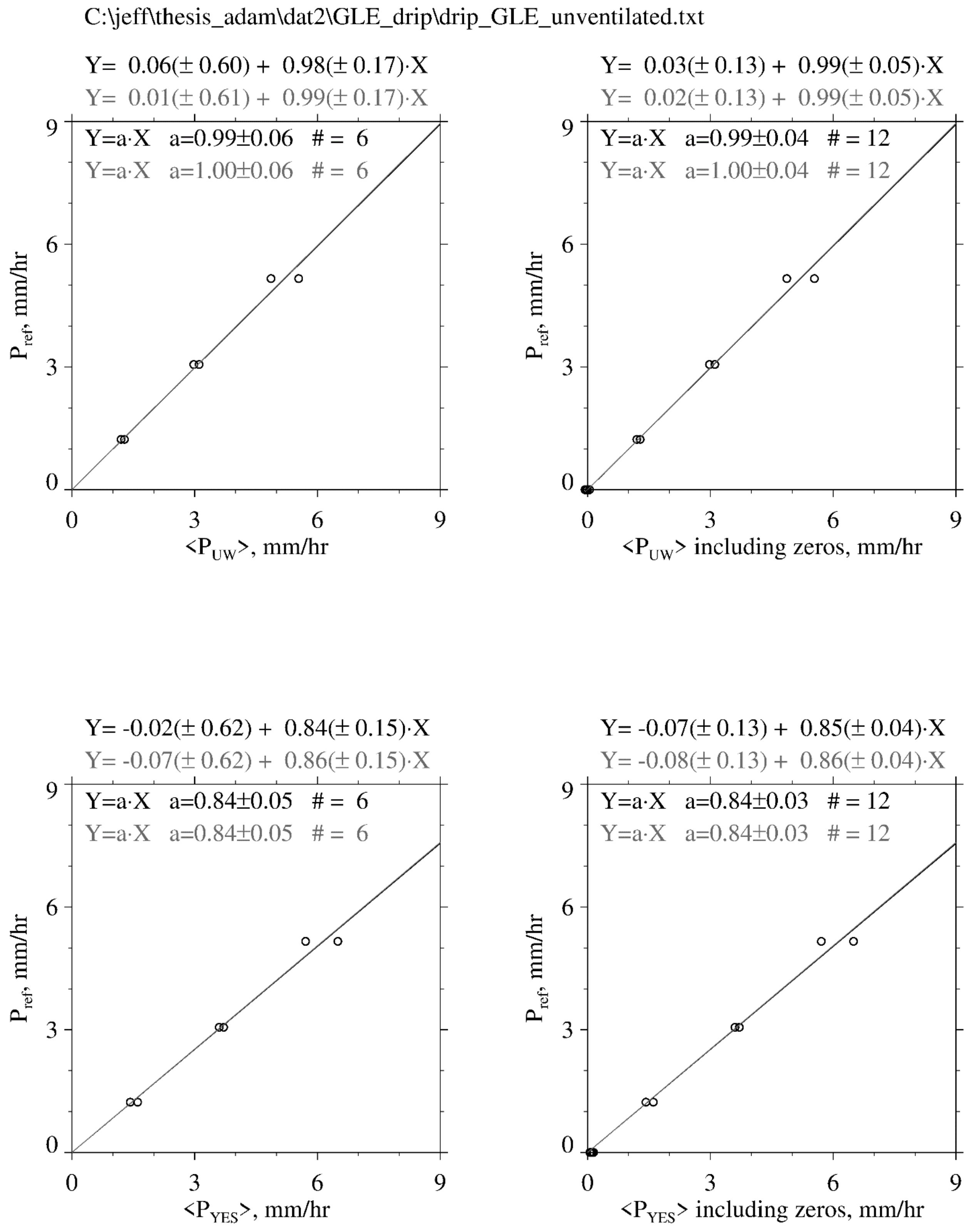
C:\jeff\thesis_adam\dat2\GLE_drip\drip_GLE_unventilated.txt
Y= 0.06(± 0.60) + 0.98(± 0.17)·X
Y= 0.01(± 0.61) + 0.99(± 0.17)·X
Y=a·X a=0.99±0.06 # = 6
Y=a·X a=1.00±0.06 # = 6
P_ref, mm/hr
<P_UW>, mm/hr
Y= 0.03(± 0.13) + 0.99(± 0.05)·X
Y= 0.02(± 0.13) + 0.99(± 0.05)·X
Y=a·X a=0.99±0.04 # = 12
Y=a·X a=1.00±0.04 # = 12
P_ref, mm/hr
<P_UW> including zeros, mm/hr
Y= -0.02(± 0.62) + 0.84(± 0.15)·X
Y= -0.07(± 0.62) + 0.86(± 0.15)·X
Y=a·X a=0.84±0.05 # = 6
Y=a·X a=0.84±0.05 # = 6
P_ref, mm/hr
<P_YES>, mm/hr
Y= -0.07(± 0.13) + 0.85(± 0.04)·X
Y= -0.08(± 0.13) + 0.86(± 0.04)·X
Y=a·X a=0.84±0.03 # = 12
Y=a·X a=0.84±0.03 # = 12
P_ref, mm/hr
<P_YES> including zeros, mm/hr

Also it isn't clear to me what role the minimum threshold plays here. In normal operations, I thought that a 0.2 mm hr^{-1} threshold was used to differentiate between noise and precipitation, but Fig. 4 only seems to include a 0 mm hr^{-1} threshold (to remove negative precipitation), and it is only for the YES sensor.

All one can say about the YES output - when it is thresholded to 0 mm/hr - is that the value is ≤ to the threshold. In the case of the UW, and because we did not threshold (see below), we see what the value is, even when it's < 0 mm/hr. Yet, the reader needs to wait till section 5.3 to understand the thresholding we do in the UW algorithm.

To fix this problem, in the revision, we added this sentence to the end of L381:

In fact, thresholding is not desired for the drip tests. Thus, the UW sequence is not thresholded in Fig. 4.

Both the UW and the R11 algorithms include a threshold if I recall correctly.

Please previous discussion.

In normal operations how would the zero precipitation periods be handled for both algorithms? If I recall correctly, the YES sensors in SPICE had very few false- positives. The same methods recommended for normal field use should be employed in the evaluation, or at an explanation of why the thresholds weren't used should be added to the manuscript. The evaluation of the total accumulation should be performed with the thresholds applied, although it could certainly also be performed without the thresholds to help demonstrate the potential effects of the threshold in normal field use.

These things are addressed in section 5.3. Please previous discussion.

Ln 404. Add an explanation of how events were defined. For example, more than x amount of precipitation, over x amount of time, beginning and ending with x minutes of zero precipitation... Also state whether the NOAH or the hotplate precipitation gauge was used to determine events.

For the OWL snow cases, this was based on three conditions. 1) Existence of a manual (snow board) collection by University of Utah. (Utah collection times are documented at https://data.eol.ucar.edu/dataset/382.021). 2) The Utah collection interval is contained within the start and stop times of a UW hotplate data file. 3) Data from both the UW hotplate and the Utah NOAH-II gauges are available. For the OWL rain cases, there were two conditions. 1) The precipitation event is contained within the start and stop times of a UW hotplate data file. 2) Data from both the UW hotplate and the Utah NOAH-II gauges are available.

At GLE, and BTL, there were two conditions: 1) An event interval is contained within the start and stop times of a UW hotplate data file. 2) Data are available from both the hotplate and NOAH-II gauges.

GLE, BTL, and OWL hotplate files contain 24 hr of data.

The most restrictive of these conditions is that an event fall within a 24-hour hotplate data file interval. A few more events would have been included had we not applied this condition, but this would have required knitting together two adjacent 24-hour-duration hotplate data files. We decided against doing that in this analysis.

In the manuscript, we do not discuss the conditions mentioned in the previous four paragraphs. However, but we did document the events in Table 5.

At the end of this document, we plot of the 27 event intervals analyzed in the manuscript. The event intervals are marked with vertical bold dashed lines and the event name is printed above the graphs.

Ln 414. Add “an” as follows: “and *an* upper-limit temperature…”.

Yes.

Ln 427 and 428. “Re extends smaller” and “there is an order of magnitude narrower Re range” are awkward as written.

Agreed. Interested readers can compare for themselves. In the revision, we changed the phrase to this:

…our Re extends over a much larger range.

Ln 441-442. Try to find a different term for “upwelling longwave”. For many readers, the term “upwelling longwave radiation” already has a specific use that differs from the longwave radiation leaving the surface of the top hotplate. And throughout the manuscript the correct usage is “longwave radiation”, not “longwave”. The same rule applies to the use of “shortwave”.

Agreed, and changes were made in earlier sections of the revisions. However, at this point in the manuscript, after having defined the terms in the power budget by way of Eq. 3 (section 2), and having used the same formulae for the power budget terms in both Eq. 3 and Fig.8, we think it is appropriate to use the modifiers “sensible, latent, and longwave”, for the output terms, and modifiers “top plate, longwave, and shortwave”, for the input terms. The caption of Fig. 8 was similarly changed.

Ln 446. Rewrite as, “The first step in the calculation is *the* conversion of the latent *energy* term…”.

Yes, however, early in the revision we define “latent power output.”

Ln 447. Change “latent term” to “latent energy term” or “latent heat term”.

We reserved “latent heat” for the quantity of energy absorbed during a phase transition. This is consistent with the definition in the American Meteorological Society Glossary: “The specific enthalpy difference between two phases of a substance at the same temperature.”

Ln 448. One of the Methods Sections might be a more appropriate location than this Section, but a detailed explanation of this element-by-element vector multiplication should be added to the manuscript, including why it is necessary.

We have shown that f2 is a function of ambient temperature. Thus, it is logical that ambient temperature should be factored in at each instant the latent power output is available. No change was made.

Ln 473 – 475. Explore the effects and uncertainty of the field-based calibration coefficients. How sensitive is precipitation to these? What happens if you swap them from site-to-site? Based only on their variability from site-to-site, there appears to be a significant amount of uncertainty in these terms. Calculate the effects of this uncertainty on precipitation.

In our view, site-to-site variability is expected given that the coefficients (α, β, and γ) are describing sensible energy transfer, and the latter is expected to change with air density, and thus with site elevation. Plus, a component of the variability is likely coming from the servicing we discussed earlier. If we had two independent determinations of $\alpha/\beta/\gamma$, and both from the same location, and this was for a hotplate that had not had electrical components replaced in the factory, then we could comply with your recommendation. Unfortunately, we do not.

Ln 483. "…ratios significantly smaller than unity" is awkward as written.

Agreed. In the revision, we changed the text to this:

Since we do not have access to the YES algorithm, we estimated the longwave radiative effect by setting the longwave terms to zero in Eq. 3. After doing this, a larger UW/YES ratio (a = 0.83 ± 0.04) was obtained in a plot analogous to Fig. 9. From this modest increase of the UW/YES ratio, we conclude that longwave forcing *cannot* explain the shift of the best-fit line away from unity in Fig. 9. An even smaller perturbation of the UW/YES ratio was obtained in calculations that set the shortwave term to zero in Eq. 3 (results not shown).

Also, we added this finding to the second paragraph of the Conclusion:

We demonstrated that radiative forcing of the power budget is relatively unimportant for the precipitation events analyzed. This is because the hotplate's shortwave absorptance (i.e., $1 - R_h$ in Eq. 3), and its longwave emissivity, are small compared to unity, because a majority of events occurred at night, and because generally overcast conditions diminished the significance of longwave forcing.

Ln 484. "…obtained when zeroing the shortwave term…" is awkward as written.

Please see our previous response.

Ln 489. Add "the" to "values of *the* UW algorithm". Ln 490. Change, "are detecting" to "detected".

Yes.

Ln 498. Add "catch" to "event-averaged *catch* efficiency".

Yes.

Ln 506. Change “*Es*” to “values of *E*” – *Es* could be mistaken as a separate term, rather than the plural form of *E*.

Yes.

Ln 508. Delete “statistically” used at both the beginning and the end of this line.

Yes.

Ln 521. Specify that the new radiation terms were only for the top plate.

In the revision, we have made it clear that Eq.1 and Eq. 3 are power budgets for the top plate. Please see previous comments.

Ln 524. Delete “have” in “we have used”.

Yes.

Ln. 565. Specify which component “Component of longwave flux” refers to. Based on Ln 118, it looks like it is the entire longwave flux, rather than a component.

In the revised Appendix, this referred to as an “Upwelling or downwelling component of longwave flux.” Also, the L117 has the upwelling longwave flux (emitted by the hotplate), and the “IR_d” in L118, is indicating “downwelling” with the subscript “d”.

Ln 596. Add *hp* (hotplate) to the list of subscripts.

Yes, but subscript “h”, not subscript “hp.” Note the later appears incorrectly in Table 3.

Figure 3. Use consistent terminology. Change “New Algorithm” to “UW algorithm”.

At this point in the manuscript, “UW Algorithm” is not yet defined. No change made.

Also in the caption explain that the Fig. 3b wind speeds were adjusted to account for the different heights.

Please see L310 to L319, the labeling of Fig. 3b, and the reference back to the text for “details.” No change made.

Buisán, S. T., Earle, M. E., Collado, J. L., Kochendorfer, J., Alastrué, J., Wolff, M., Smith, C. D., and López-Moreno, J. I.: Assessment of snowfall accumulation underestimation by tipping bucket gauges in the Spanish operational 5 network, Atmos. Meas. Tech., 10, 1079-1091, 10.5194/amt-10-1079-2017, 2017.

Fortin, V., Therrien, C., and Anctil, F.: Correcting wind-induced bias in solid precipitation measurements in case of limited and uncertain data, Hydrological Processes, 22, 3393-3402, 10.1002/hyp.6959, 2008.

Kochendorfer, J., Nitu, R., Wolff, M., Mekis, E., Rasmussen, R., Baker, B., Earle, M. E., Reverdin, A., Wong, K., Smith, C. D., Yang, D., Roulet, Y. A., Meyers, T., Buisan, S., Isaksen, K., Brækkan, R., Landolt, S., and Jachcik, A.: Testing and development of transfer functions for weighing precipitation gauges in WMO-SPICE, Hydrol. Earth Syst. Sci. Discuss., 2017, 1-25, 10.5194/hess-2017-228, 2017a.

Kochendorfer, J., Rasmussen, R., Wolff, M., Baker, B., Hall, M. E., Meyers, T., Landolt, S., Jachcik, A., Isaksen, K., Brækkan, R., and Leeper, R.: The quantification and correction of wind-induced precipitation measurement errors, Hydrol. Earth Syst. Sci., 21, 1973-1989, 10.5194/hess-21-1973-2017, 2017b.

Wolff, M. A., Isaksen, K., Petersen-Overleir, A., Odemark, K., Reitan, T., and Braekkan, R.: Derivation of a new continuous adjustment function for correcting wind-induced loss of solid precipitation: results of a Norwegian field study, Hydrology and Earth System Sciences, 19, 951-967, 10.5194/hess-19-951-2015, 2015

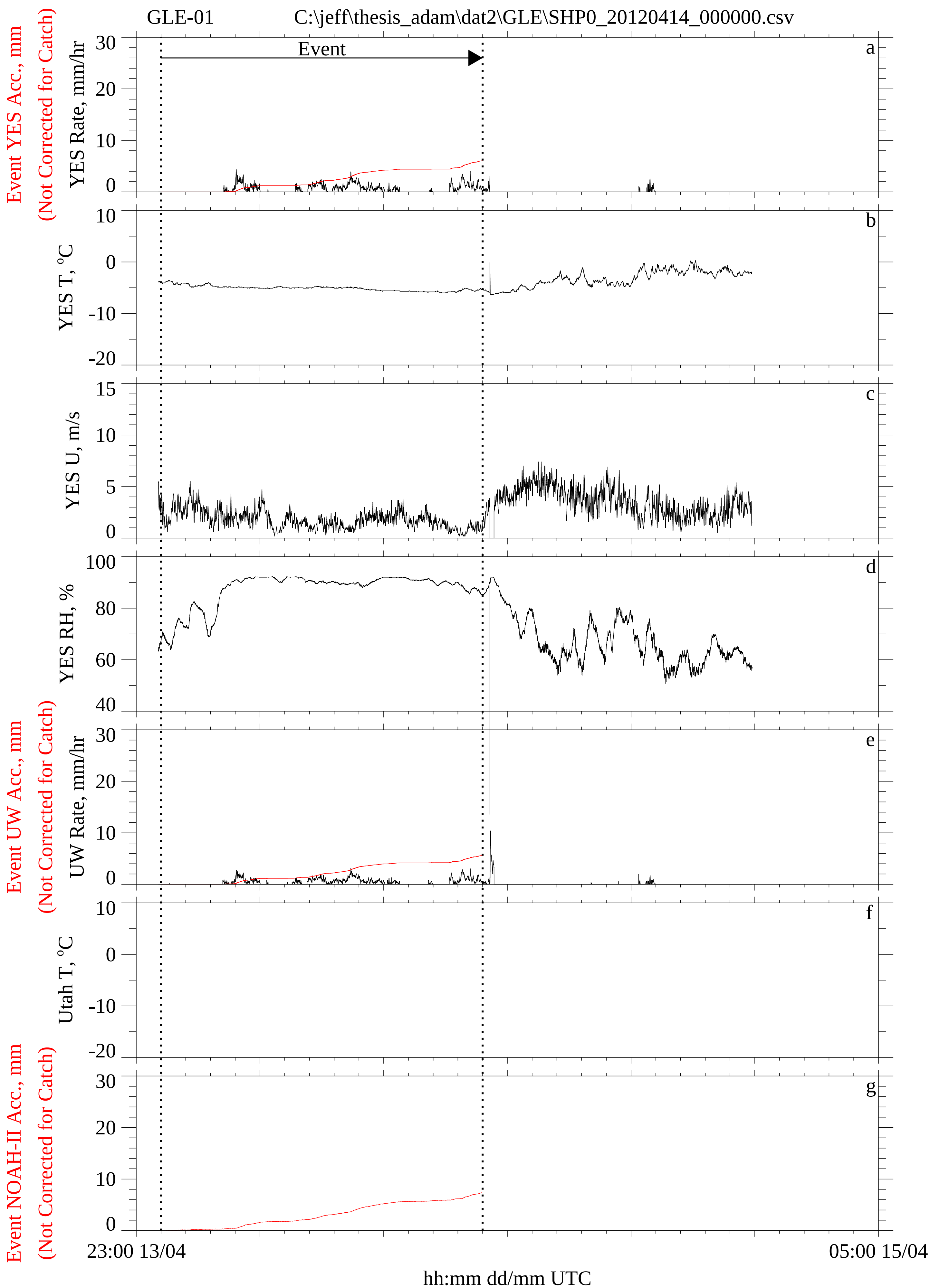
GLE-01
C:\jeff\thesis_adam\dat2\GLE\SHP0_20120414_000000.csv
Event
a
b
c
d
e
f
g
Event YES Acc., mm
(Not Corrected for Catch)
YES Rate, mm/hr
YES T, °C
YES U, m/s
YES RH, %
Event UW Acc., mm
(Not Corrected for Catch)
UW Rate, mm/hr
Utah T, °C
Event NOAH-II Acc., mm
(Not Corrected for Catch)
23:00 13/04
05:00 15/04
hh:mm dd/mm UTC

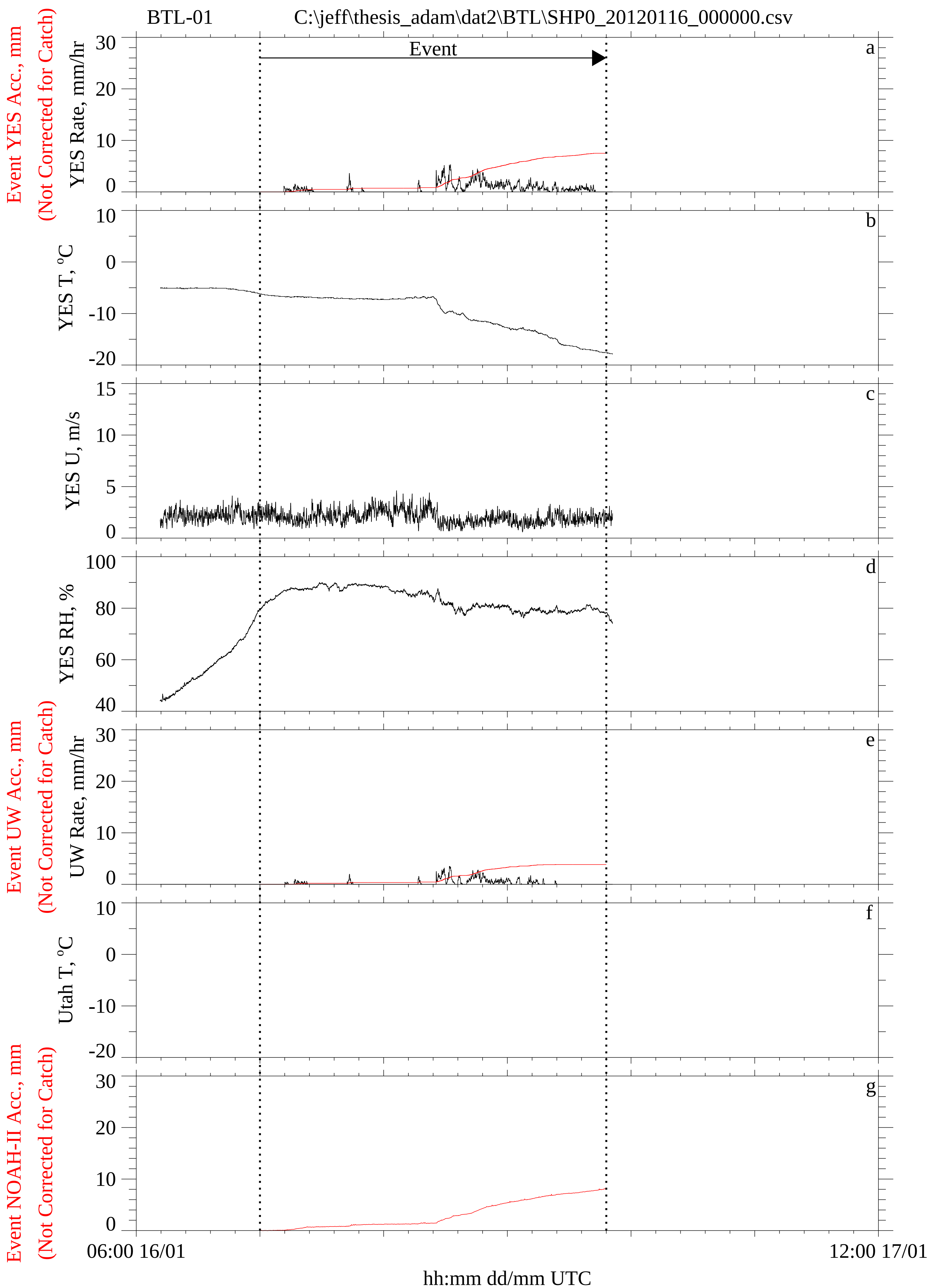

BTL-01
C:\jeff\thesis_adam\dat2\BTL\SHP0_20120116_000000.csv
Event
Event YES Acc., mm (Not Corrected for Catch)
YES Rate, mm/hr
YES T, °C
YES U, m/s
YES RH, %
Event UW Acc., mm (Not Corrected for Catch)
UW Rate, mm/hr
Utah T, °C
Event NOAH-II Acc., mm (Not Corrected for Catch)
a
b
c
d
e
f
g
06:00 16/01
12:00 17/01
hh:mm dd/mm UTC

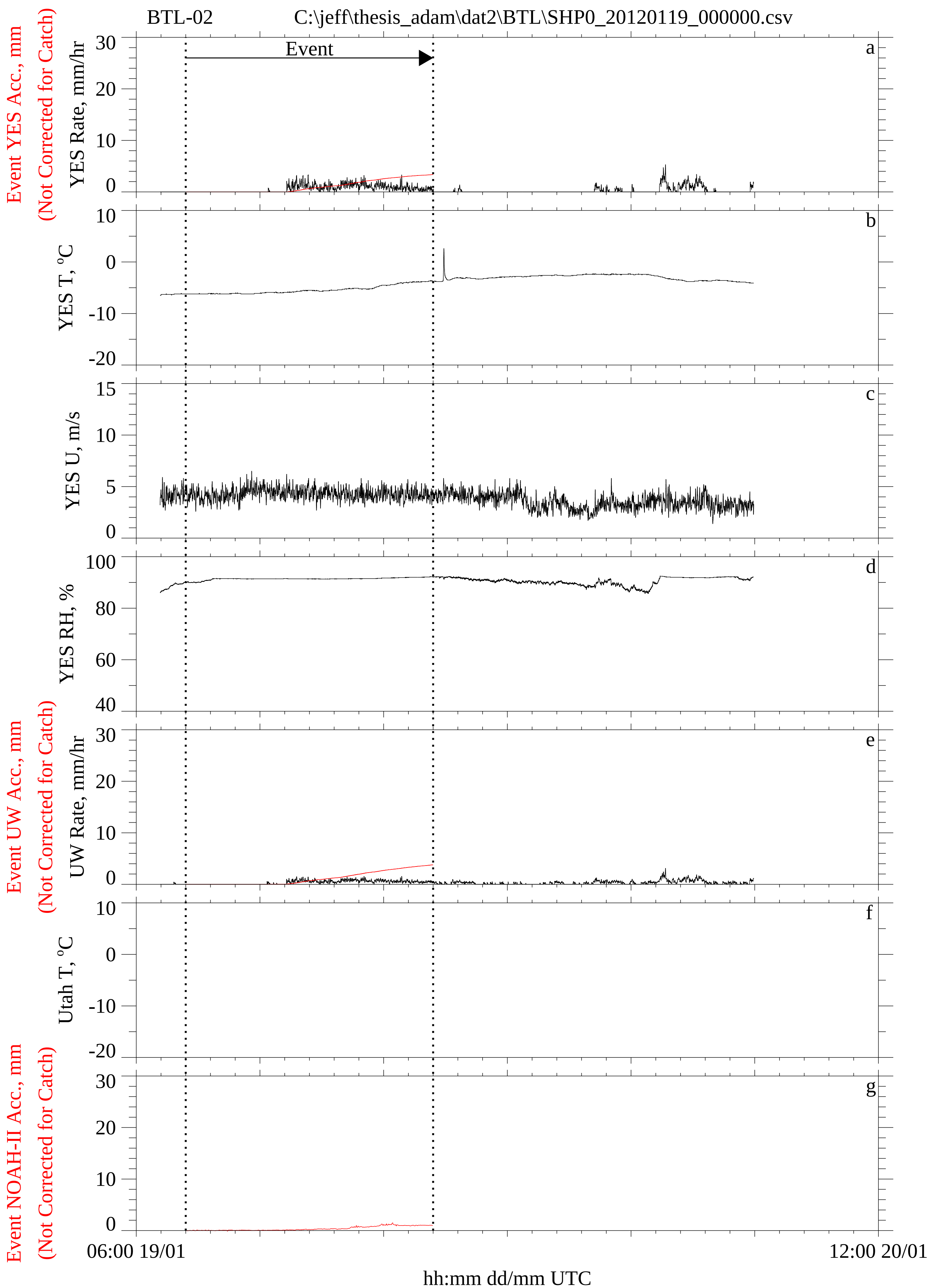
BTL-02
C:\jeff\thesis_adam\dat2\BTL\SHP0_20120119_000000.csv
Event
a
b
c
d
e
f
g
Event YES Acc., mm
(Not Corrected for Catch)
YES Rate, mm/hr
YES T, °C
YES U, m/s
YES RH, %
Event UW Acc., mm
(Not Corrected for Catch)
UW Rate, mm/hr
Utah T, °C
Event NOAH-II Acc., mm
(Not Corrected for Catch)
30
20
10
0
-10
-20
15
5
100
80
60
40
06:00 19/01
12:00 20/01
hh:mm dd/mm UTC

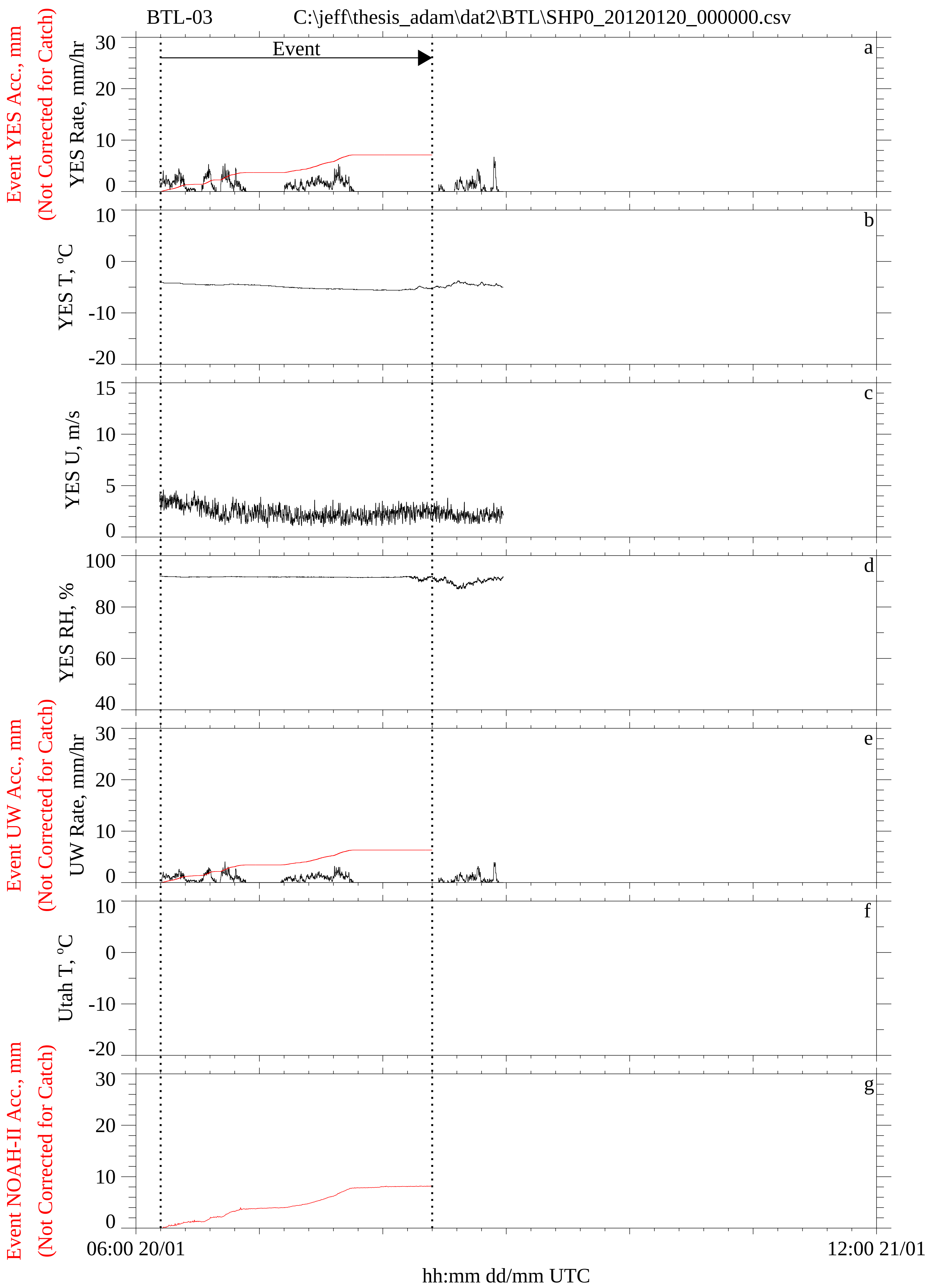

BTL-03
C:\jeff\thesis_adam\dat2\BTL\SHP0_20120120_000000.csv
Event
Event YES Acc., mm
(Not Corrected for Catch)
YES Rate, mm/hr
YES T, °C
YES U, m/s
YES RH, %
Event UW Acc., mm
(Not Corrected for Catch)
UW Rate, mm/hr
Utah T, °C
Event NOAH-II Acc., mm
(Not Corrected for Catch)
a
b
c
d
e
f
g
06:00 20/01
12:00 21/01
hh:mm dd/mm UTC

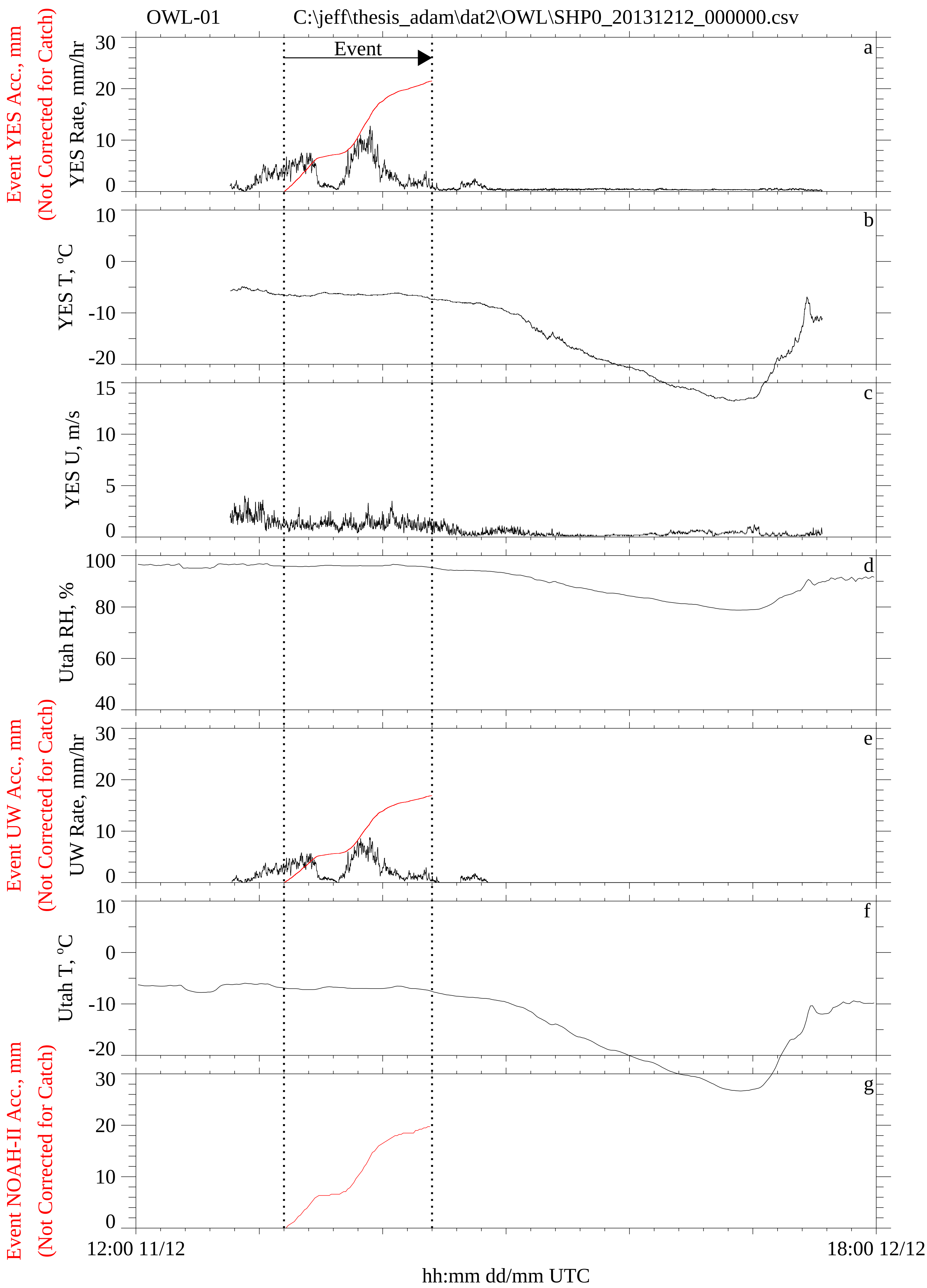

OWL-01
C:\jeff\thesis_adam\dat2\OWL\SHP0_20131212_000000.csv
Event
Event YES Acc., mm
(Not Corrected for Catch)
YES Rate, mm/hr
YES T, °C
YES U, m/s
Utah RH, %
Event UW Acc., mm
(Not Corrected for Catch)
UW Rate, mm/hr
Utah T, °C
Event NOAH-II Acc., mm
(Not Corrected for Catch)
a
b
c
d
e
f
g
12:00 11/12
18:00 12/12
hh:mm dd/mm UTC

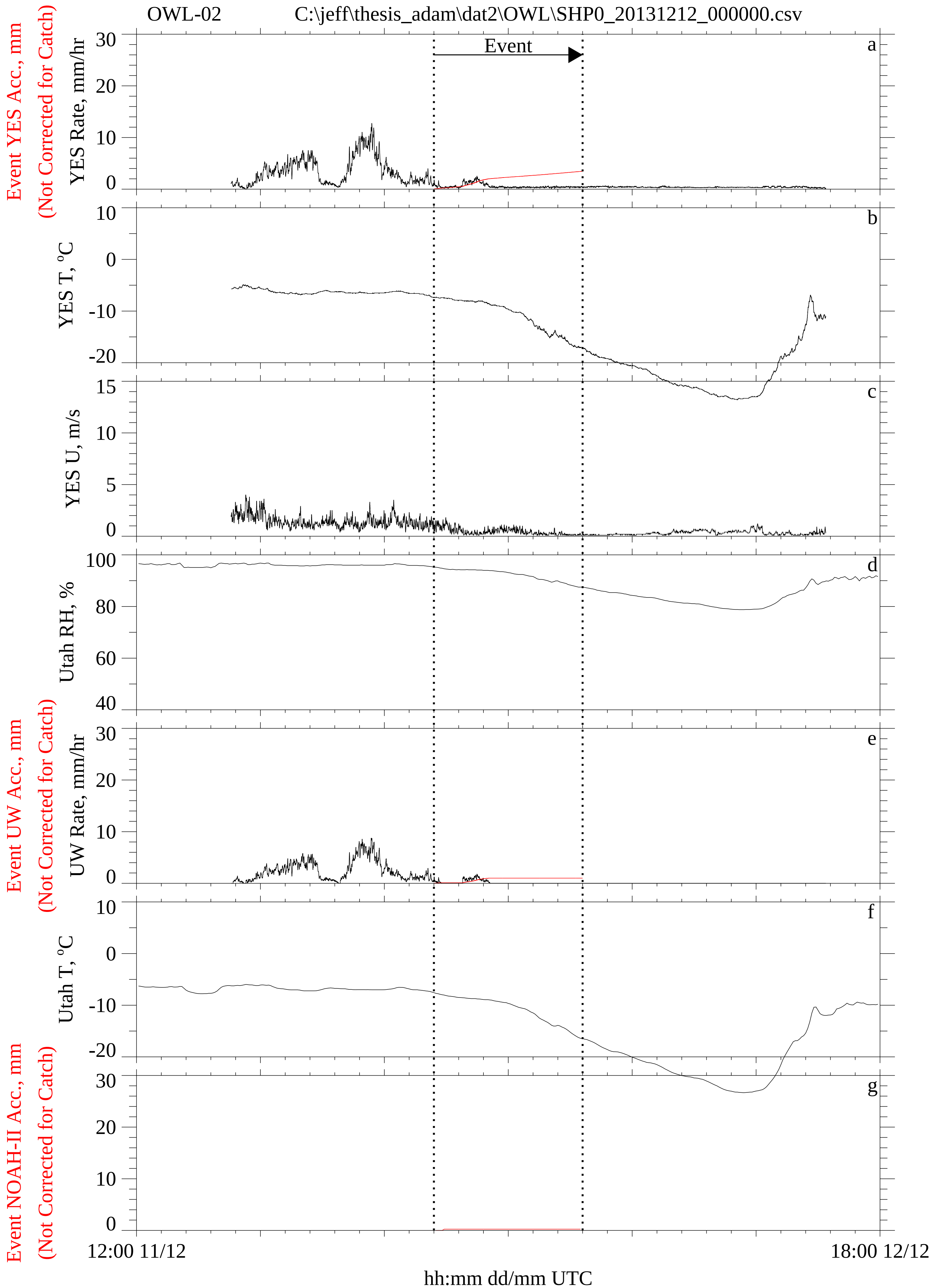
OWL-02
C:\jeff\thesis_adam\dat2\OWL\SHP0_20131212_000000.csv
Event
Event YES Acc., mm (Not Corrected for Catch)
YES Rate, mm/hr
YES T, °C
YES U, m/s
Utah RH, %
Event UW Acc., mm (Not Corrected for Catch)
UW Rate, mm/hr
Utah T, °C
Event NOAH-II Acc., mm (Not Corrected for Catch)
a
b
c
d
e
f
g
12:00 11/12
18:00 12/12
hh:mm dd/mm UTC

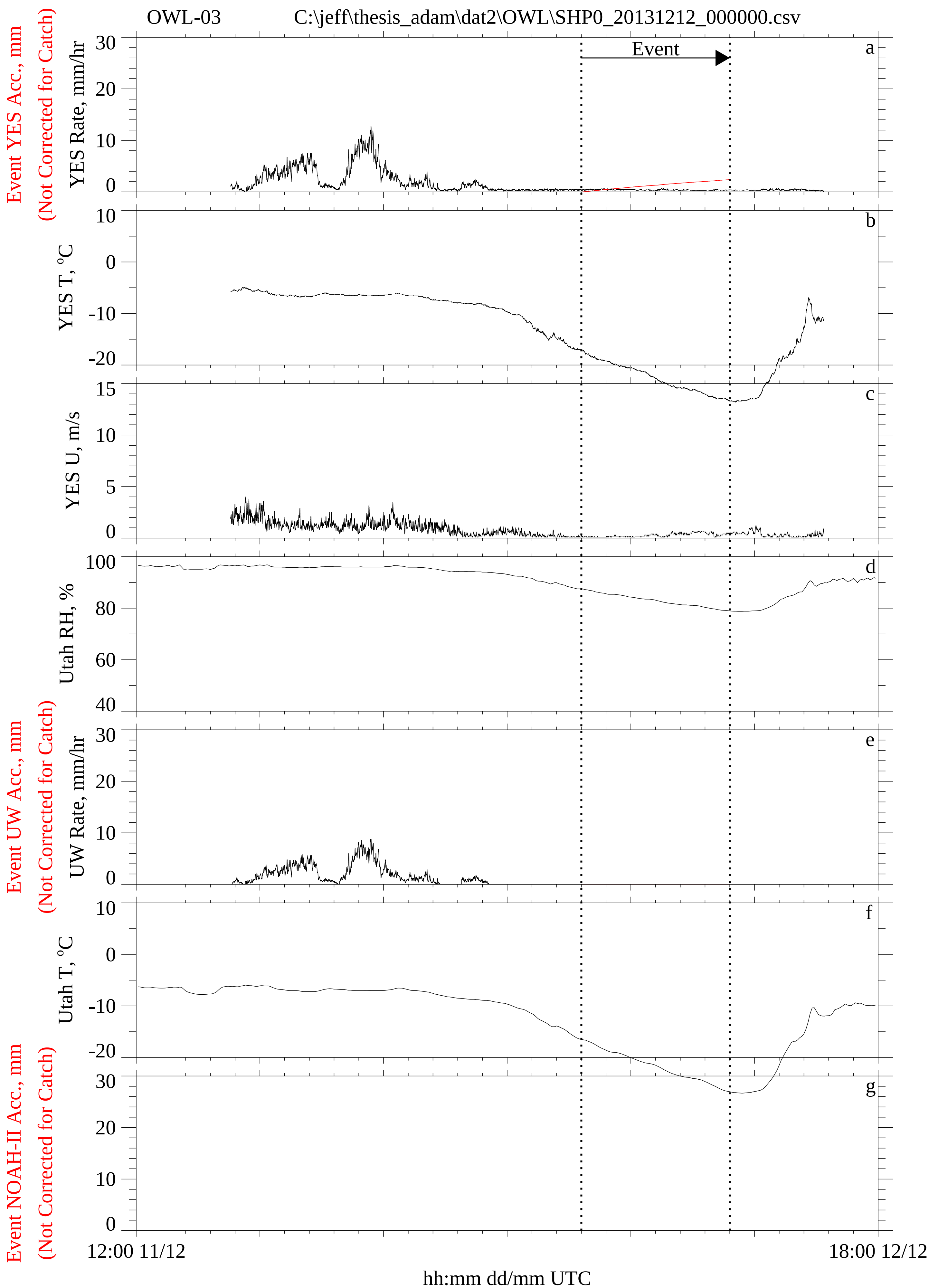
OWL-03
C:\jeff\thesis_adam\dat2\OWL\SHP0_20131212_000000.csv
Event
Event YES Acc., mm
(Not Corrected for Catch)
YES Rate, mm/hr
a
YES T, °C
b
YES U, m/s
c
Utah RH, %
d
Event UW Acc., mm
(Not Corrected for Catch)
UW Rate, mm/hr
e
Utah T, °C
f
Event NOAH-II Acc., mm
(Not Corrected for Catch)
g
12:00 11/12
18:00 12/12
hh:mm dd/mm UTC

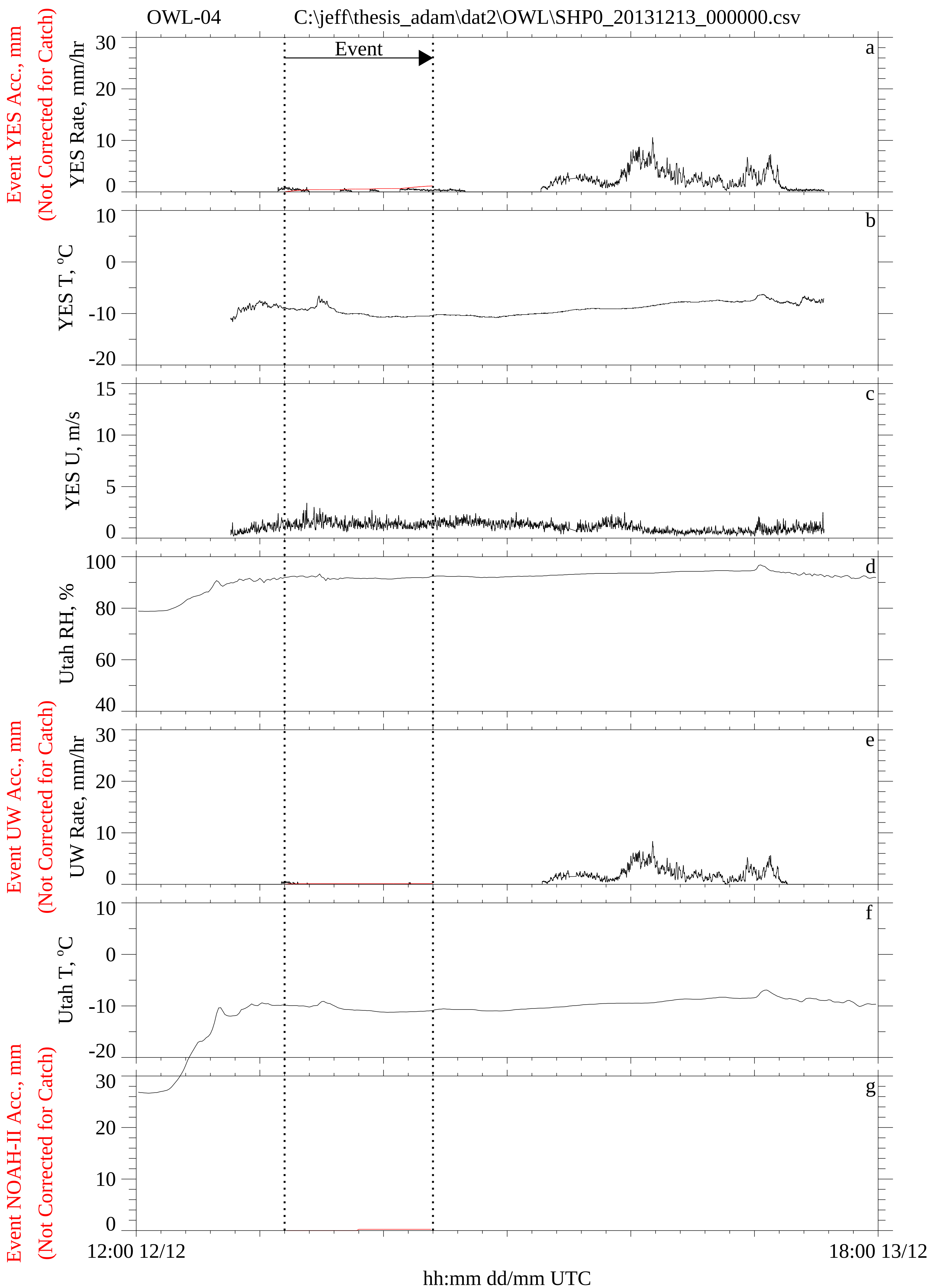

OWL-04
C:\jeff\thesis_adam\dat2\OWL\SHP0_20131213_000000.csv
Event
a
b
c
d
e
f
g
YES Rate, mm/hr
Event YES Acc., mm
(Not Corrected for Catch)
YES T, °C
YES U, m/s
Utah RH, %
UW Rate, mm/hr
Event UW Acc., mm
(Not Corrected for Catch)
Utah T, °C
Event NOAH-II Acc., mm
(Not Corrected for Catch)
12:00 12/12
18:00 13/12
hh:mm dd/mm UTC

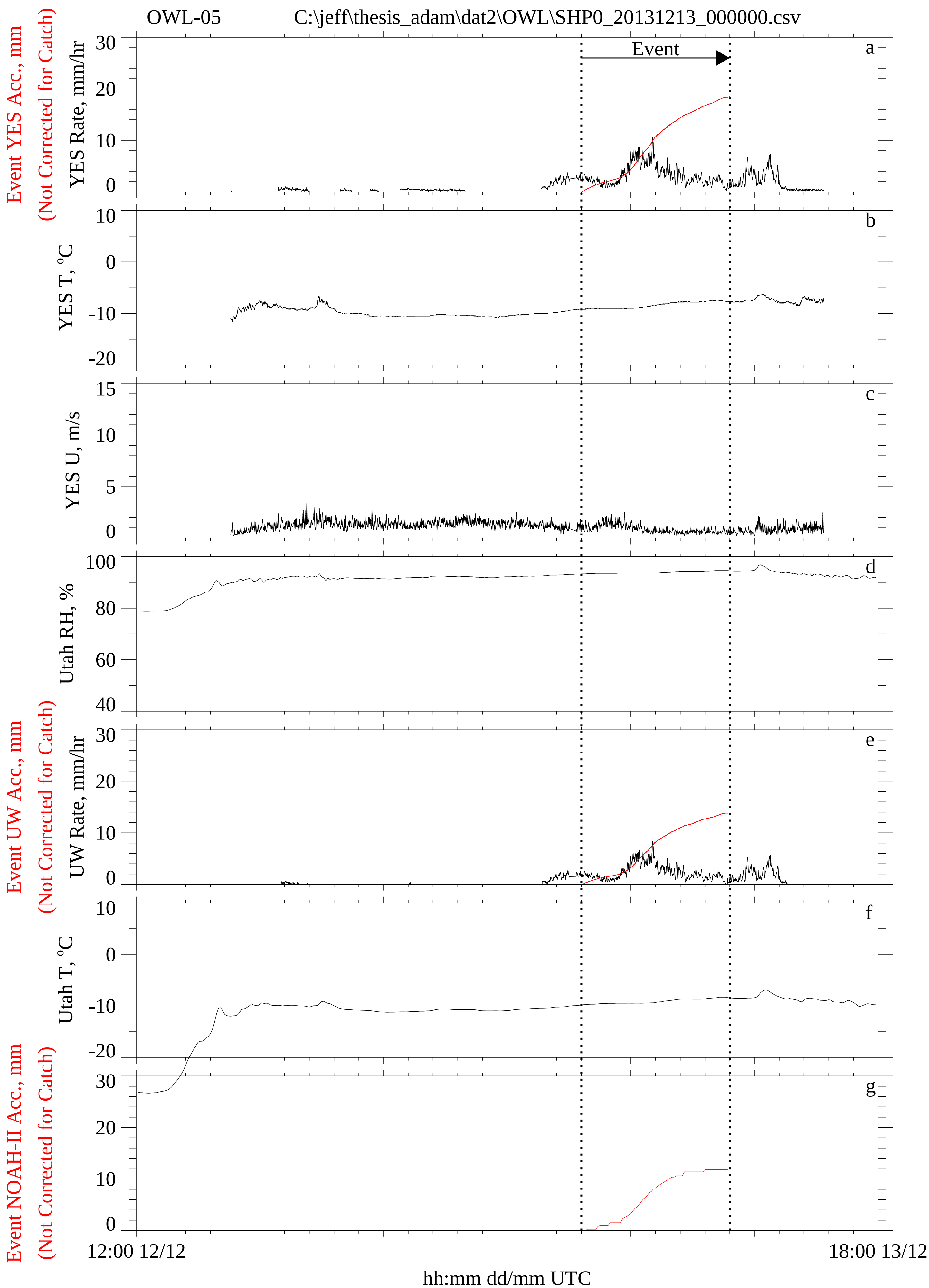

OWL-05
C:\jeff\thesis_adam\dat2\OWL\SHP0_20131213_000000.csv
Event
a
b
c
d
e
f
g
Event YES Acc., mm (Not Corrected for Catch)
YES Rate, mm/hr
YES T, °C
YES U, m/s
Utah RH, %
Event UW Acc., mm (Not Corrected for Catch)
UW Rate, mm/hr
Utah T, °C
Event NOAH-II Acc., mm (Not Corrected for Catch)
12:00 12/12
18:00 13/12
hh:mm dd/mm UTC

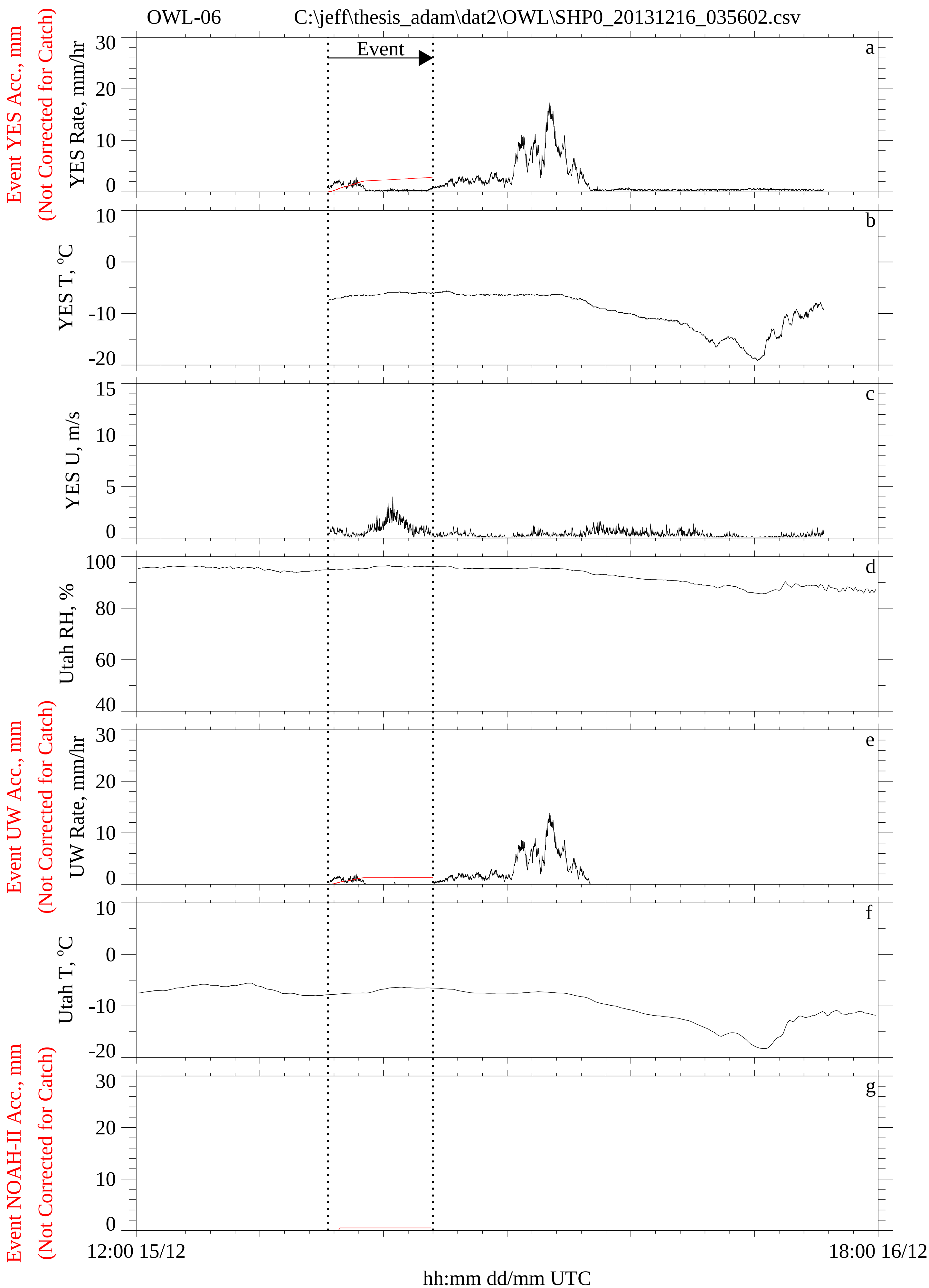

OWL-06
C:\jeff\thesis_adam\dat2\OWL\SHP0_20131216_035602.csv
Event
Event YES Acc., mm
(Not Corrected for Catch)
YES Rate, mm/hr
YES T, °C
YES U, m/s
Utah RH, %
Event UW Acc., mm
(Not Corrected for Catch)
UW Rate, mm/hr
Utah T, °C
Event NOAH-II Acc., mm
(Not Corrected for Catch)
a
b
c
d
e
f
g
12:00 15/12
18:00 16/12
hh:mm dd/mm UTC

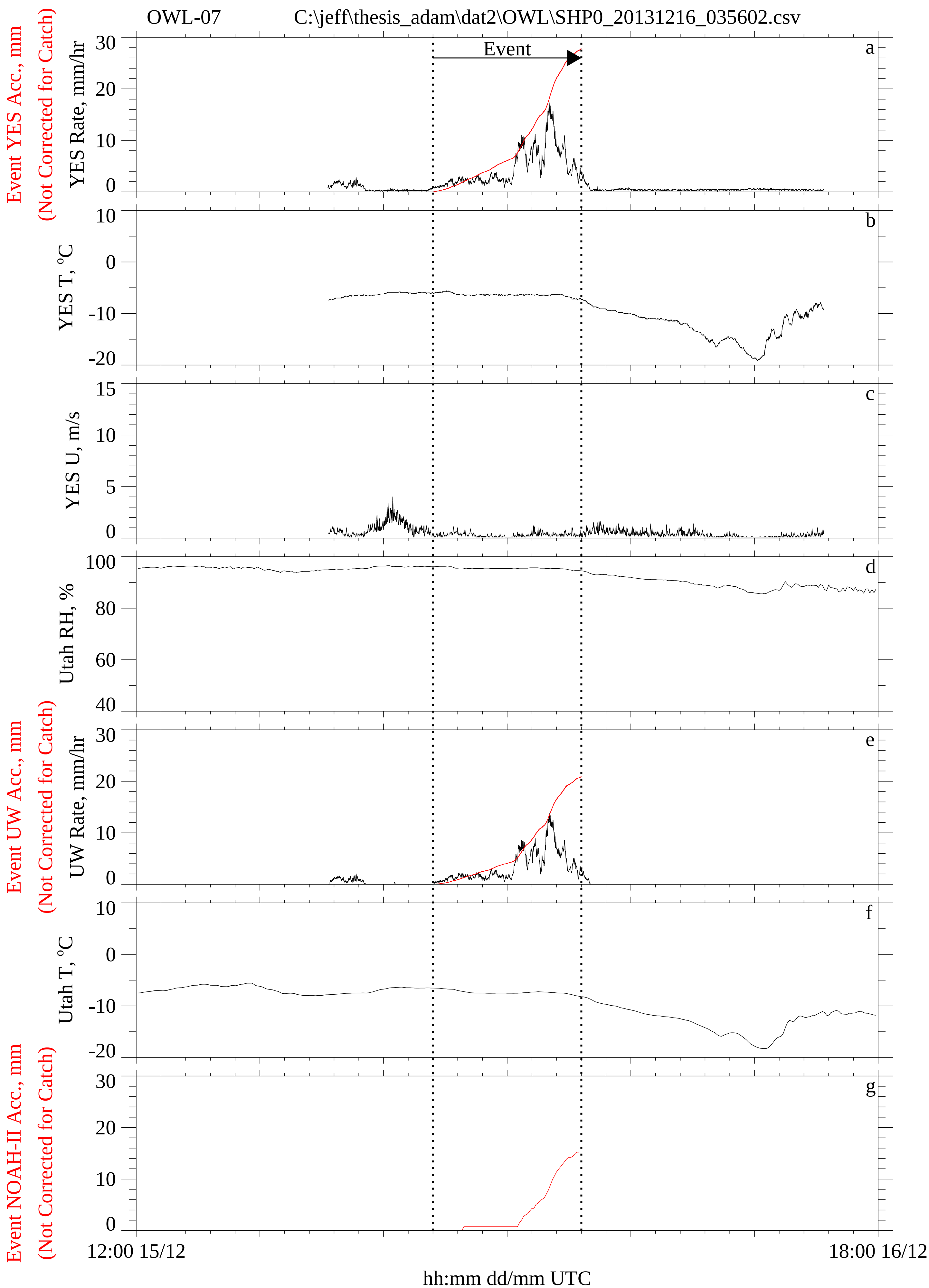

OWL-07
C:\jeff\thesis_adam\dat2\OWL\SHP0_20131216_035602.csv
Event
Event YES Acc., mm (Not Corrected for Catch)
YES Rate, mm/hr
YES T, °C
YES U, m/s
Utah RH, %
Event UW Acc., mm (Not Corrected for Catch)
UW Rate, mm/hr
Utah T, °C
Event NOAH-II Acc., mm (Not Corrected for Catch)
a
b
c
d
e
f
g
12:00 15/12
18:00 16/12
hh:mm dd/mm UTC

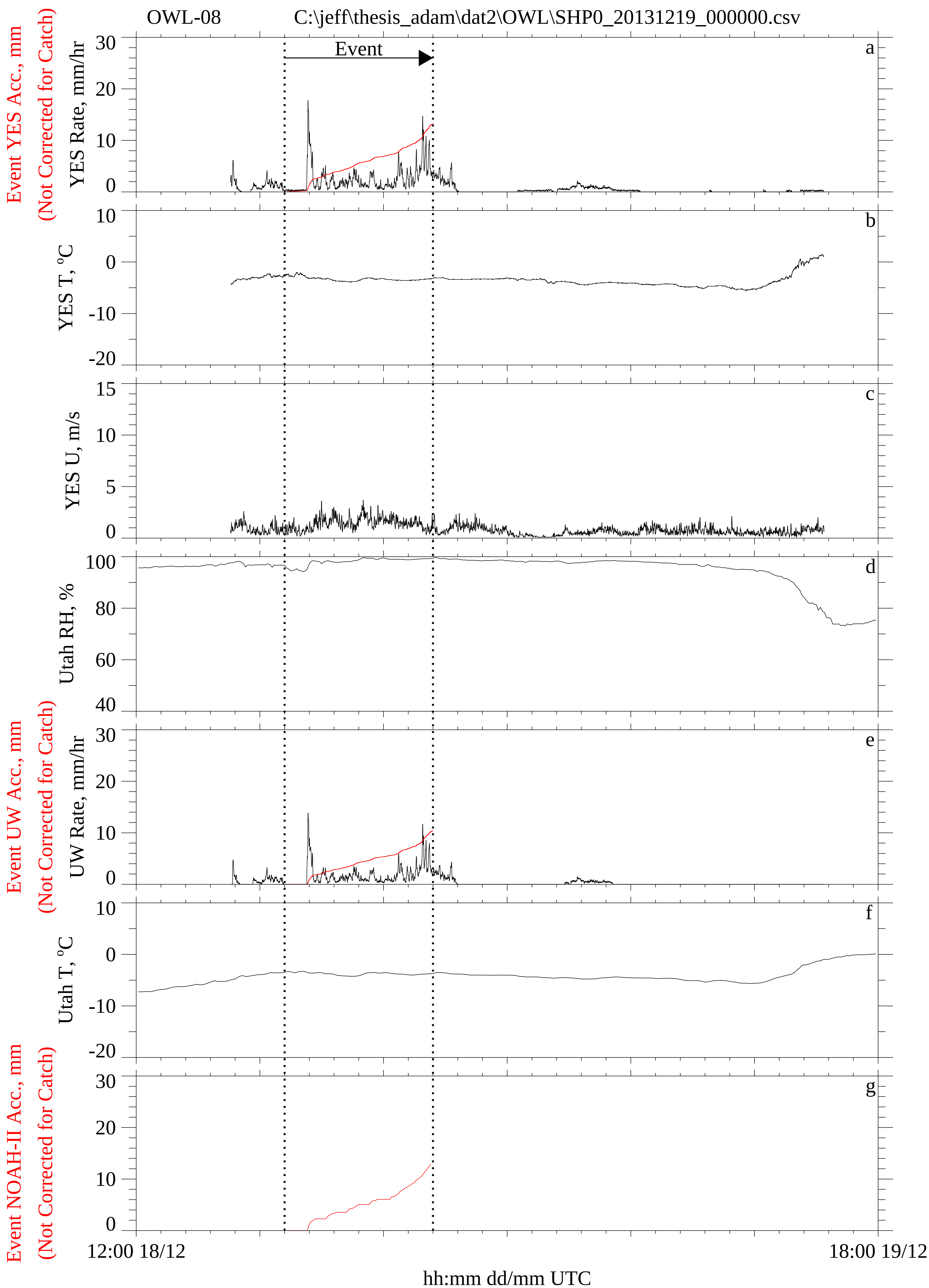

OWL-08
C:\jeff\thesis_adam\dat2\OWL\SHP0_20131219_000000.csv
Event
Event YES Acc., mm (Not Corrected for Catch)
YES Rate, mm/hr
YES T, °C
YES U, m/s
Utah RH, %
Event UW Acc., mm (Not Corrected for Catch)
UW Rate, mm/hr
Utah T, °C
Event NOAH-II Acc., mm (Not Corrected for Catch)
a
b
c
d
e
f
g
12:00 18/12
18:00 19/12
hh:mm dd/mm UTC

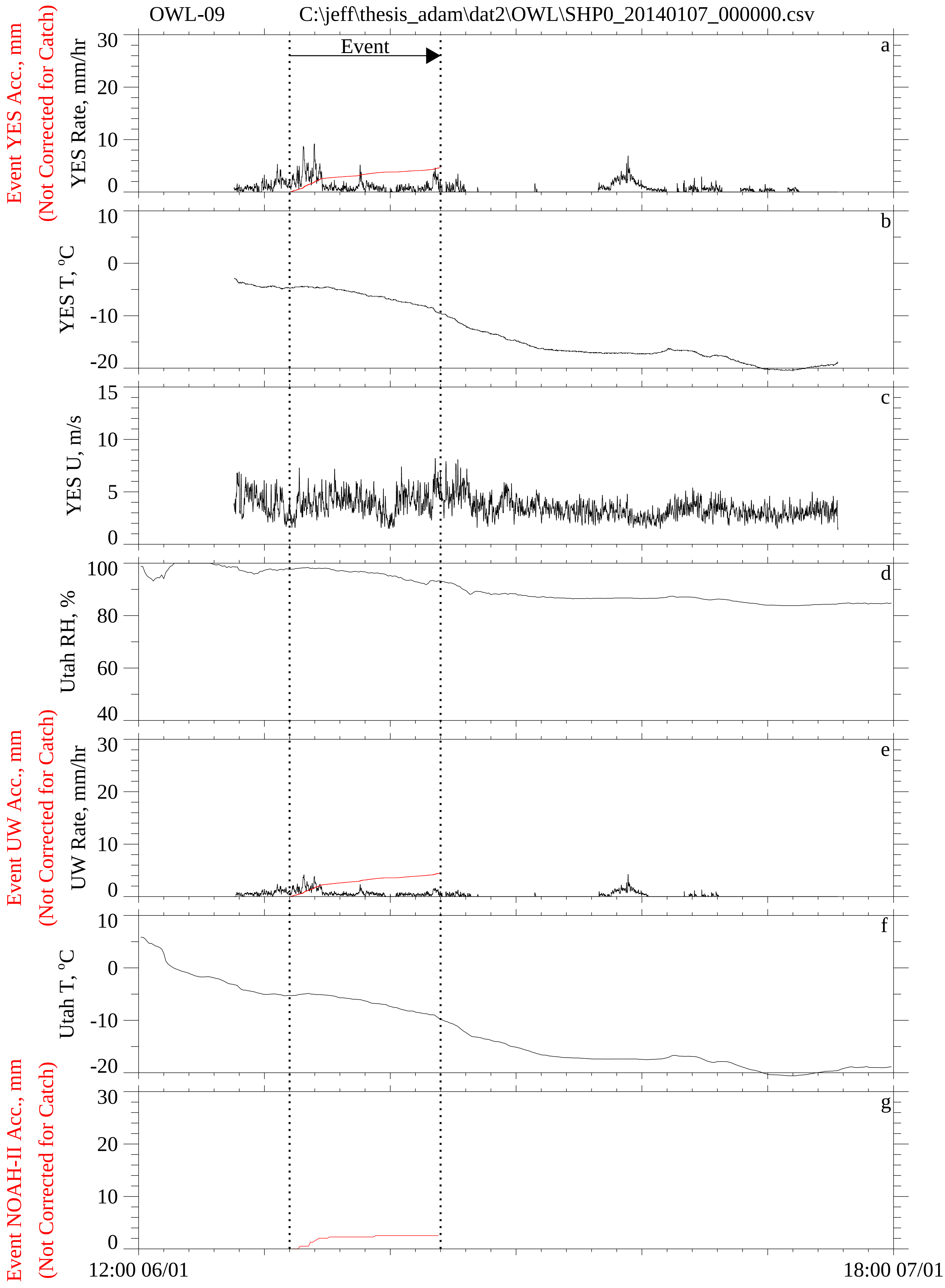

OWL-09
C:\jeff\thesis_adam\dat2\OWL\SHP0_20140107_000000.csv
Event
a
b
c
d
e
f
g
Event YES Acc., mm
(Not Corrected for Catch)
YES Rate, mm/hr
YES T, °C
YES U, m/s
Utah RH, %
Event UW Acc., mm
(Not Corrected for Catch)
UW Rate, mm/hr
Utah T, °C
Event NOAH-II Acc., mm
(Not Corrected for Catch)
12:00 06/01
18:00 07/01
hh:mm dd/mm UTC

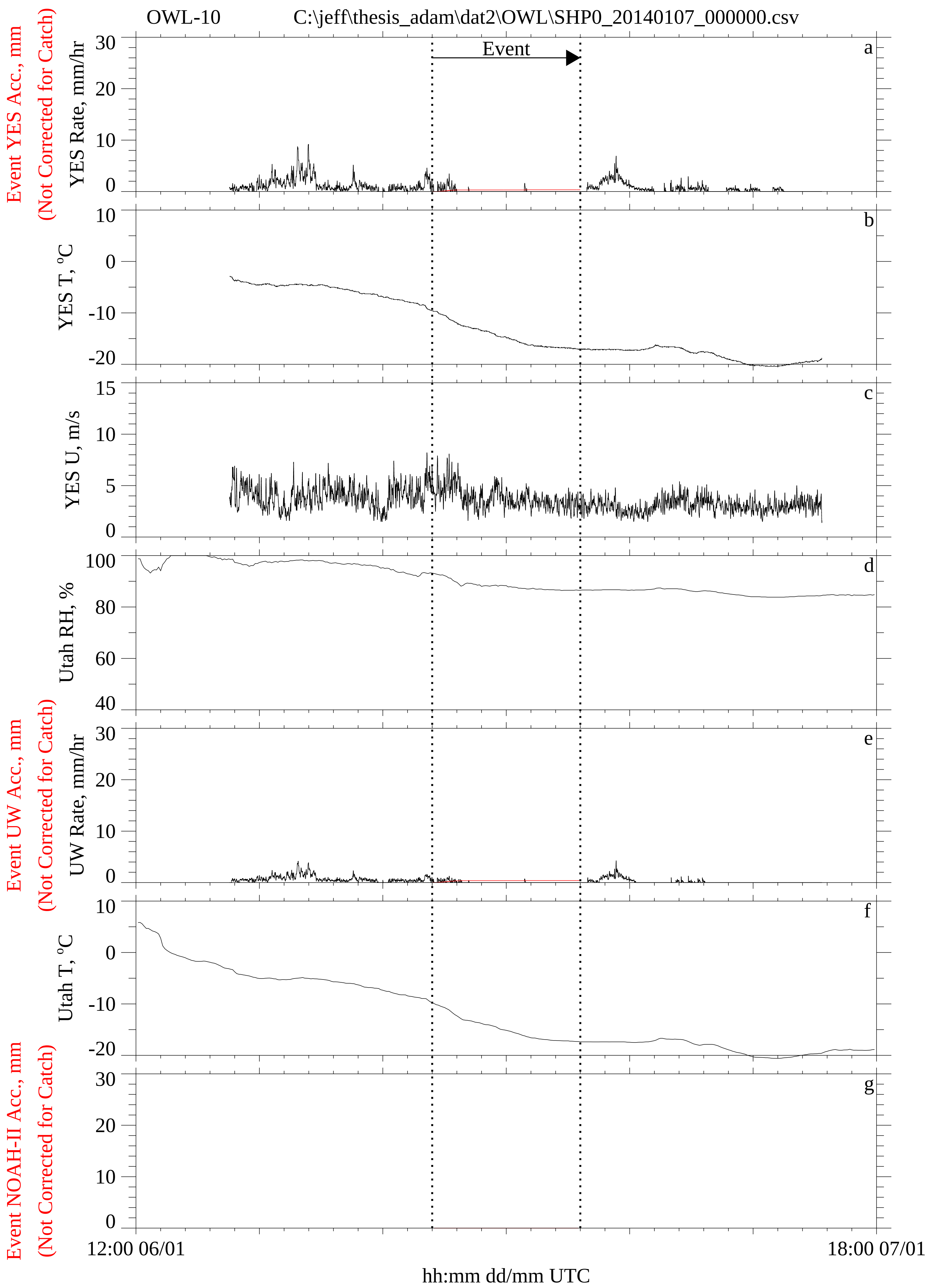

OWL-10
C:\jeff\thesis_adam\dat2\OWL\SHP0_20140107_000000.csv
Event
Event YES Acc., mm
(Not Corrected for Catch)
YES Rate, mm/hr
YES T, °C
YES U, m/s
Utah RH, %
Event UW Acc., mm
(Not Corrected for Catch)
UW Rate, mm/hr
Utah T, °C
Event NOAH-II Acc., mm
(Not Corrected for Catch)
a
b
c
d
e
f
g
12:00 06/01
18:00 07/01
hh:mm dd/mm UTC

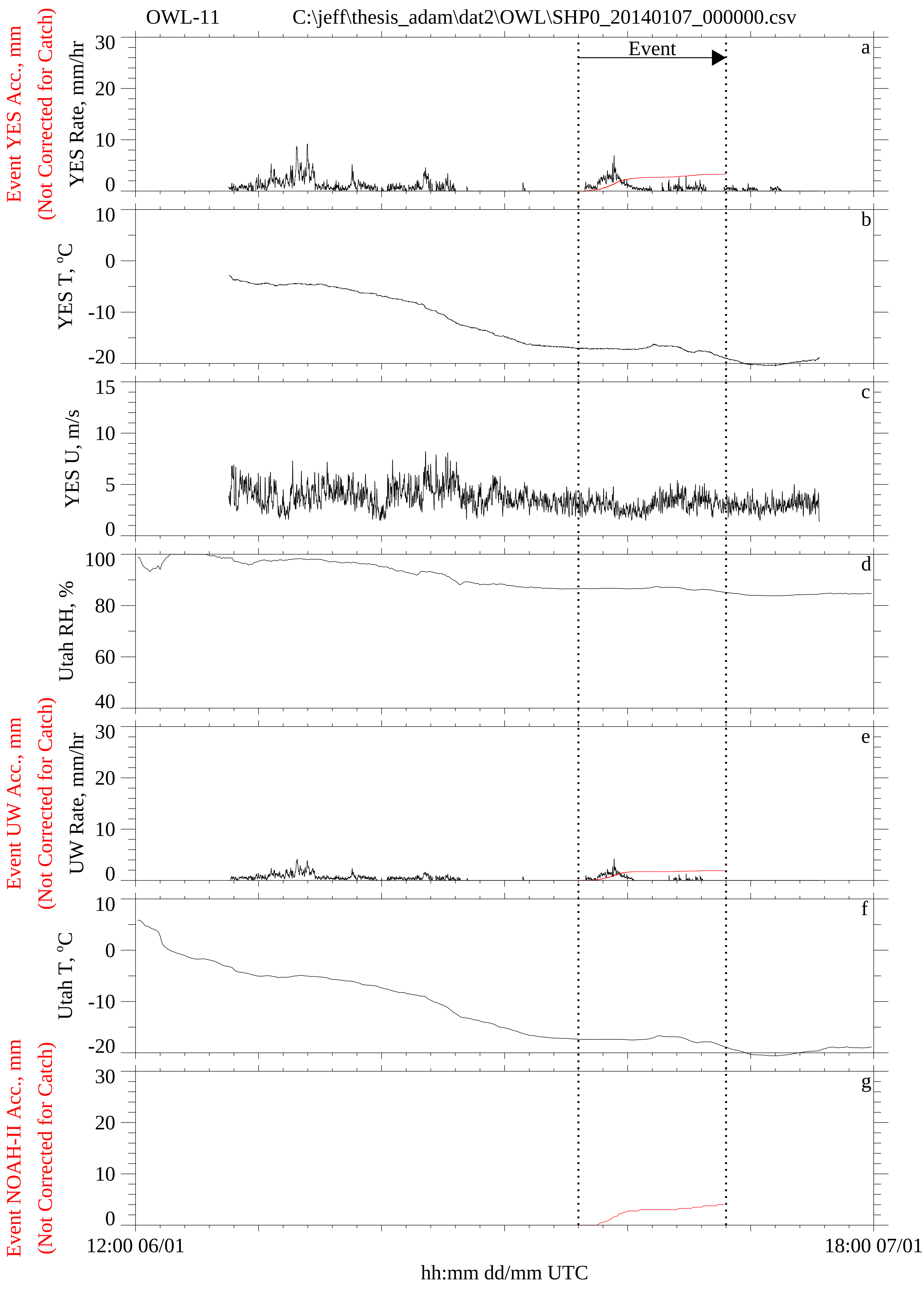

OWL-11
C:\jeff\thesis_adam\dat2\OWL\SHP0_20140107_000000.csv
Event
Event YES Acc., mm (Not Corrected for Catch)
YES Rate, mm/hr
YES T, °C
YES U, m/s
Utah RH, %
Event UW Acc., mm (Not Corrected for Catch)
UW Rate, mm/hr
Utah T, °C
Event NOAH-II Acc., mm (Not Corrected for Catch)
a
b
c
d
e
f
g
12:00 06/01
18:00 07/01
hh:mm dd/mm UTC

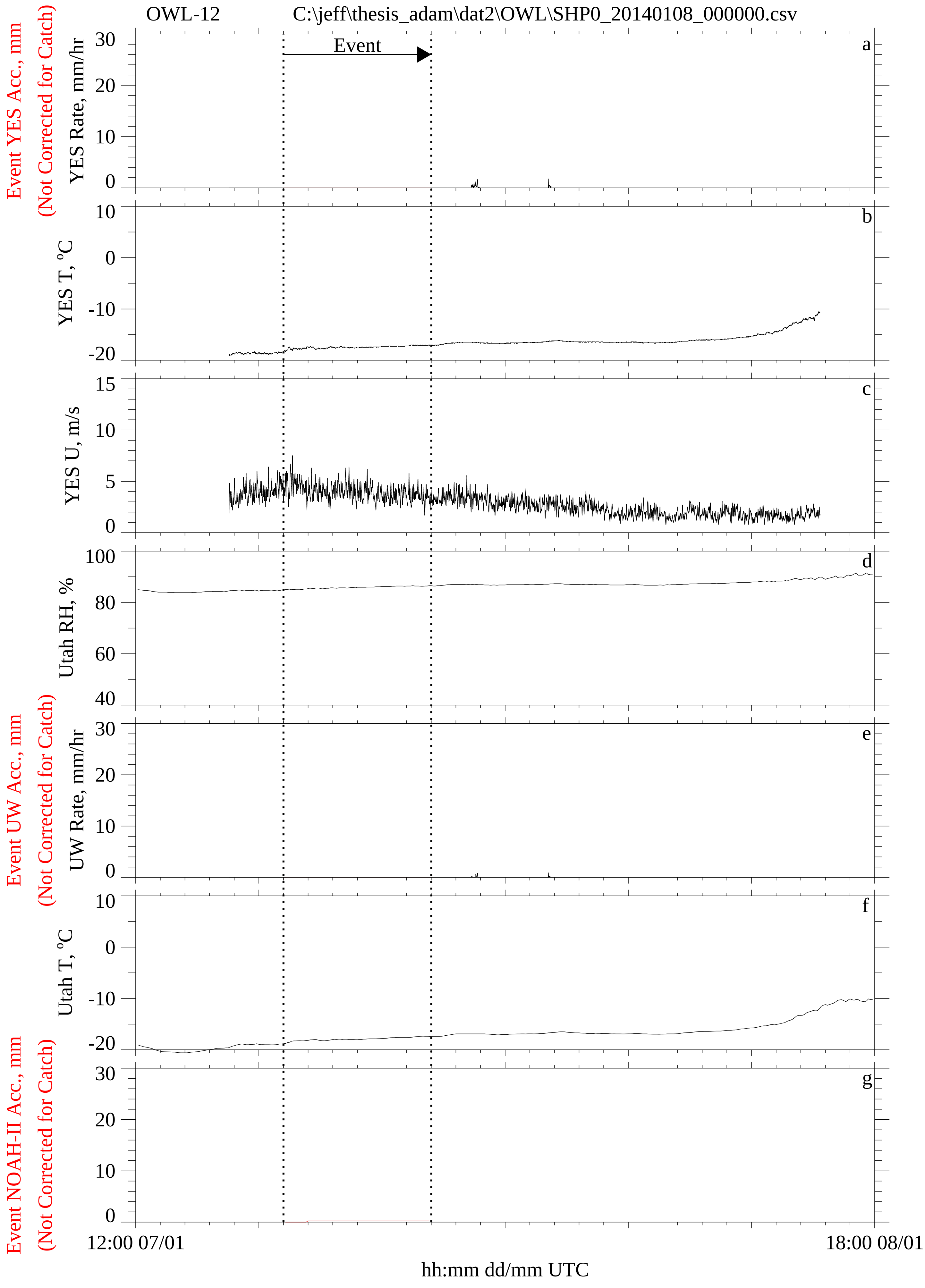
OWL-12
C:\jeff\thesis_adam\dat2\OWL\SHP0_20140108_000000.csv
Event
Event YES Acc., mm
(Not Corrected for Catch)
YES Rate, mm/hr
a
YES T, °C
b
YES U, m/s
c
Utah RH, %
d
Event UW Acc., mm
(Not Corrected for Catch)
UW Rate, mm/hr
e
Utah T, °C
f
Event NOAH-II Acc., mm
(Not Corrected for Catch)
g
12:00 07/01
18:00 08/01
hh:mm dd/mm UTC

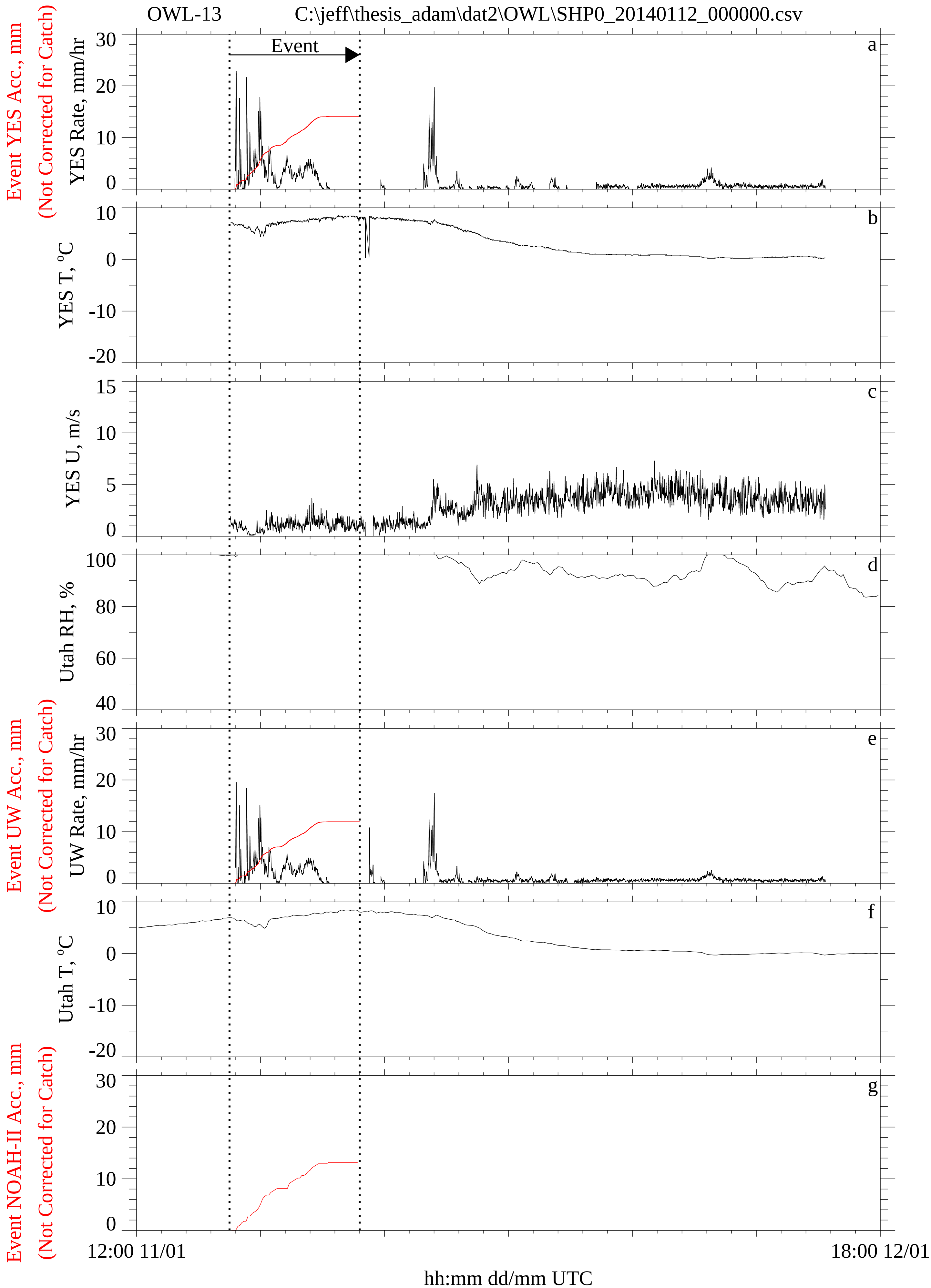

OWL-13
C:\jeff\thesis_adam\dat2\OWL\SHP0_20140112_000000.csv
Event
Event YES Acc., mm (Not Corrected for Catch)
YES Rate, mm/hr
YES T, °C
YES U, m/s
Utah RH, %
Event UW Acc., mm (Not Corrected for Catch)
UW Rate, mm/hr
Utah T, °C
Event NOAH-II Acc., mm (Not Corrected for Catch)
a
b
c
d
e
f
g
12:00 11/01
18:00 12/01
hh:mm dd/mm UTC

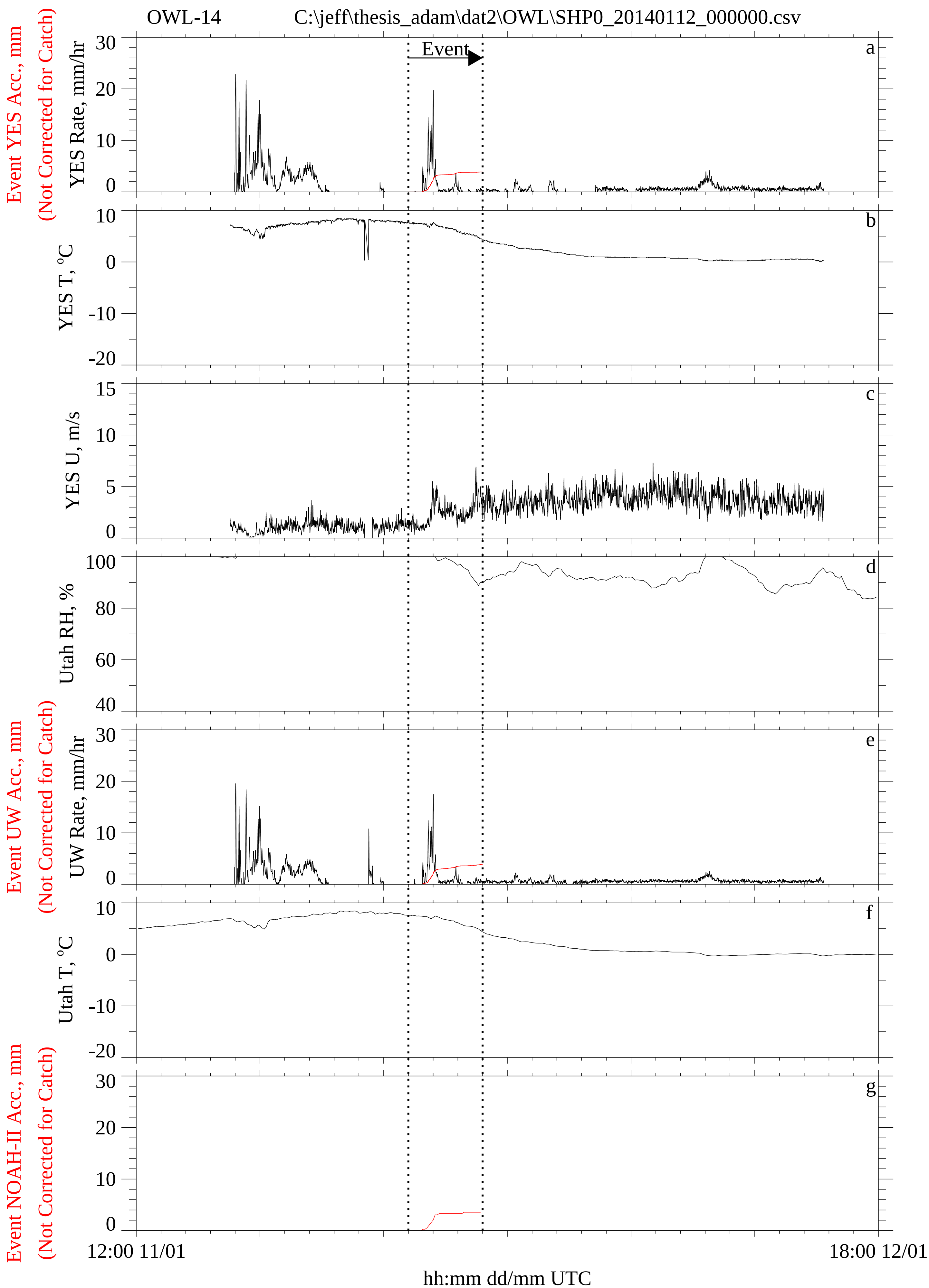

OWL-14
C:\jeff\thesis_adam\dat2\OWL\SHP0_20140112_000000.csv
Event
Event YES Acc., mm (Not Corrected for Catch)
YES Rate, mm/hr
YES T, °C
YES U, m/s
Utah RH, %
Event UW Acc., mm (Not Corrected for Catch)
UW Rate, mm/hr
Utah T, °C
Event NOAH-II Acc., mm (Not Corrected for Catch)
a
b
c
d
e
f
g
12:00 11/01
18:00 12/01
hh:mm dd/mm UTC

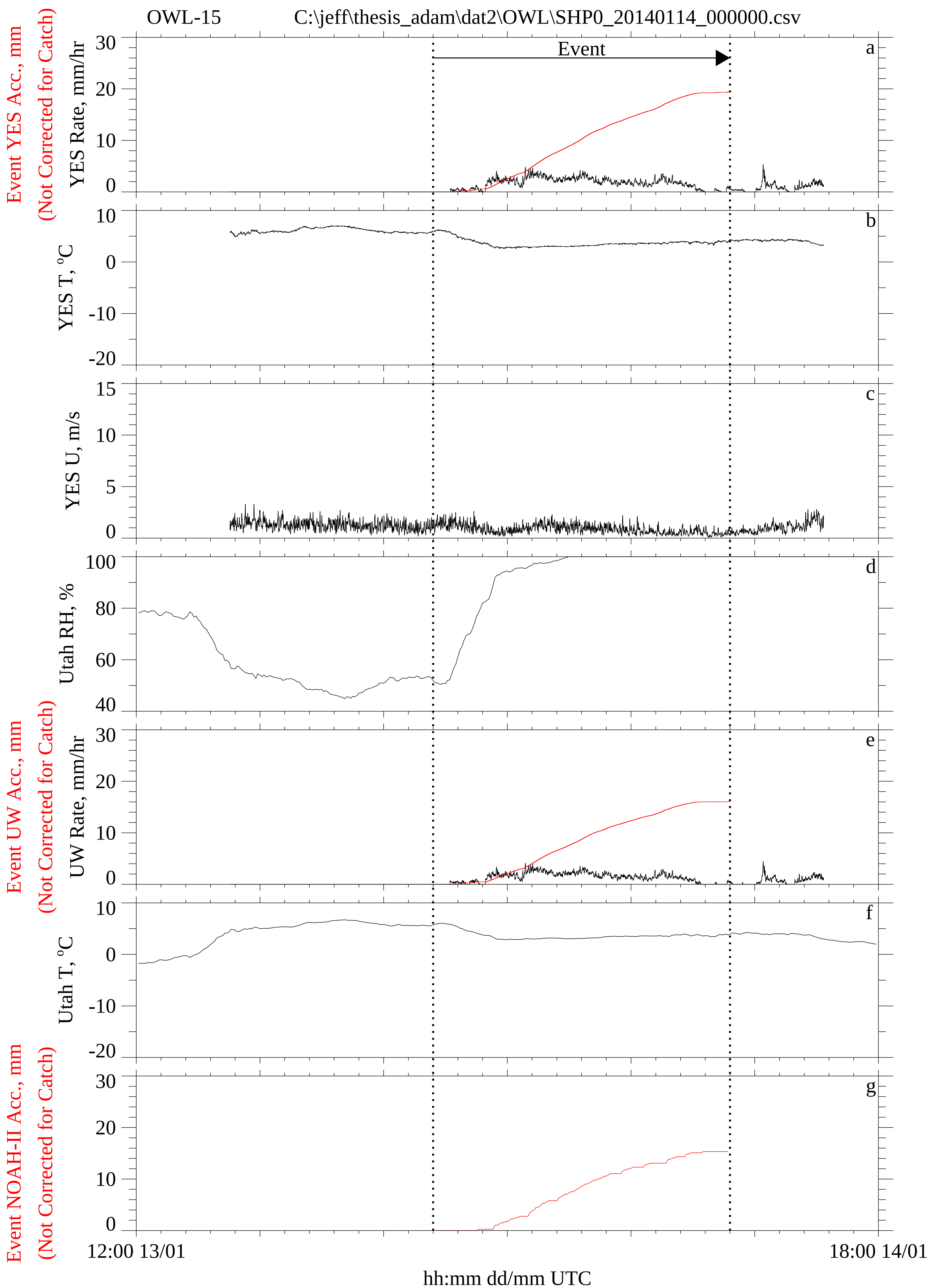
OWL-15
C:\jeff\thesis_adam\dat2\OWL\SHP0_20140114_000000.csv
Event
Event YES Acc., mm (Not Corrected for Catch)
YES Rate, mm/hr
YES T, °C
YES U, m/s
Utah RH, %
Event UW Acc., mm (Not Corrected for Catch)
UW Rate, mm/hr
Utah T, °C
Event NOAH-II Acc., mm (Not Corrected for Catch)
a
b
c
d
e
f
g
12:00 13/01
18:00 14/01
hh:mm dd/mm UTC

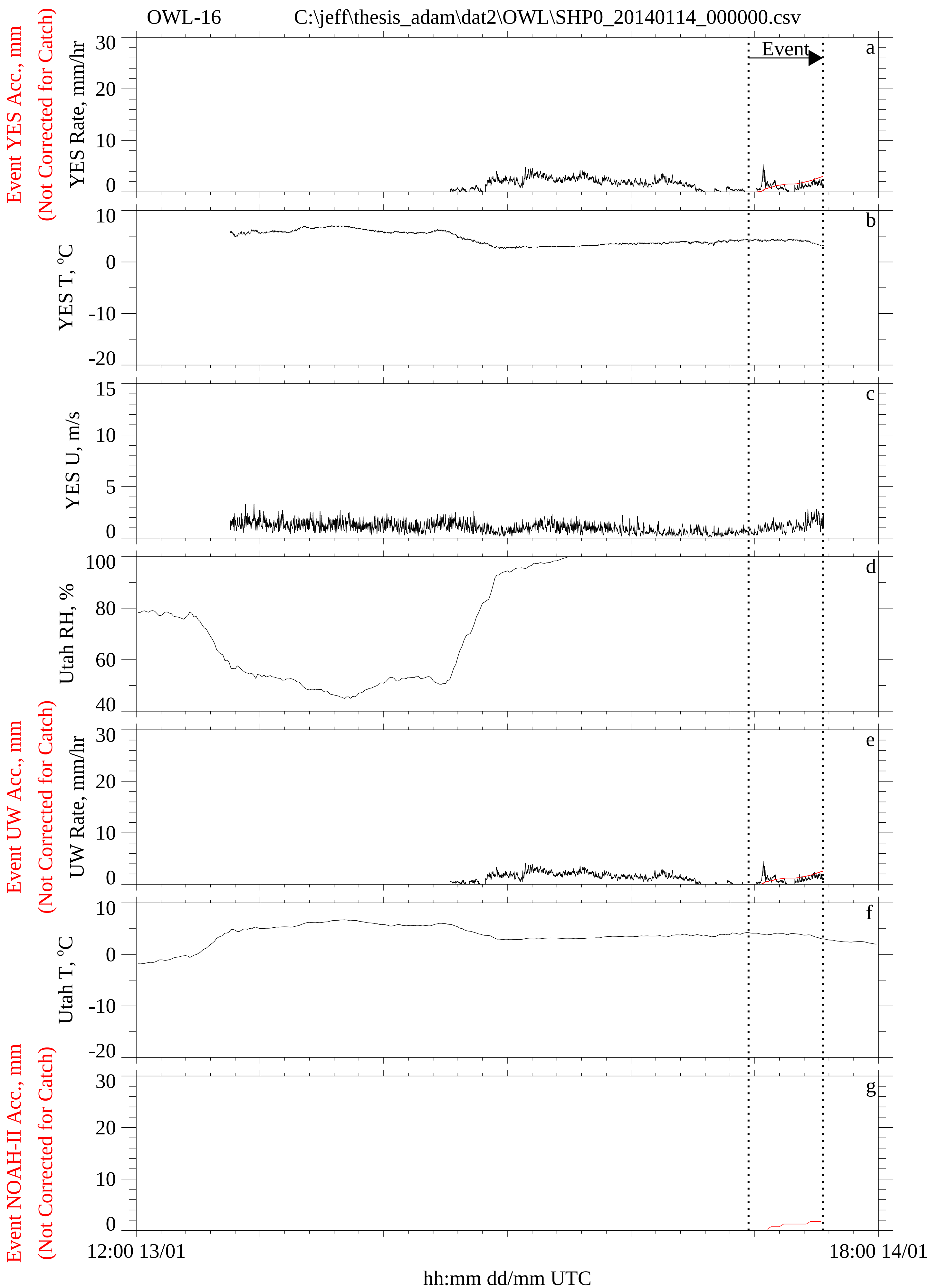

OWL-16
C:\jeff\thesis_adam\dat2\OWL\SHP0_20140114_000000.csv
Event
Event YES Acc., mm
(Not Corrected for Catch)
YES Rate, mm/hr
YES T, °C
YES U, m/s
Utah RH, %
Event UW Acc., mm
(Not Corrected for Catch)
UW Rate, mm/hr
Utah T, °C
Event NOAH-II Acc., mm
(Not Corrected for Catch)
a
b
c
d
e
f
g
12:00 13/01
18:00 14/01
hh:mm dd/mm UTC

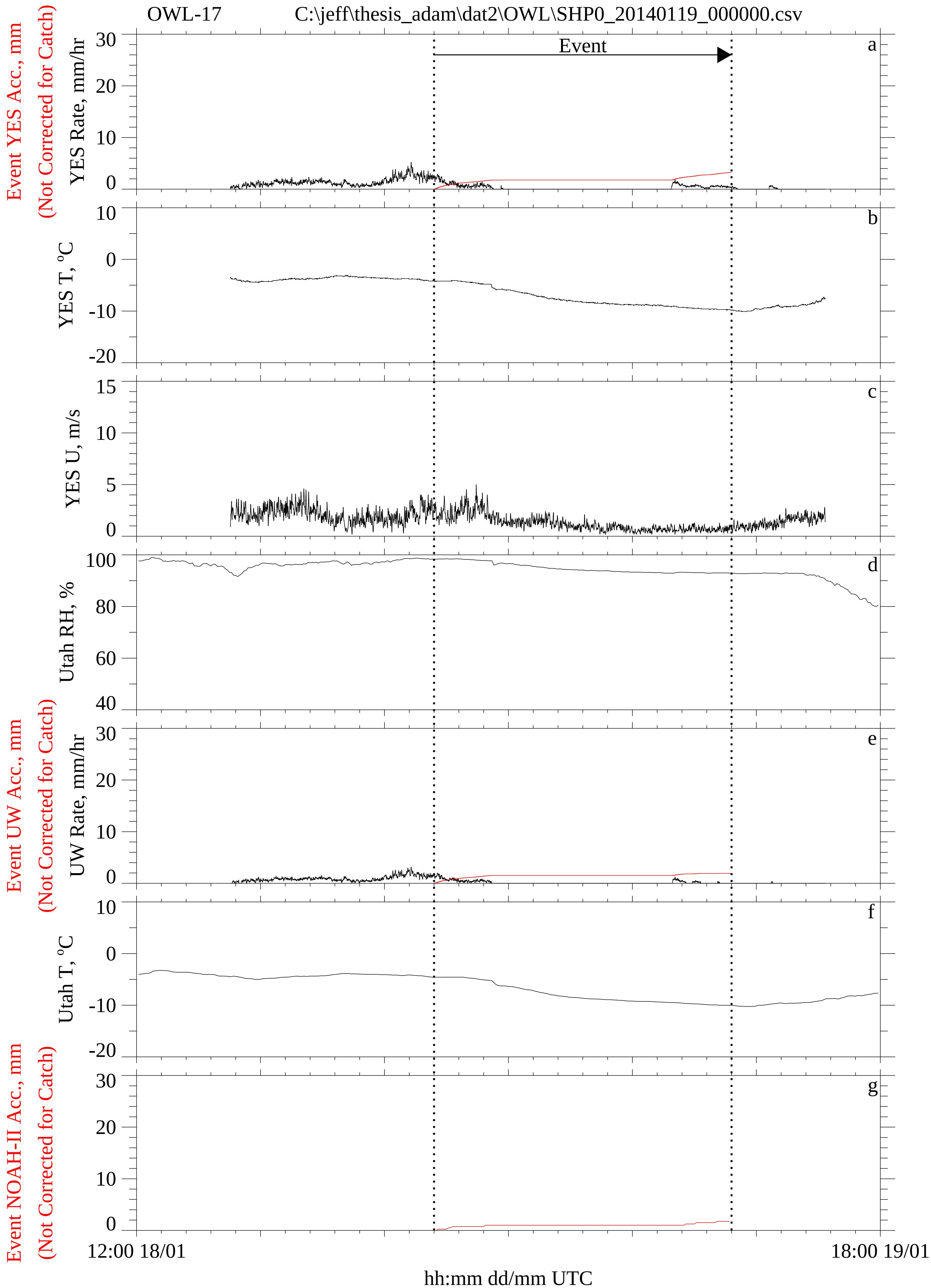

OWL-17
C:\jeff\thesis_adam\dat2\OWL\SHP0_20140119_000000.csv
Event
a
b
c
d
e
f
g
Event YES Acc., mm (Not Corrected for Catch)
YES Rate, mm/hr
YES T, °C
YES U, m/s
Utah RH, %
Event UW Acc., mm (Not Corrected for Catch)
UW Rate, mm/hr
Utah T, °C
Event NOAH-II Acc., mm (Not Corrected for Catch)
12:00 18/01
18:00 19/01
hh:mm dd/mm UTC

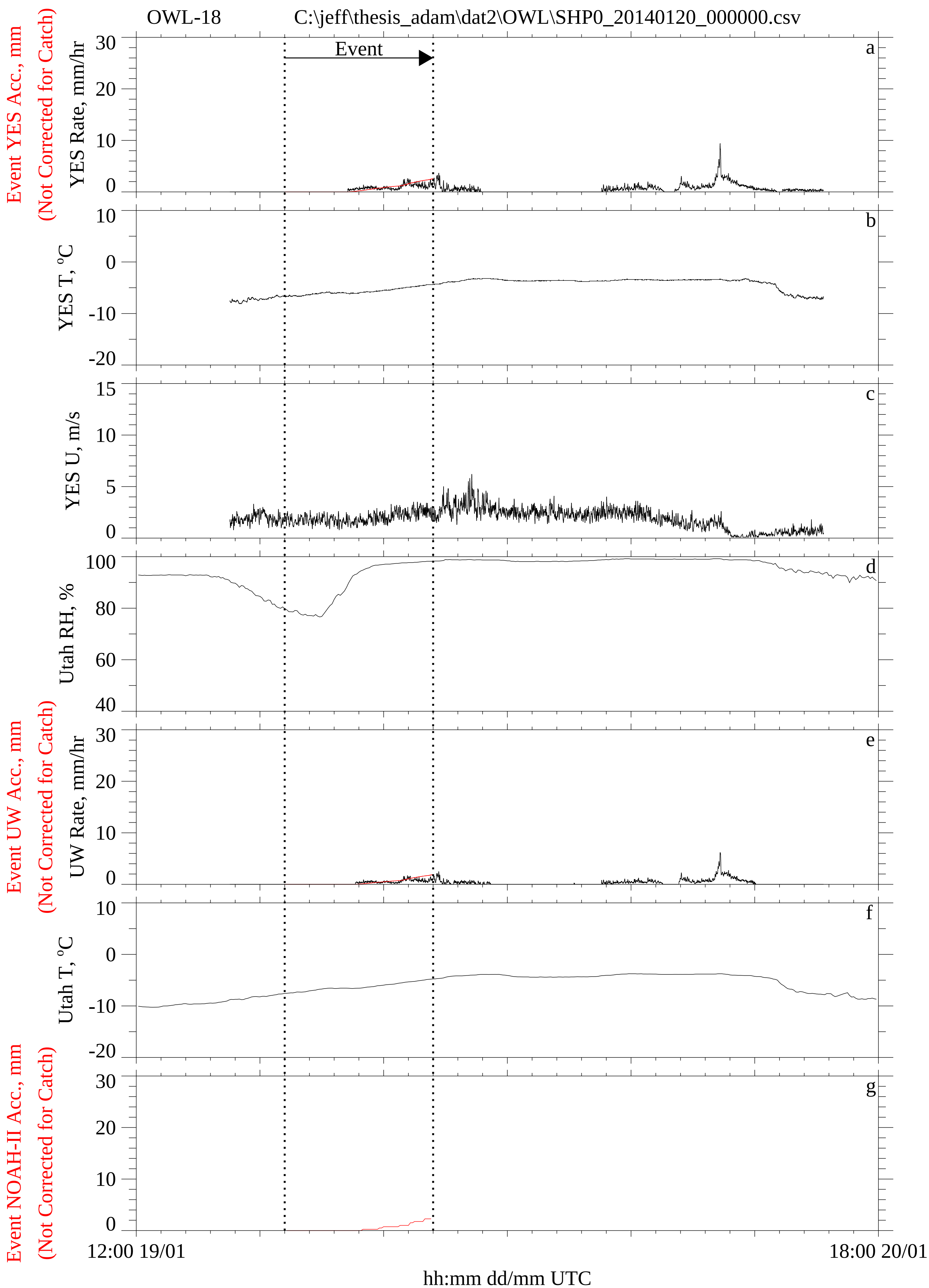

OWL-18
C:\jeff\thesis_adam\dat2\OWL\SHP0_20140120_000000.csv
Event
a
b
c
d
e
f
g
Event YES Acc., mm (Not Corrected for Catch)
YES Rate, mm/hr
YES T, °C
YES U, m/s
Utah RH, %
Event UW Acc., mm (Not Corrected for Catch)
UW Rate, mm/hr
Utah T, °C
Event NOAH-II Acc., mm (Not Corrected for Catch)
12:00 19/01
18:00 20/01
hh:mm dd/mm UTC

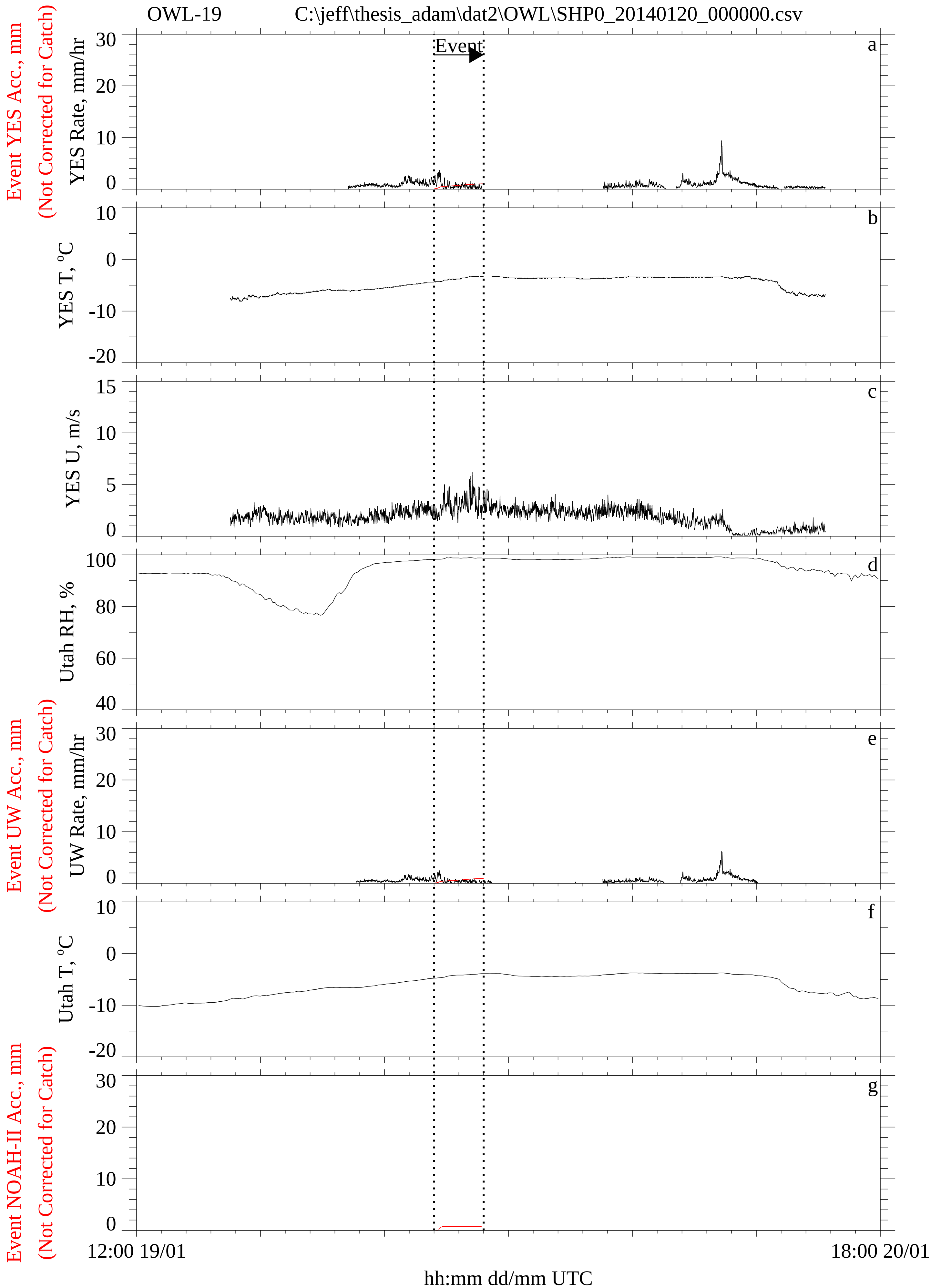
OWL-19
C:\jeff\thesis_adam\dat2\OWL\SHP0_20140120_000000.csv
Event
Event YES Acc., mm
(Not Corrected for Catch)
YES Rate, mm/hr
a
YES T, °C
b
YES U, m/s
c
Utah RH, %
d
Event UW Acc., mm
(Not Corrected for Catch)
UW Rate, mm/hr
e
Utah T, °C
f
Event NOAH-II Acc., mm
(Not Corrected for Catch)
g
12:00 19/01
18:00 20/01
hh:mm dd/mm UTC

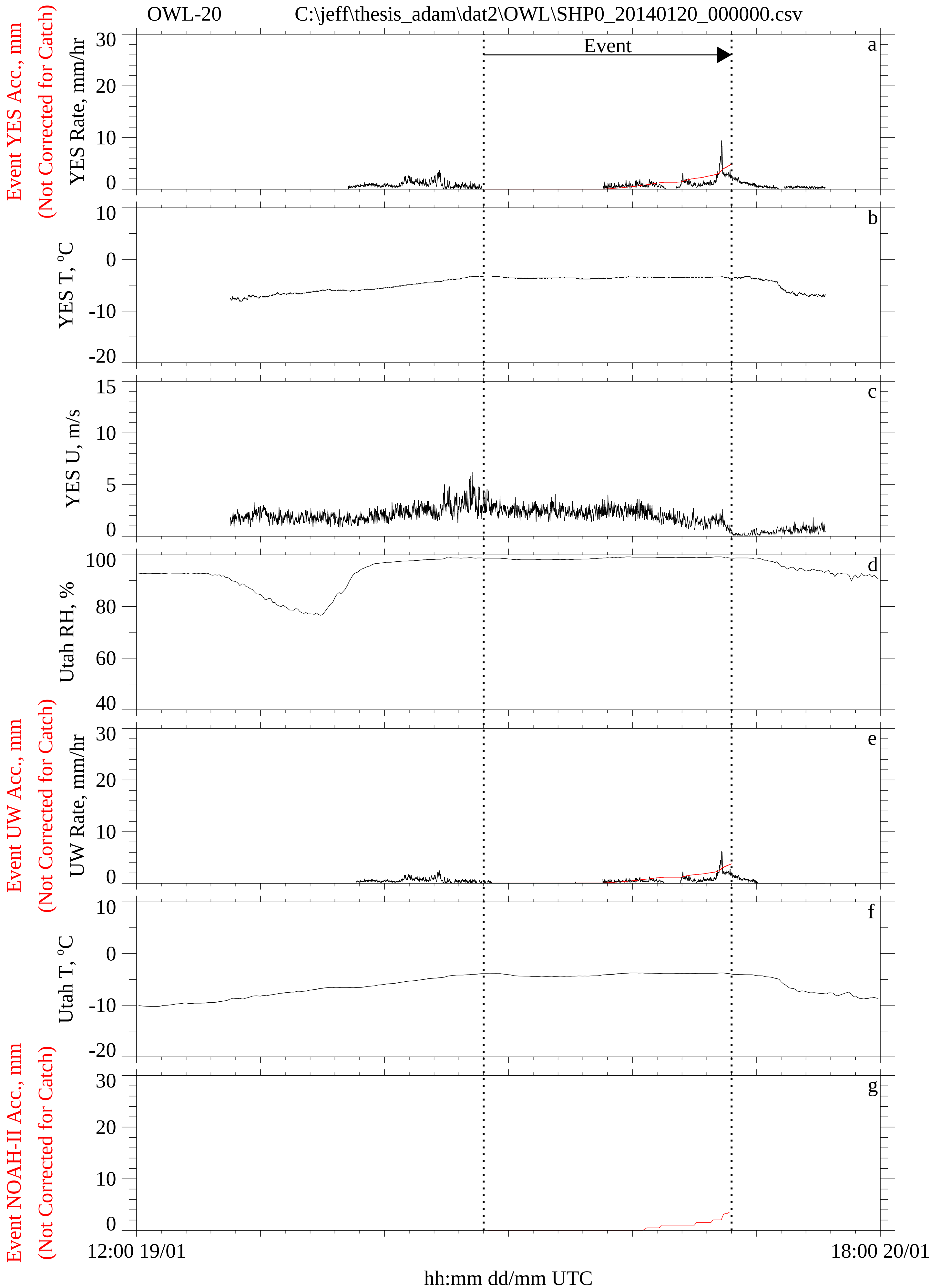

OWL-20
C:\jeff\thesis_adam\dat2\OWL\SHP0_20140120_000000.csv
Event
a
b
c
d
e
f
g
Event YES Acc., mm
(Not Corrected for Catch)
YES Rate, mm/hr
YES T, °C
YES U, m/s
Utah RH, %
Event UW Acc., mm
(Not Corrected for Catch)
UW Rate, mm/hr
Utah T, °C
Event NOAH-II Acc., mm
(Not Corrected for Catch)
12:00 19/01
18:00 20/01
hh:mm dd/mm UTC

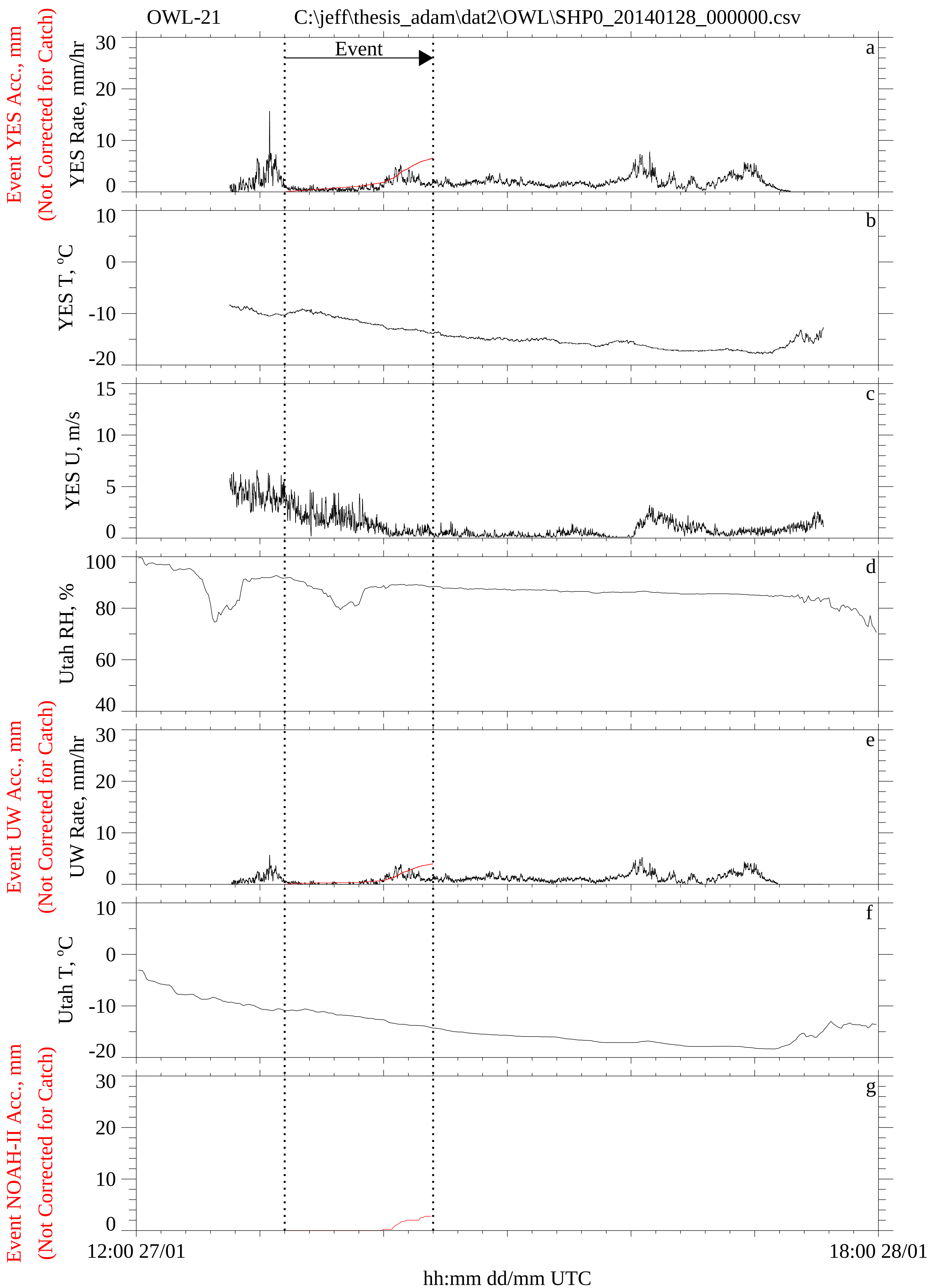

OWL-21
C:\jeff\thesis_adam\dat2\OWL\SHP0_20140128_000000.csv
Event
Event YES Acc., mm
(Not Corrected for Catch)
YES Rate, mm/hr
YES T, °C
YES U, m/s
Utah RH, %
Event UW Acc., mm
(Not Corrected for Catch)
UW Rate, mm/hr
Utah T, °C
Event NOAH-II Acc., mm
(Not Corrected for Catch)
a
b
c
d
e
f
g
12:00 27/01
18:00 28/01
hh:mm dd/mm UTC

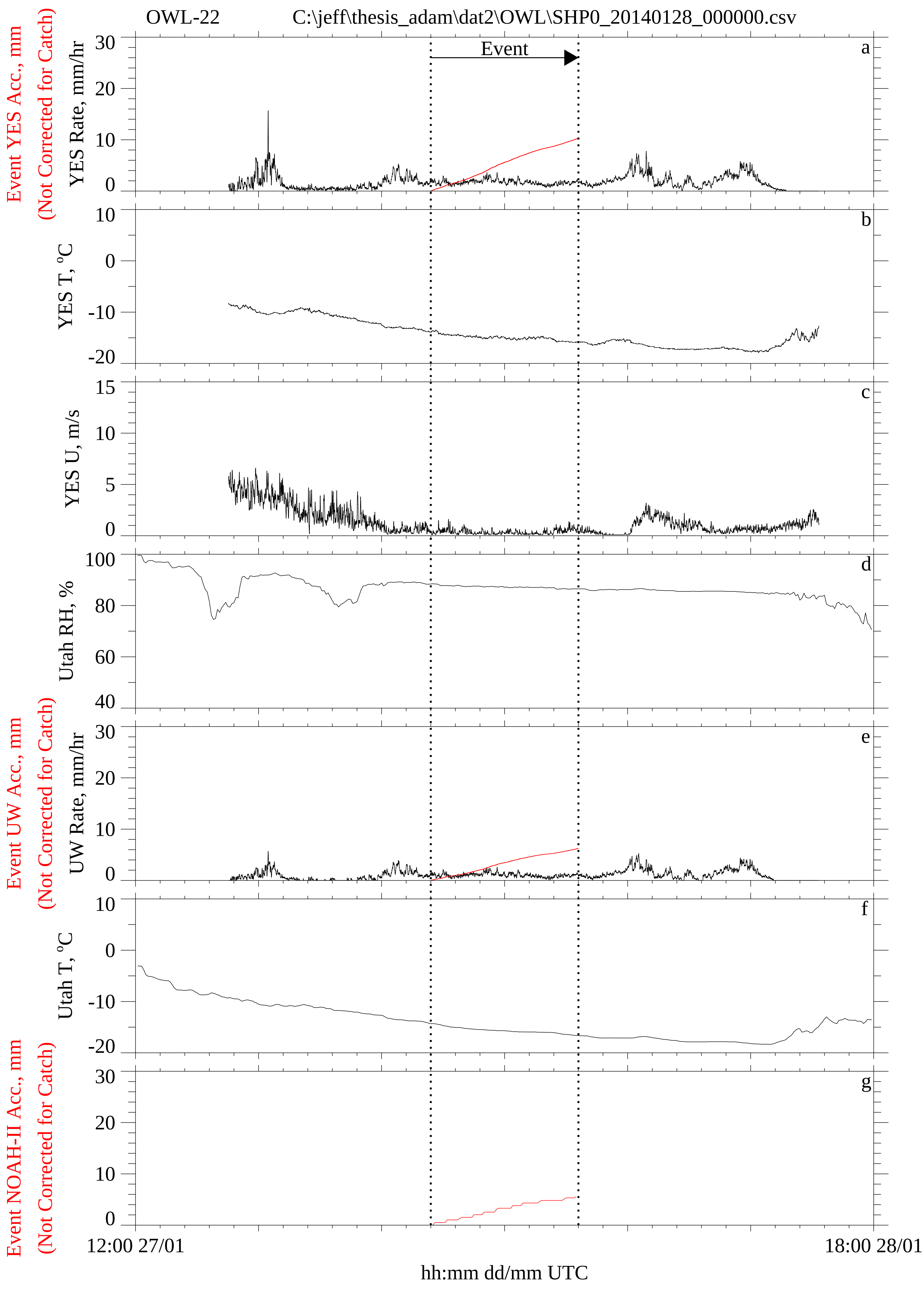

OWL-22
C:\jeff\thesis_adam\dat2\OWL\SHP0_20140128_000000.csv
Event
Event YES Acc., mm (Not Corrected for Catch)
YES Rate, mm/hr
YES T, °C
YES U, m/s
Utah RH, %
Event UW Acc., mm (Not Corrected for Catch)
UW Rate, mm/hr
Utah T, °C
Event NOAH-II Acc., mm (Not Corrected for Catch)
a
b
c
d
e
f
g
12:00 27/01
18:00 28/01
hh:mm dd/mm UTC

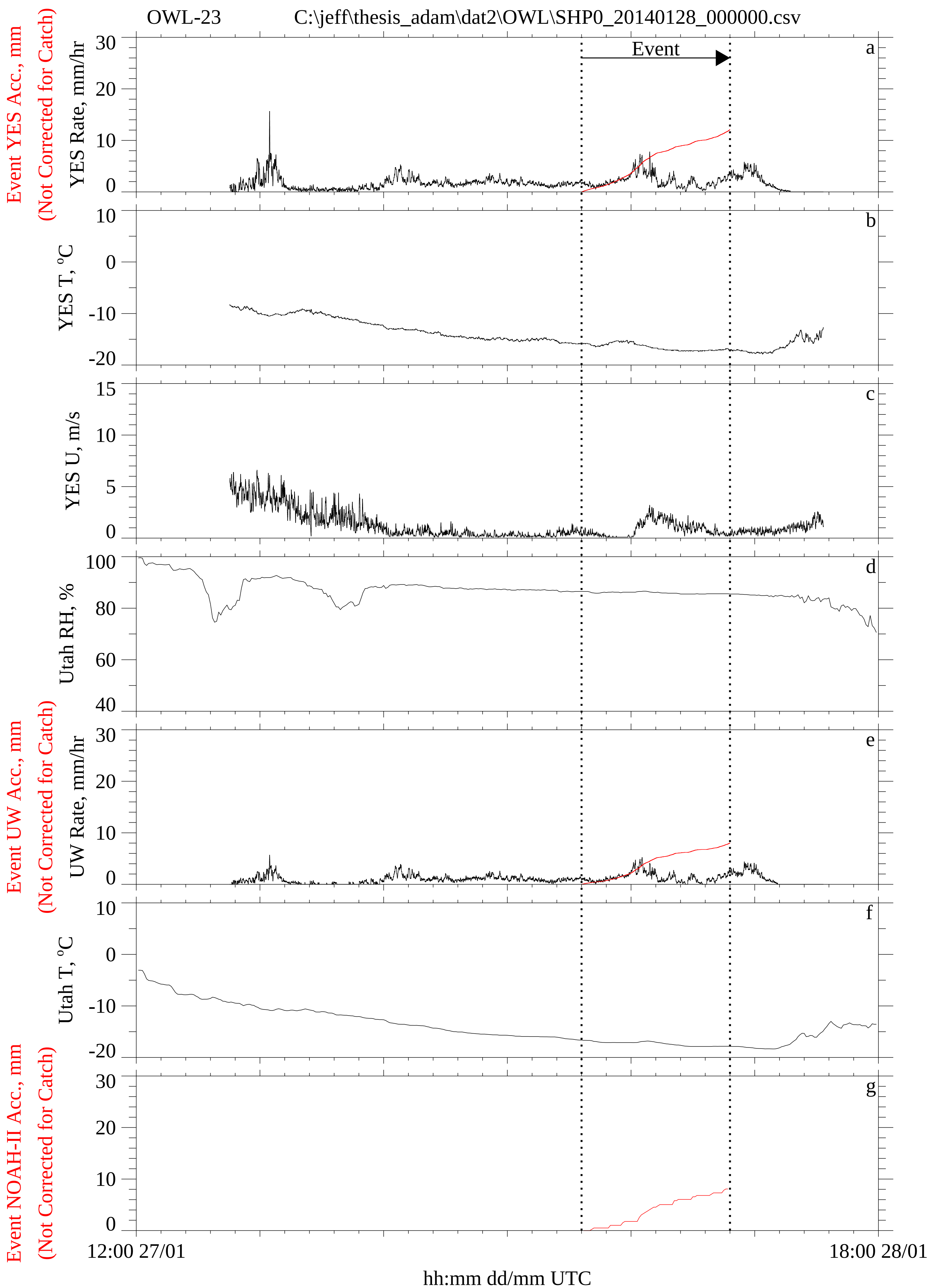

OWL-23
C:\jeff\thesis_adam\dat2\OWL\SHP0_20140128_000000.csv
Event
a
b
c
d
e
f
g
Event YES Acc., mm (Not Corrected for Catch)
YES Rate, mm/hr
YES T, °C
YES U, m/s
Utah RH, %
Event UW Acc., mm (Not Corrected for Catch)
UW Rate, mm/hr
Utah T, °C
Event NOAH-II Acc., mm (Not Corrected for Catch)
12:00 27/01
18:00 28/01
hh:mm dd/mm UTC

Hotplate Precipitation Gauge Calibrations and Field Measurements

Nicholas Zelasko [1], Adam Wettlaufer [1], Bujidmaa Borkhuu [1], Matthew Burkhart [1], Leah S. Campbell [2], W. James Steenburgh [2], and Jefferson R. Snider [1, 3]

[1] University of Wyoming Department of Atmospheric Science

[2] University of Utah Department of Atmospheric Sciences

[3] Corresponding Author

Abstract –

First introduced in 2003, approximately 70 Yankee Environmental Systems (YES) hotplate precipitation gauges have been purchased by researchers and operational meteorologists. A version of the YES hotplate is described in Rasmussen et al. (2011; R11). Presented here is indoor- and field-based testing of a newer version of the hotplate; this device is equipped with longwave and shortwave radiation sensors. Hotplate surface temperature, coefficients describing natural and forced convective sensible energy transfer, and radiative properties (longwave emissivity and shortwave reflectance) are reported for two of the new-version YES hotplates. These parameters are applied in a new algorithm, are used to derive liquid-equivalent accumulations (snowfall and rainfall), and these accumulations are compared to values derived by the internal algorithm used in the YES hotplates (hotplate-derived accumulations). In contrast with R11, the new algorithm accounts for radiative terms in a hotplate's energy budget, applies an energy conversion factor which does not differ from a theoretical energy conversion factor, and applies a surface area that is correct for the YES hotplate. Radiative effects are shown to be relatively unimportant for the precipitation events analyzed. In addition, this work documents a 10 % difference between the hotplate-derived and new-algorithm-derived accumulations. This difference seems consistent with R11's application of a hotplate surface area that deviates from the actual surface area of the YES hotplate, and with R11's recommendation for an energy conversion factor that differs from that calculated using thermodynamic theory.

1 - Introduction

Two types of instrumentation are available ~~have been developed~~ for making point measurements of ~~measuring~~ liquid-equivalent snowfall rates and liquid-equivalent snow accumulations: ~~1) Weighing gauges that measure snowfall as it collects in a container or on a surface (WMO, 2008),~~ 1) Weighing gauges and related devices that measure snowfall as it collects in a container or on a surface (Brock and Richardson, 2001; Chapter 9), and 2) optical gauges that measure the concentration and size of snow particles either in free fall or within a wind tunnel (Loffler-Mang and Joss, 2000; Deshler, 1988). Many of these gauges obstruct the wind and thus cause falling snow particles to deflect from the measurement zone. Consequently, rates and accumulations are underestimated and should be adjusted to account for undercatch (Jevons, 1861; Lovblad et al., 1993). Alternatively, both gauge types can be operated within a fenced enclosure that minimizes wind and the resultant undercatch (Goodison et al., 1998; Rasmussen et al., 2012). In addition, optical gauges require a snow particle density to convert concentration and size to a liquid-equivalent rate and accumulation (Brandes et al., 2007; Lempio et al., 2007). Because this density is variable and difficult to measure accurately (Locatelli and Hobbs, 1974), optical snowfall measurements are uncertain and remain uncertain even if undercatch is accounted for. A further disadvantage, for both the weighing and optical devices, is that the entrance to the device can become clogged with snow (Warnick, 1954; Currie, 1998; Stickel et al., 2005).

The Yankee Environmental Systems (YES, 2011) hotplate was developed to minimize the aforementioned uncertainties. Advantages of the hotplate are: 1) it is compact, 2) it is immune to clogging, 3) there is no requirement that snow particles fall through an opening, and 4) the derived rates and accumulations are largely independent of snow particle density, although a dependence does exist (R11; their figure 14). In some applications, a disadvantage of the hotplate relative to a weighing gauge, is the hotplate's electrical power consumption. This is ~ 200 W in Wyoming during winter.

This work furthers efforts to advance the hotplate as a snowfall measurement system (Borkhuu, 2009; R11; Boudala et al., 2014). We develop calibration constants for two hotplate systems configured with longwave and shortwave radiation sensors. These are a hotplate gauge owned by the University of Wyoming (UW) and ~~a hotplate gauge owned~~ by the National Center for Atmospheric Research (NCAR; Boulder, CO)~~.~~[1]. In addition, we develop a new hotplate data processing algorithm, derive liquid-equivalent rates and accumulations for 27 precipitation events (snowfall and rainfall), compare accumulations obtained with the new algorithm to those derived by an internal algorithm (hotplate-derived accumulations), and compare accumulations to values derived using weighing gauges.

2 - Algorithm Development

The two ~~vertically~~ stacked circular aluminum plates seen in Fig. 1 are the precipitation measurement portion of the YES hotplate system. The plate diameter (D_h) is 0.130 m and both plates have concentric rings that extend vertically either 3 mm (inner and middle rings) or 1 mm (outer ring) from the plate surface. One of the plates faces upward and is exposed to precipitation, the other faces downward. Temperature sensors monitor the top and bottom plates and feedback-controlled heaters maintain the plates at approximately 75 °C (R11). ~~Electrical power supplied to the top plate (Q_{top}) compensates for power lost via sensible, net radiative, and latent (vapor mass) transfer.~~ Electrical power supplied to the top plate (Q_{top}) compensates for

Formatted: Font: Italic

Formatted: Font: Italic, Subscript

[1] When a distinction is needed, we indicate the hotplate, followed by a forward slash, and the location of the deployment. For example, the UW hotplate, deployed at the OWL site, is designated UW/OWL.

power lost via sensible energy, radiative, and vapor mass transfer. Henceforth, we refer to the latter process as latent power output. ~~The power input to the bottom plate (Q_{bot}) is the source term in that plate's energy budget and is assumed to only compensate for sensible power output. This compensation is the basis for the hotplate's determination of wind speed (U). Values of U are commonly used to evaluate a Reynolds number (Re). The Reynolds number controls sensible heat transfer from a ventilated surface (Kobus and Wedekind, 1995). A complete description of our nomenclature is provided in the Appendix.~~The hotplate-derived wind speed, evaluated using the "factory calibration" discussed in R11, is used in this analysis. The bottom plate power (Q_{bot}) is likely a measurement used in the calculation of that wind speed, but this is speculative because the factory wind speed algorithm is proprietary. We symbolize this wind speed as U and use it to evaluate a Reynolds number (Re), and use the latter to parameterize sensible energy transfer from the ventilated surface of the top plate. R11 also derived wind speeds by fitting Q_{bot}, ambient temperature, and a wind speed measured at 10 m above ground level (AGL). This wind speed is not used in this analysis. The hotplate ambient temperature (T) measurement comes from the sensor seen below the radiation instruments (Fig. 1), the relative humidity (RH) measurement comes from a sensor that protrudes below the electronics box (Fig. 1), and the hotplate pressure sensor is contained within the electronics box. A complete description of our nomenclature is provided in the Appendix.

Formatted: Font: Italic

Formatted: Font: Italic, Subscript

Formatted: Font: Italic

Formatted: Font: Italic

Formatted: Font: Italic

Formatted: Font: Italic, Subscript

Formatted: Font: Italic

Formatted: Font: Italic

Formatted: Indent: First line: 0.5", Line spacing: Double

Since the hotplate was introduced in 2003, two teams (Borkhuu, 2009; R11) have reported data processing algorithms. The algorithm in Borkhuu (2009) can be explained by reference to the equation she used to model the top plate’s power budget:

$0 =$	Implied Steady-state	
Q_{top}	Electrical Power Supplied to Top Plate	
$- D_h \cdot K_x \cdot (T_h - T) \cdot (\gamma + \alpha \cdot Re^{\beta})$	Sensible Power Output	
$- P \cdot E / f_2$	Latent Power Output	(1)

In Eq. 1, there are three terms that sum to zero in an assumed steady-state. The last of these, the latent power output, is proportional to the precipitation rate (P) and a snow particle catch efficiency (E) and inversely proportional to f_2, an electrical-to-precipitation conversion factor. Also i~~I~~n Eq. 1~~addition~~, the sensible power output ~~term~~ has contributions from natural convection (proportional to -γ) and forced convection (proportional to $\alpha \cdot Re^{\beta}$), where α, β, and γ are fitted constants. These convective regimes are discussed in Kobus and Wedekind (1995) and are shown graphically in their Figure 6. Eq. 1 is similar to the algorithm used by King et al. (1978) to derive cloud liquid water concentration using a heated airborne sensor.

The algorithm in R11 is based on Eq. 2.

$$P = [Q_{top} - Q_{bot} - f_1(U)] \cdot f_2 / E \qquad (2)$$

Here, $f_1(U)$ is a wind speed-dependent function. Also in Eq. 2, we see the conversion factor introduced in the previous paragraph. Somewhat different from how R11 formulated their conversion factors for rain and snow, we formulate f_2 to account for the warming of ice, melting, warming of the liquid, and liquid evaporation. For rain, we formulate f_2 to account for the warming of liquid and its evaporation. With an exception that we justify later, we applied the conversion factors ~~as~~ recommended by R11: 1) if $T < 0\ ^{o}C$, the snow f_2 is applied, and 2) if $T > 4\ ^{o}C$ the rain f_2 is applied.

In Eq. 1, the sensible power output ~~term~~ is a function of Re, and thus U, and also a function of T. Hence, Eq. 1 can be rearranged to look similar to Eq. 2 with P dependent on T, U, Q_{top}, f_2, and E. A difference between the Eq. 1 and Eq. 2 formulations is the explicit dependence on Q_{bot}, in Eq. 2; this is in addition to the implicit Q_{bot}-dependent wind speed in Re (Eq. 1) and in $f_1(U)$ (Eq. 2).

Borkhuu (2009), YES (2011), and R11 surmised that the energetic effect of longwave and shortwave radiation could, in some settings, be comparable to the latent power output~~term~~. ~~Consequently, our hotplate (Wolfe and Snider, 2012) was upgraded by YES in 2011.~~ Consequently, our hotplate (Wolfe and Snider, 2012) was upgraded to firmware version 3.1.2 in 2011. The upgrade included radiation sensors for the measurement of downwelling longwave and shortwave fluxes. An objective of this paper is the incorporation of the radiation measurements into a new precipitation rate algorithm.

We used the following equation to analyze the top plate's power budget:~~The following budget equation is the basis for our analysis:~~

$0 =$	Implied Steady-state	
Q_{top}	Electrical Power Supplied to Top Plate	
$- D_h \cdot K_x \cdot (T_h - T) \cdot (\gamma + \alpha \cdot Re^{\beta})$	Sensible Power Output	
$- A_h \cdot \varepsilon_h \cdot \sigma \cdot T_h^4$	Longwave Power Output	
$+ A_h \cdot \varepsilon_h \cdot IR_d$	Longwave Power Input	
$+ A_h \cdot (1 - R_h) \cdot SW$	Shortwave Power Input	
$- P \cdot E / f_2$	Latent Power Output	(3)

Compared to Eq. 1, Eq. 3 has three additional terms. These describe the interaction of the top plate ~~hotplate~~ with its environment via radiative transfer. Two of these terms are inputs (longwave and shortwave) and one is an output (longwave).

~~**2.1 - Hotplate Data Files**~~

~~The hotplate outputs data to two files. The previously discussed~~ $\sout{Q_{top}}$ ~~and~~ $\sout{Q_{bot}}$ ~~are two of several recorded variables and both of these are essential for the analysis described here. One of the files is known as the UHP or "user" hotplate file. The UHP file is provided to all YES customers. The second file is the SHP or "sensor" file. Table 1 has the list of all recorded variables and how some of these are symbolized. A complete list of variables (measured and computed), and constants, is provided in the Appendix. With the exception of Unix time, all variables in Table 1 are available as 60-s running averages, sampled at 1 Hz (YES, 2011).~~

2.1 - Hotplate Data Files

Formatted: j_title_2

The hotplate outputs data to two files. The previously discussed Q_{top} and Q_{bot} are two of several recorded variables and both of these are essential for the analysis described here. One of the files is known as the UHP or "user" hotplate file. The UHP file is provided to all YES customers. The second file is the SHP or "sensor" file. The SHP file is proprietary but we were granted access to it by NCAR. Table 1 has the list of all recorded variables and how some of these are symbolized. A complete list of variables (measured and computed), and constants, is provided in the Appendix. With the exception of Unix time, all variables in Table 1 are provided as 60-s averages, sampled at 1 Hz (YES, 2011).

2.2 - Radiative Properties

Two radiative properties are applied ~~in this analysis~~in our analysis of the top plate's power budget (Eq. 3). In the infrared, or longwave, the emissivity of the top plate~~hotplate~~ is the key~~relevant~~ property. The material used to fabricate the plates is aluminum, which when exposed to air becomes covered with an aluminum oxide layer. Hence, the hotplate emissivity was taken to be that of oxidized aluminum (~~m. The value we picked is~~ $\varepsilon_h = 0.14$; ~~(~~Weast, 1975; Section E). Furthermore, we made two assumptions: 1) the longwave output (Eq. 3) is the product of ε_h ~~(assumed constant)~~, hotplate area (A_h), and the flux emitted by a black body at T_h, and 2) the longwave input (Eq. 3) is the product ε_h, A_h and the downwelling longwave flux (IR_d). In a later section, we explain how we derive IR_d.

In the visible, or shortwave, the top plate~~hotplate~~'s reflectance (R_h) is the key ~~relevant~~ property. Eq. 3 shows how we factored into ~~a hotplate's~~ the power ~~energy~~ budget the top plate's reflectance, a measured downwelling shortwave flux (SW; Table 1), and A_h. A value for R_h was determined as follows. We exposed the UW hotplate to solar illumination, while measuring the solar flux, and then shaded the hotplate to establish a baseline for the determination of R_h. During these experiments, there was negligible wind and therefore natural convection dominated forced convection in the budget. The ~~energy~~ budget equation we used to analyze these measurements has three terms: Q_{top}, sensible power output, and solar input. In two experiments, the values R_h = 0.66 and R_h = 0.61 were derived. We apply the average of these ($R_h = 0.63$) in our analysis of measurements from both UW and NCAR hotplates. Because of the oxide layer, the derived reflectance is smaller than the value reported for polished aluminum reflecting "incandescent" light (0.69; Weast, 1975; Section E) and significantly smaller than the value for vacuum-deposited aluminum at visible wavelengths (0.97; Hass, 1955).

3 - Methods

3.1 Temperature Measurements

Ice bulb temperatures at OWL were calculated using temperature, *RH*, and pressure measurements made within a fully shielded housing (Steenburgh et al., 2014). At GLE and BTL ice bulb temperatures were calculated using the hotplate-derived temperature, *RH*, and pressure values (Table 1). Because the hotplate temperature sensor is incompletely shielded (Fig. 1), there is concern that its measurement is positively biased by solar heating. We investigated this by differencing hotplate-derived temperatures, acquired during precipitation events at OWL, and values acquired by the fully shielded temperature sensor operated at OWL. On average, the hotplate values were larger (0.4 ± 0.4 ^{o}C). We did not attempt to correct for this bias.

Formatted: j_ind

Formatted: Font: Italic

Formatted: Font: Italic

Formatted: Superscript

3.2~~1~~ - Site Description

Indoor testing was conducted in a high-bay weather balloon hangar and in a laboratory. These facilities are at the University of Wyoming (UW) and are abbreviated hangar and lab. During wintertime, and especially at night, the hangar is cold (~ 0 ^{o}C); the lab is warm year round (~ 20 ^{o}C). Field measurements (Table 2) were conducted in Southeast Wyoming at the Glacier Lakes Ecosystem Experiments Site (GLE), in Southeast Wyoming near the summit of Battle Pass (BTL), and at the North Redfield site in Western New York (OWL). During both indoor and field measurements, all parameters reported by the hotplate (UHP and SHP variables; section 2.1) were recorded using a custom-built data system.

~~The accuracy of a hotplate-estimated precipitation rate is dependent on assessment of whether the sensed hydrometeors are rain or snow (R11 and Fig. 3a).~~ The accuracy of a hotplate-estimated precipitation rate depends on whether the sensed hydrometeors are rain or snow (R11). We infer the latter using a calculated ice-bulb temperature (T_{IB}) (Iribarne and Godson, 1981; Chapter 7). ~~Our basis for the T_{IB}s are measurements of relative humidity (RH; 100 % when saturated with respect to liquid), temperature, and pressure (Table 1).~~ Measurements used to derive the T_{IB}s are described in section 3.1. The lower limits on these derived values~~on the T_{IB}s~~, assuming the measured *RH* is overestimated by 5 % (YES, 2011), is no more than 0.4 °C colder than the values we report. In instances with ~~lower-limit~~ T_{IB}s larger than 0 °C, we assume the sensed hydrometeors were liquid.

3.3~~2~~ - NOAH-II Gauge

The NOAH-II is a weighing-type gauge manufactured by ETI Instrument Systems Inc. (www.etisensors.com). NCAR operated a NOAH-II at GLE and BTL during 2012, and coauthors (Campbell and Steenburgh) operated a NOAH-II at OWL (Dec. 2013 through Jan. 2014; Campbell et al., 2016). The three NOAH-II gauges were outfitted with Alter shields (Goodison et al., 1998; hereafter G98).

3.4~~3~~ – Indoor Testing

Indoor testing of the UW hotplate was conducted every year from 2011 to 2015; the NCAR hotplate was only tested in 2012. Based on our testing of the UW hotplate, we have no evidence indicating that the calibration changed over the duration of any of the field deployments; however, ~~Wettlaufer (2013) does demonstrate that calibration constants did change over the 2011 to 2015 interval in response to servicing conducted twice at YES.~~ Wettlaufer (2013) demonstrates that calibration constants did change over the 2011 to 2015 interval, and

Formatted: Font: Italic

likely in response to servicing conducted twice at YES. In this paper we present ~~and apply~~ calibration constants appropriate for the UW hotplate sensor deployed at GLE (April 2012) and at OWL (December 2013 through January 2014).

During testing, we controlled the hotplate's radiation environment by placing a material with known emissivity (painted-steel sheeting, $\varepsilon_s = 0.84$) above and below the hotplate. The steel sheets were positioned to dominate the hotplate's upward and downward fields of view (Fig. 2); however, the sheets were positioned ~~vertically~~ so that they were not heated by the hotplate. In that case, the sheet temperature (T_s) can be assumed equal to T.

3.5~~4~~ - Downwelling Longwave Flux

As we have already mentioned, previous work concluded that the hotplate method of determining precipitation ~~amount~~ can be affected by longwave radiation. ~~In response to that finding, YES incorporated a device that measures the net downward longwave flux (pyrgeometer, e.g., Albrecht et al., 1974) into the system (Table 1).~~ In response to that finding, newer versions of the hotplate have a device that measures longwave radiation (pyrgeometer, e.g., Albrecht et al., 1974) (Fig. 1 and Table 1).

$$M_{IR} = IR_d - IR_u \qquad (4)$$

The left-hand side of Eq. 4 represents the longwave~~ radiant~~ measurement (M_{IR}) and the right-hand side has the downwelling~~nward~~ and upwelling~~ward~~ components contributing to M_{IR}.

Because IR_d appears in the top ~~hot~~plate's power budget (Eq. 3), and since M_{IR} is the only term in Eq. 4 that is measured, the upwelling component (IR_u) must be evaluated. This is possible because the signal from the pyrgeometer is adjusted, within the hotplate electronics package, to make the source of the upwelling ~~infrared~~ flux a virtual blackbody at the ambient temperature (YES 2012, personal communication). In that case, IR_d can be formulated as

$$IR_d = M_{IR} + \sigma \cdot T^4 \qquad (5)$$

where σ is the Stefan-Boltzmann constant and T is the hotplate-measured ambient temperature. We also use Eq. 6 to calculate the downwelling longwave~~infrared~~ flux

$$IR_d = \varepsilon_s \cdot \sigma \cdot T_s^4 \qquad (6)$$

3.6~~5~~ – Warm-Cold Ambient Temperature Tests

Procedures described here were applied during testing conducted indoors (hangar and lab, section 3.2~~1~~) at two different temperatures and are hereafter referred to as the warm/cold test. We show how values of a warm (T_w) and cold (T_c) ambient temperature, combined with other recorded hotplate variables (Table 1), can be used to derive two calibration parameters~~settings~~ in Eq. 3 (T_h and γ). In our analysis, the temperature of the steel sheeting (T_s) was~~is~~ assumed equal to the ambient temperature (either T_w or T_c) and IR_d was~~is~~ calculated using~~with~~ Eq. 6. By design these tests had negligible forced-convective and latent energy transfers. In that case, Eq. 7a - b are the top plate budget equations.

$$0 = Q_{top,w} - D_h \cdot K_x \cdot (T_h - T_w) \cdot \gamma - A_h \cdot \varepsilon_h \cdot \sigma \cdot T_h^4 + A_h \cdot \varepsilon_h \cdot \varepsilon_s \cdot \sigma \cdot T_w^4 + A_h \cdot (1 - R_h) \cdot SW_w \qquad (7a)$$

$$0 = Q_{top,c} - D_h \cdot K_x \cdot (T_h - T_c) \cdot \gamma - A_h \cdot \varepsilon_h \cdot \sigma \cdot T_h^4 + A_h \cdot \varepsilon_h \cdot \varepsilon_s \cdot \sigma \cdot T_c^4 + A_h \cdot (1 - R_h) \cdot SW_c \qquad (7b)$$

The measurements applied in these equations were T_w and T_c, the warm and cold plate powers ($Q_{top,w}$ and $Q_{top,c}$), the warm and cold shortwave fluxes (SW_w and SW_c), and constants (Appendix). Values of T_h and γ (hereafter referred to as T_h/γ pairs) were derived by minimizing departures from zero simultaneously in Eq. 7a - b. Minimization was conducted using a Newton's method equation solver (Exelis Visual Information Solutions, Inc.); the convergence tolerance was $1\text{x}10^{-4}$ J s^{-1}.

3.7~~6~~ - Nusselt-Reynolds Relationship

The Nusselt number ($Nu = \gamma + \alpha \cdot Re^{\beta}$), is a component of the sensible power output term in Eq. 3. ~~In this section, we develop a relationship between *Nu* and *Re* based on measurements recorded in the field when precipitation was not occurring; in a later section we show how that relationship is applied in a calculation of the precipitation rate.~~In this section, we develop a relationship between *Nu* and *Re* based on measurements recorded in the field when precipitation was not occurring; in a later section we show how that relationship was applied in the new algorithm.

Formatted: Character scale: 105%

Conceptually, Nu is a dimensionless representation of the sensible power output. Eq. 8a was used to calculate Nu with measurements (Q_{top}, T, and SW), a calculated variable (IR_d; section 3.5~~4~~), and constants (Appendix and Table 3).

$$Nu = [Q_{top} - A_h \cdot \varepsilon_h \cdot \sigma \cdot T_h^4 + A_h \cdot \varepsilon_h \cdot IR_d + A_h \cdot (1 - R_h) \cdot SW] / [D_h \cdot K_x \cdot (T_h - T)] \qquad (8a)$$

In the numerator are the terms contributing to the sensible power output, and in the denominator ~~of Eq. 8a~~ is a term proportional to the sensible power ~~output~~ due to molecular conduction.

Conceptually, Re is a dimensionless representation of the wind speed. Eq. 8b was used to calculate Re with a measurement (U) and constants (Appendix).

$$Re = p_x \cdot D_h \cdot U / (R_d \cdot T_x \cdot \mu_x) \qquad (8b)$$

Two criteria were used to select a site-specific data subset for the Nu-Re development: 1) no precipitation, and 2) at least three hours of continuous measurements with a broad range of wind speeds. We fitted the selected Nu-Re pairs using a non-linear least squares procedure (curvefit; Exelis Visual Information Solutions, Inc.); the convergence tolerance for the relative decrease in chi-squared was 1×10^{-3}.

3.8~~7~~ - Electrical-to-precipitation Conversion Factor

Equilibrium thermodynamics, with the assumptions that ice melts at T_o = 0 °C and vaporization occurs at T_h, was used to derive the conversion factor in Eq. 3 (f_2). Adopting the temperature criteria from R11 (also see section 2), and a framework from Iribarne and Godson (1981; Chapter 7), we formulated the theoretical conversion factors as

$$f_2(T, T_h) = \{\rho \cdot A_h \cdot [\, C_i \cdot (T_o - T) + L_f(T_o) + C \cdot (T_h - T_o) + L_v(T_h)]\}^{-1} \quad (T < 0\ ^{o}\mathrm{C}) \qquad (9a)$$

$$f_2(T, T_h) = \{\rho \cdot A_h \cdot [\, C \cdot (T_h - T) + L_v(T_h)]\}^{-1} \quad (T > 4\ ^{o}\mathrm{C}) \qquad (9b)$$

This formulation is graphed in Fig. 3a (solid line) where we extended Eq. 9b into the temperature range (0 ºC < T < 4 ºC) where the distinction between rain and snow is ambiguous ~~because falling snow particles remain unmelted in situations with T > 0 ºC and low humidity~~ (R11).

We now compare the conversion factor derived using Eq. 9a – b with that reported in R11. To be consistent with R11, we assume $T = T_h = 0$ ºC. We find that the ratio of f_2 (Eq. 9a) divided by the factor reported in R11 for snow (3.99 x 10^{-8} m J^{-1}) and the ratio of f_2 (Eq. 9b) divided by the factor reported in R11 for rain (4.52 x 10^{-8} m J^{-1}), are both 0.666. Since these ratios are equal to the area in R11 (A_h = 0.008844 m^2), divided by the area applied in our calculation ($A_h = (\pi/4)\cdot 0.130^2 = 0.01327$ m^2), we conclude that the discrepancy is not due to differing thermodynamic parameters applied in R11's and our calculations (e.g., the latent heat of vaporization), rather it stems from the different values used for the hotplate area. Further, R11 changed their theoretical f_2 to an actual conversion factor that was "..lower because of the imperfect heat transfer from the precipitation to the hot plate (losses to the air, e.g.)." We do not find justification for this in R11, nor do we agree with R11's assignment of A_h = 0.008844 m^2 assuming they were recommending that value for the hotplate sold by YES. Recently, Boudala et al. (2014) addressed the second of these two points, making it clear that A_h = 0.01327 m^2 is appropriate for the hotplate sold by YES.

In light of the above, the ratio of our f_2 (Eq. 9a – b with $T = T_h = 0$ ºC), divided by the actual conversion factor in R11, is 0.86 for snow and 0.89 for rain. Since a derived precipitation rate is proportional to f_2 (e.g., Eq. 2), we expect the ratio of a precipitation rate from the new algorithm (assuming $T = T_h = 0$ ºC), divided by a synchronous hotplate-derived precipitation rate, to be between 0.86 and 0.89. Our expectation hinges on the assumption that the YES algorithm has incorporated R11's surface area and R11's distinction between theoretical and actual conversion factors.

We calculate f_2 in the new algorithm two ways: 1) In a comparison made to a hotplate-derived accumulation, our f_2 is set to 2.66×10^{-8} m J^{-1} (snow) and 3.01×10^{-8} m J^{-1} (rain). These values were obtained from Eq. 9a – b with $T = T_h = 0$ °C and are displayed as a dotted line in Fig. 3a. 2) In comparisons made to either a NOAH-II accumulation or to a laboratory reference precipitation rate, we evaluate f_2 using Eq. 9a – b with a T_h from Table 3 and with the hotplate-measured ambient T (Table 1). In addition to the step change due to the difference between the latent heats of sublimation and vaporization, our conversion factor has a weak temperature dependence (Fig. 3a, solid line). ~~This is accounting for the warming discussed in section 2.~~ This is due to the warming discussed in section 2. Also, in Fig. 3a we display the actual conversion factor from R11 (dashed line). Our classification of measurements into snow and rain is discussed in a later section.

3.9~~8~~ – Snow Particle Catch Efficiency

In this section, we evaluate a wind speed-dependent function and use it to account for the top plate's snow particle catch efficiency (*E*; section 2). The physical processes this function accounts for are, 1) snow particle bouncing subsequent to collision with the top plate, followed by transfer away from the top plate by wind, and 2) shearing off of a snow particle after it has landed on the top plate (R11). ~~The hotplate's snow particle catch efficiency (*E*; section 2) is accounted for using a wind speed-dependent function (R11). The function accounts for the fact that snow particles landing on the hotplate can bounce, and be carried away by the wind, or be sheared off by the wind after they land.~~ This conceptual description of catch on the hotplate is different from that used to describe catch by weighing gauges where undercatch results because a

Formatted: Font: Italic

subset of snow particles are carried over the gauge by a vertically-accelerated flow (Nespor and Servuk, 1999; Thériault et al., 2012). Both R11 and G98 derive catch efficiencies as the ratio of two paired values of liquid-equivalent accumulation, one obtained from the gauge of interest and the other obtained from a second gauge operated inside a Double Fence Intercomparison Reference Shield (DFIR).

The snow particle catch efficiency functions applied here are both gauge- and location-specific~~dependent~~. For the UW hotplate (at GLE and OWL), and the NCAR hotplate (at BTL), we apply the function recommended by YES (YES 2012, personal communication; hereafter Y12). Wind speeds used in the efficiency calculation are the hotplate-derived *U*. In addition, the hotplate catch efficiency function described by R11 (their Equation 6) was also applied. This was~~is~~ based on the hotplate *U* adjusted to the 10-m level with a roughness length z_o = 0.3 m (G98, their Equation 4.3.1) and was only used in analysis of measurements made at OWL. The z_o we picked corresponds to a surface with “Many trees, hedges, few buildings” (Panofsky and Dutton, 1984; their Table~~Figure~~ 6.2). This assignment is consistent with the presence of shrubs and trees (Steenburgh et al., 2014), and a two-story barn, at the OWL site. The barn was located at the eastern edge of a fallow field, 80 m west of the gauges at OWL. For the NOAH-II gauge, we applied a function developed for an 8-inch (diameter) Alter-shielded gauge (G98; their Equation 4.7.1). Wind speeds used in that calculation are from the hotplate (at GLE and BTL) or from an anemometer (at OWL) (Campbell et al., 2016). Of course, we are assuming that the function from G98 mimics undercatch by our 12-inch (diameter) Alter-shielded NOAH-II gauge.

In Fig. 3b, we present the three catch efficiency functions (R11 with U adjusted to 10 m, Y12, and G98). In this graph, the wind speed applied in the R11 function is the value plotted on the abscissa multiplied by 2.9. This adjustment corresponds to the lowest installation of the hotplate at OWL and decreases to 2.0 for measurements made after 20131217 [2]. In our calculation of the R11 catch efficiency functions, the snow depth for the interval of interest (20131211 to 20140129) was set equal to the average (0.7 m) derived using an ultrasonic snow depth instrument operated at OWL (Campbell et al., 2016). This average, and the AGL altitudes of the hotplate installation (Table 2), were used to derive the two wind-speed adjustment factors (2.9 and 2.0). The basis for this calculation is G98's gauge-height correction formula (their Equation 4.3.1).

Since the anemometer at OWL was operated at nearly the same height as the top of the NOAH-II gauge (Steenburgh et al., 2014), and the G98 catch efficiency formula (their Equation 4.7.1) assumes speeds are measured at the height of the gauge opening, a vertical adjustment of the wind speed was not factored into the G98 catch efficiencies.

[2] AGL a~~A~~ltitudes of the two hotplate installations are provided in Table 2.

4 – Testing and Calibration Results

4.1 – Warm-Cold Tests

Results from the warm-cold tests are described here. The derived T_h/γ pairs (section 3.6~~5~~) are in Table 3. The T_h values are 42.2 ^{o}C for the NCAR hotplate deployed at BTL (NCAR/BTL), 52.2 ^{o}C the UW hotplate deployed at (UW/GLE), and 65.5 ^{o}C for the UW gauge deployed at OWL (UW/OWL). The first two T_hs differ from those presented in Wettlaufer (2013) where, for the NCAR hotplate, he reported agreement with the nominal plate temperature (75 ^{o}C; R11) and for the UW hotplate (GLE) he reported a larger temperature (T_h = 109 ^{o}C). The T_h/γ pair reported in Table 3, for the UW/OWL study, was evaluated after Wettlaufer (2013) reported his warm-cold test results.

In our analysis of the warm-cold measurements we only used data acquired in the hangar. As we describe below, this may have improved the accuracy of the resultant T_h/γ pairs. This is because all data needed to derive a T_h/γ pair can be obtained without turning off the hotplate. Wettlaufer (2013) analyzed both hanger and lab data. Both in his work and in ours, the relevant hotplate properties were derived by averaging over a 5 minute warm interval and a 5 minute cold interval, and applying these averages in Eq. 7a – b. ~~In our analysis of the warm-cold measurements we only used data acquired in the hangar; Wettlaufer (2013) analyzed both hangar and lab data.~~ For us the warm-cold temperature pairings are 5.4/-4.3 °C (NCAR/BTL), 7.0/-1.1 °C (UW/GLE), and 29.5/10.4 °C (UW/OWL). Compared to Wettlaufer (2013), our T_ws are 15 °C colder (NCAR/BTL and UW/GLE~~OWL~~ experiments only). Using our T_h/γ pairs (Table 3) and the first two T_ws (i.e., for NCAR/BTL and UW/GLE), we evaluated the term in Eq. 7a representing natural-convective transfer ($D_h \cdot K_x \cdot (T_h - T_w) \cdot \gamma$) and compared to values derived using T_h/γ pairs in Wettlaufer (2013; his Table 2). In the NCAR/BTL comparison T_w was set at

5.4 °C and in the UW/GLE comparison T_w was set at 7.0 °C. Our natural-convective term agrees within ± 0.1 W of those derived by Wettlaufer (2013). Also in good agreement is the product of T_h and γ. Relative to Wettlaufer (2013), our $T_h \times \gamma$ product is 6 % larger (NCAR/BTL), and 7 % larger (UW/GLE). We expect that our T_h/γ pairs (Table 3), when applied in Eq. 3, will produce a reasonable estimate of the precipitation rate. We test that expectation in the next section.

Error limits on T_h and γ, in Table 3, were derived by perturbing $Q_{top,w}$ (i.e., the value acquired in the warm test) by ± 0.5 W and repeating the analysis (Eq. 7a - b). Our estimate of the $Q_{top,w}$ error (± 0.5 W) came from a comparison of values acquired before and after power to the hotplate was stopped and restarted. These tests were conducted in the hangar and the 10 min warm up recommended by the manufacturer was adhered to (YES, 2011).

4.2 - Drip Tests

This section compares two time sequences of precipitation rate: one calculated with the new algorithm, the other is the hotplate-derived value (Table 1). The basis for the comparison is measurements of artificially-produced liquid precipitation made in the hangar. We applied water drops to the NCAR and UW hotplates using a volumetric water pump (Ismatec Inc.; Model 7618). Each of these tests has a drip period (4 min) and a nondrip period (5 min). Drops (4 mm volume-equivalent diameter) were added uniformly to the top plate at a constant volumetric rate. ~~Assuming all of the pumped water is delivered to the hotplate, the pump rate is proportional to a precipitation rate. We see no reason to question this assumption. Hence, we~~ We convert the pump rate to a reference precipitation rate (P_{REF}) and apply the P_{REF} in subsequent analyses [3]. These drip tests were conducted at $T > 4$ °C.

[3] The value of the multiplier that converts the volumetric pump rate ($cm^3\ min^{-1}$) to precipitation rate ($mm\ hr^{-1}$) is 4.51.

Because the drip tests were conducted with the hotplate operating as in Fig. 2, and unventilated, the recorded data were analyzed with $T_s = T$, in Eq. 6 (section 3.5), and with the sensible power output formulated as $D_h \cdot K_x \cdot (T_h - T) \cdot \gamma$ (Appendix and Table 3). Also, because all of the pumped water is delivered to the top plate, the catch efficiency is $E = 1$. ~~With these constraints,~~ Hotplate precipitation rates were derived by inputting measurements (Q_{top}, T, U, and SW) and a calculated variable (IR_d; section 3.5~~4~~) into Eq. 3 and solving for a precipitation rate sequence ($P(t)$). We symbolize this $P(t)$ as P_{UW} and refer to calculations leading to that sequence as the UW algorithm. Also, we refer to sequences obtained from the UHP file (Table 1) as P_{YES} and refer to that calculation as the YES algorithm.

We now compare values of P_{UW} to synchronous values of P_{YES}. Typically, these rates exhibit a maximum ~ 3 min after the nondrip-to-drip transition (Fig. 4). We interpret these maxima as overestimates, possibly due to a violation of the steady-state assumption. Also evident, particularly in the P_{UW} sequence, is a minimum. This occurs during the time the instrument is relaxing to its rest state; i.e. ~ 2 min after a drip-to-nondrip transition. The figure also demonstrates that thresholding is applied to the P_{YES} sequence, i.e. the YES algorithm thresholds the output to 0 mm hr^{-1} if values decrease to < 0 mm hr^{-1}. This is evident at ~ 16:11 UTC and at three other times in the P_{YES} sequence. In fact, thresholding is not desired for the drip tests. Thus, the UW sequence is not thresholded in Fig. 4.

Two 1-min averaging intervals are shown in Fig. 4. ~~We set the end of these at the drip-to-nondrip transitions.~~ We set the end of these at the drip-to-nondrip transitions and symbolize the averages as <P_{UW}> and <P_{YES}>. Fig. 5 is a compilation of the two tests already discussed ~~(Fig. 4)~~ plus four additional P_{REF} vs <P_{UW}> comparisons and four additional P_{REF} vs <P_{YES}> comparisons.

Formatted: Font: Italic
Formatted: Font: Italic, Subscript
Formatted: Font: Italic
Formatted: Font: Italic, Subscript

We now use linear least-squares regression analysis, and a regression equation of form $y = a \cdot x$, to derive the ratio of two precipitation rates. In Fig. 5 it is apparent that the regression slope (ratio), derived for the P_{REF} vs $<P_{UW}>$ comparison, does not differ from one by more than ± 1 standard deviation. Ratios for the two hotplates (UW and NCAR) and for three drip tests are summarized in Table 4. In the third column (P_{REF} vs $<P_{UW}>$), we see that none of the ratios differ from one by more than ± 1 standard deviation. Different from Fig. 5 and Table 4, we also evaluated intercepts of regressions that were not forced through the origin; none of these intercepts differ significantly from zero (results not shown). From the statistical comparisons in Table 4, we conclude the T_h/γ pairs (Table 3) applied in the UW algorithm (Eq. 3) produce a precipitation rate consistent with the reference.

Values of the reference rate and the hotplate-derived rate ($<P_{YES}>$) are compared as ratios in Fig. 5 and in the fourth column of Table 4. These ratios are seen to deviate systematically from unity, and in the direction discussed in section 3.8~~7~~. In the unforced regressions (not shown) the intercepts are negative, but only one of these differed significantly from zero (NCAR/BTL; intercept = -0.3 ± 0.1). Negative intercepts are expected because P_{YES} is positively offset, by ~ 0.2 mm hr^{-1}, during most of the nondrip periods (e.g., 16:21 UTC in Fig. 4).

5 - Field Measurements

This section is organized as follows: Section 5.1 presents field measurements of ambient temperature and ambient ice-bulb temperature. We use this information to classify 27 precipitation events as snowfall or rainfall. Section 5.2 presents the *Nu*-*Re* relationship we use to account for the sensible power output ~~term~~ in Eq. 3. Section 5.3 describes how we derive a precipitation rate for a hotplate based on measurements made in the field. Section 5.4 compares time-integrated precipitation rates (accumulations) derived using the two algorithms. In section 5.4, we also compare hotplate accumulations to values from the NOAH-II.

5.1 – Field-measured Temperatures and Ice-bulb Temperatures

The 27 precipitation events are summarized in Table 5. Measurements were made during 2012, at the two Southeast Wyoming field sites (BTL and GLE), and during 2013 and 2014 at the Western New York site (OWL). Table 5 and Fig. 6 have event-averaged ambient temperatures (<*T*>) and ~~the~~ event-averaged ambient ice-bulb temperatures (<T_{IB}>~~; section 3.1~~). Twenty-three of the events have <*T*> ≤ -3.3 °C and upper-limit temperature (<*T*> plus two standard deviations) no warmer than -2.3 °C. We classified these as snowfall. In addition, we classified four events as rainfall. These had <T_{IB}> ≥ +2.9 °C and lower-limit temperature (<*T*> minus two standard deviations) no colder than +2 °C.

5.2 - Nusselt-Reynolds Relationship

Fig. 7b shows a plot of the *Nu*-*Re* fit function with the data used to constrain the function. ~~This result is for the UW hotplate operating at the GLE site.~~ This result is based on UW hotplate measurements (GLE site) and formulas developed in section 3.7. Fit coefficients (α, β, and γ) are reported in Table 6 for each field site. Hansen and Webb (1992) reported α = 0.09 and a β between 0.69 and 0.72 for a surface similar to the hotplate (circular with three concentric rings); however, their flow direction was perpendicular to the plate surface. The values of α and β we report may differ from those in Hansen and Webb (1992) because the flow is principally parallel to the plate surface at our field sites. There are two other differences relative to Hansen and Webb (1992): 1) Our geometrically-averaged *Nu* (~ 360) is about a factor of five larger, and 2) our~~-~~ *Re* extends over a much larger range.~~*Re* extends smaller by a factor of two and larger by a~~

Formatted: Font: Italic

~~factor of three.~~ Finally, we note that compared to Fig. 7b there is an order of magnitude narrower *Re* range in the NCAR/BTL and UW/OWL *Nu*-*Re* plots (not shown).

Formatted: Character scale: 105%

Fig. 7a is a companion to Fig. 7b showing the γ based on the warm-cold test. The error limit on this datum is explained in section 4.1. Since *Nu* is dependent on the T_h derived in the warm-cold test (section 3.6~~5~~), we expect the *Nu*-*Re* function to converge to the warm-cold γ in the limit of small *Re*. In our assessment of convergence, we evaluated the limiting *Nu* at the *Re* corresponding to the minimum *U* reported in the hotplate data output (0.1 m s^{-1}). This minimum *U* establishes the left end of the function in Fig. 7b. Convergence of the *Nu*-*Re* relationship to within the error limit on the warm-cold γ, at the former's left-most limit, is evident in Fig. 7a – b. Convergence is also evident in the NCAR/BTL and UW/OWL plots analogous to Fig. 7a – b (not shown) and this in spite of narrower *Re* range in those datasets.

5.3 - Precipitation Rate from Field Measurements

~~Fig. 8 shows energy-budget terms (Eq. 3) for one of the four rainfall events in our dataset (OWL-15 in Fig. 6). The three output terms (sensible, latent, and upwelling longwave), and three input terms (top plate power, downwelling longwave, and shortwave) are shown in Fig. 8a - b. In this section we begin with the sequence of latent power output (i.e., the sequence labeled~~ ~~$P \cdot E/f_2$~~ ~~in Fig. 8a) and describe how we calculate the sequence of rainfall rate.~~ Fig. 8 shows budget terms (Eq. 3) for one of the four rainfall events in our dataset (OWL-15). The three output terms (sensible, latent, and longwave), and three input terms (top plate, longwave, and shortwave) are shown in Fig. 8a - b. In this section we begin with the latent power output (i.e., $P \cdot E/f_2$ in Fig. 8a) and describe how we calculate the rainfall rate. We also contrast that calculation with steps followed in the case of snowfall.

Formatted: Font: Italic

Formatted: Font: Italic, Subscript

The first step in the calculation is conversion of the latent power output~~term~~ term (Fig. 8a) to a provisional precipitation rate; this is done by multiplying each element of the ~~latent~~ term by the corresponding element of f_2 (Eq. 9b). This operation is referred to as element-by-element vector multiplication. Thresholding is applied next. Both a 300-s running average of the provisional rate and a 10-s running average of the provisional rate are computed. If the 300-s average exceeds 0.25 mm hr^{-1}, and the 10-s average exceeds 0 mm hr^{-1}, the rate is stored as the 10-s average; otherwise the rate is stored as 0 mm hr^{-1}. We refer to the resultant as P_{UW}, but we note that in section 4.2 the P_{UW} sequences ~~were~~ are unthresholded. Both the thresholded and unthresholded sequences are presented in Fig. 8c – d. The thresholded P_{UW} is identical to the unthresholded P_{UW} where the 300-s average exceeds 0.25 mm hr^{-1} and the 10-s average exceeds 0 mm hr^{-1}.

In the case of snowfall, the f_2 is calculated using Eq. 9a and applied as discussed in the previous paragraph. Finally, the precipitation rate is derived as the resultant of element-by-element vector multiplication of the thresholded P_{UW} and the reciprocal of the snow particle catch efficiency (section 3.9~~8~~).

5.4 – Comparisons of Liquid-equivalent Accumulation

Here we use linear least-squares regression analysis, with a regression equation of form $y = a{\cdot}x$, to derive the ratio of two measures of liquid-equivalent accumulation for snow. In Fig. 9, these measures are the accumulations derived using the UW and YES algorithms. In the these algorithms the particle catch efficiency function is the one described in Y12 and f_2 is 2.66 × 10^{-8} m J^{-1} (~~(~~section 3.8~~7~~). The data points correspond to measurements made at GLE (UW hotplate), at BTL (NCAR hotplate), and at OWL (UW hotplate). We note that 19 of 23 y-axis values are from the same instrument (UW hotplate) and are derived using the same calibration (UW/OWL) used~~applied~~ to produce the result shown in the third row of Table 4. Statistical consistency between the ratio in Fig. 9 (0.79 ± 0.05) and the ratio in the third row of Table 4 (i.e., 0.79 ± 0.03 for the P_{REF} vs $<P_{YES}>$ ratio) suggest~~s~~ a systematic error in the YES-derived precipitation rates and accumulations. This assertion is reinforced by the three NCAR hotplate points straddling the best-fit line, in Fig. 9, and by the ratio reported in Table 4 for the NCAR hotplate (i.e., 0.81 ± 0.03 for the P_{REF} on $<P_{YES}>$ ratio). However, we cannot exclude the possibility that bias in our field-based calibration coefficients (α, β, and γ; Table 6) is the reason for a UW/YES ratio significantly smaller than unity in Fig. 9.

As was discussed in section 4.2, and demonstrated in Fig. 4, during the indoor nondrip periods the P_{YES} sequence is positively offset. A plausible reason for this, and for the ratios < 1 reported in the previous paragraph, is disregard for longwave forcing in the YES algorithm. ~~Since we do not have access to the YES algorithm, we estimated the longwave radiative effect by setting the downwelling and upwelling longwave terms to zero in Eq. 3. After doing this, a larger UW/YES ratio was obtained in a plot analogous to Fig. 9 (0.83 ± 0.04). From this modest increase of the UW/YES ratio, we conclude that offset due to longwave forcing *cannot* explain UW/YES ratios significantly smaller than unity. An even smaller-magnitude perturbation of the UW/YES ratios was obtained when zeroing the shortwave term in Eq. 3 (results not shown).~~Since we do not have access to the YES algorithm, we estimated the longwave radiative effect by setting the longwave terms to zero in Eq. 3. After doing this, a larger UW/YES ratio (a = 0.83 ± 0.04) was obtained in a plot analogous to Fig. 9. From this modest increase of the UW/YES ratio, we conclude that longwave forcing *cannot* explain the shift of the best-fit line away from unity in Fig. 9. An even smaller perturbation of the UW/YES ratio was obtained in calculations that set the shortwave term to zero in Eq. 3 (results not shown).

Formatted: Font: Italic

Further evidence for systematic error in the YES values comes from Fig. 10. With the exception that these data are for rain observed at OWL (section 5.1) the comparison in Fig. 10 is similar to Fig. 9. Although the number of points is small, Fig. 10 establishes that our finding of a UW/YES ratio significantly smaller than unity is true for both rainfall and snowfall. In addition, Fig. 11 strengthens this conclusion by showing agreement between values of the UW ~~algorithm~~ accumulation and the NOAH-II accumulation when both gauges detected~~are detecting~~ rain.

An additional assessment of snowfall at OWL is presented in Fig. 12a – c. In these graphs the NOAH-II measurements are plotted on the abscissa and different interpretations of the UW hotplate measurements are plotted on the ordinate. For both devices, we plot the ratio of a liquid-equivalent accumulation divided by an event-averaged ~~particle~~ catch efficiency, and we note that the numerator of these~~is~~ ratios ~~is an accumulation~~ are accumulations that were~~that was~~ not corrected for inefficient catch [4] ~~and that values contributing to these ratios are in Table 5~~. Table 5 demonstrates two features of the OWL snow data set: 1) The event-averaged catch efficiency based on Y12 (<*E Y12*>) is consistently larger than the event-averaged efficiency based on R11 (<*E R11*>), and 2) the event-averaged efficiency <*E R11*> is comparable to <*E Y12 An*>, where the latter is the event-averaged efficiency derived with the anemometer *U* and the Y12 catch efficiency function. These features are consistent with the altitude adjustment in R11, which increases the wind speed (section 3.9~~8~~), and thus decreases <*E R11*> relative to <*E Y12*>. They are also consistent with a low bias in the hotplate-derived *U*. The latter is supported by a comparison of the hotplate *U* vs anemometer *U* where the fit-line slope is 0.55 ± 0.05 for the 19 snow events at OWL (results not shown).

[4] This comparison was also made using accumulations corrected with a time-dependent catch efficiency (section 5.3), but we found that the fit-line slopes differed by less than ± 5 % from those in Fig. 12.

Consistent with the ranking of event-averaged values of E ~~E_s~~ (Table 5), Fig. 12a shows that the hotplate values, derived with the hotplate U and the Y12 catch efficiency function, are ~~statistically~~ smaller (on average) than the NOAH-II-derived values. We also see that the 15% ~~statistical~~ underestimate in the hotplate (Fig. 12a) reverses to a slight overestimate when using the R11 catch efficiency function (Fig. 12b) and when using the anemometer U with the Y12 function (Fig. 12c). T~~Unfortunately, t~~hese results do not allow us to specify ~~relative~~ contributions to the 15% ~~statistical~~ underestimate (Fig. 12a), coming from the fact that the Y12 function does not use a height-adjusted U, or from the suspected hotplate underestimate of U. Further studies focused on development of a hotplate catch efficiency function dependent on the local wind speed, as opposed to the wind speed at 10 m (R11), and investigation of the hotplate's determination of wind speed, are needed to resolve this issue. Since there is error in the NOAH-II values used in this comparison, there is also need for characterization of that uncertainty (random and systematic). Error can propagate from the NOAH-II measurements themselves and from the catch efficiency function we applied to those data (section 3.9).

Formatted: Font: Italic

6 - Conclusions

Starting with m~~M~~easurements acquired from~~ made with~~ two YES hotplates, we ~~were used to~~ derived precipitation rates and accumulations for 27 snowfall and rainfall events. The basis for this is a power ~~n energy~~ budget equation similar to that in King et al. (1978). We changed ~~that energy budget~~ the budget equation ~~(Eq. 1)~~ by including terms ~~that~~ describing the e longwave and shortwave radiant energy transfers. ~~(Eq. 3).~~ To the best of our knowledge, this is the first time that radiative terms have been incorporated into a hotplate data analysis algorithm and reported in the scientific literature.

We demonstrated that radiative forcing of the budget is relatively unimportant for the precipitation events analyzed. This is because the top plate's shortwave absorptance (i.e., $1 - R_h$ in Eq. 3), and its longwave emissivity, are small compared to unity, because a majority of events occurred at night, and because generally overcast conditions diminished the significance of the longwave forcing.

Formatted: Font: Italic

Formatted: Font: Italic, Subscript

In this paper, we ~~have~~ used computational methods different from those in R11, and we derived and applied different calibration coefficients. In spite of these changes we report precipitation rates and accumulations that strongly correlate with the output of two YES hotplates. However, a systematic difference is evident in our comparisons of the UW and YES algorithms. We surmise that the difference comes from the following: 1) R11's assignment of A_h (0.00884 m^2 vs 0.01327 m^2 in the UW algorithm), 2) R11's distinction between a theoretical and an actual energy conversion factor, and 3) the incorporation of #1 and #2 into the YES algorithm. Clearly, R11's A_h is not justified for hotplates sold by YES (Boudala et al., 2014; YES 2017, personal communication). R11's distinction between conversion factors is more problematic.

That distinction can be interpreted two ways: either 1) The distinction accounts for environmental thermal energy input that assists the conversion of precipitation mass to vapor, or 2) the distinction accounts for the loss of snow particles from the top surface of the hotplate due to removal by wind. Because early in the warming process a precipitation element attains a temperature larger than that of the air, we assert that the first of these phenomena is unlikely to contribute significantly to the energy budget. The second may be significant, but it is our opinion that removal of precipitation mass by wind is best accounted with a catch efficiency, not with a distinction between conversion factors. Lastly, accounting for either of these phenomena, independent of an adjustment of the catch efficiency, should be accomplished with an increase of an actual conversion factor relative to the theoretical value, not with the decrease proposed by R11.

Acknowledgements -

We gratefully acknowledge the support provided by the UW Department of Atmospheric Science Engineering Group. We also thank Ontario Winter Lake-effect Systems (OWLeS) project PIs Bart Geerts and Dave Kristovich for their leadership and Philip Bergmaier for maintaining the UW hotplate during OWLeS. This work was supported by the United States National Science Foundation (Award EPS 1208909), the Wyoming Water Development Commission (Award WWDC40395H), and by the U.S. Department of Interior (Award 1000628L).

Appendix – Nomenclature

A_h	Area of YES hotplate = 0.01327 m^2
C	Liquid H_2O specific heat capacity = 4218 J kg^{-1} K^{-1} (assumed independent of temperature; Iribarne and Godson, 1981; their Table IV-5)
C_i	Solid H_2O specific heat capacity = 2106 J kg^{-1} K^{-1} (assumed independent of temperature; Iribarne and Godson, 1981; their Table IV-5)
D_h	Diameter of YES hotplate = 0.130 m
E	Snow particle catch efficiency (section 3.9~~8~~)
f_1	Wind speed-dependent property in Eq. 2 [W]
f_2	Electrical-to-precipitation conversion factor [m J^{-1}]
IR	Upwelling or downwelling c~~C~~omponent of longwave flux [W m^{-2}]
$L_f(T_o)$	Latent heat of fusion evaluated at the thermodynamic reference temperature = $0.3337 x 10^6$ J kg^{-1} (Iribarne and Godson, 1981; their Table IV-5)
$L_v(T_h)$	Latent heat of vaporization at T_h (Iribarne and Godson, 1981; their Equation 4.103) [J kg^{-1}]
M_{IR}	Measured ~~net~~ longwave flux (section 3.5~~4~~) [W m^{-2}]
Nu	Nusselt number
P	Liquid-equivalent precipitation rate [mm hr^{-1} or m^3 m^{-2} s^{-1}]
P_{Ref}	Reference precipitation rate (section 4.2) [mm hr^{-1} or m^3 m^{-2} s^{-1}]
P_{UW}	Precipitation rate derived with UW algorithm (section 5.3) [mm hr^{-1} or m^3 m^{-2} s^{-1}]
P_{YES}	Precipitation rate derived with YES algorithm (section 4.2) [mm hr^{-1} or m^3 m^{-2} s^{-1}]
Q_{bot}	Bottom plate power [W]
Q_{top}	Top plate power [W]
R_d	Dry air specific gas constant = 287 J kg^{-1} K^{-1}
Re	Reynolds number
R_h	Hotplate Reflectance = 0.63 (section 2.2)
SW	Measured shortwave flux (section 2.2) [W m^{-2}]
T	Ambient temperature [^oC or K]
T_h	Hotplate surface temperature (section 3.6~~5~~) [^oC or K]
T_o	Thermodynamic reference temperature = 0.0 ^oC
T_s	Temperature of painted-steel sheeting [^oC or K]

U Wind speed [m s^{-1}]

Greek Symbols

α Fitted *Nu-Re* Coefficient (section 3.7~~6~~)

β Fitted *Nu-Re* Coefficient (section 3.7~~6~~)

ε_h Hotplate emissivity = 0.14 (section 2.2)

ε_s Emissivity of painted-steel sheeting = 0.84 (section 3.4~~3~~)

γ Coefficient derived in warm-cold tests (section 3.6~~5~~) or a coefficient in the *Nu-Re* relationship (section 5.2)

ρ Liquid H_2O density = 1000 kg m^{-3} (assumed independent of temperature)

σ Stefan-Boltzmann constant = 5.67×10^{-8} W m^{-2} K^{-4}

Subscripts

c Indoor cold setting

d Downwelling

h Hotplate

IB Ice-bulb

s Painted-steel sheeting

u Upwelling

w Indoor warm setting

x Property of air film adjacent to the hotplate surface: p_x = standard-atmosphere pressure at the altitude of the measurement. The following three film properties are held constant in calculation of the Reynolds number (section 3.7~~6~~) and in calculation of the sensible power output due to molecular conduction (section 3.7~~6~~): 1) temperature (T_x = 303.15 K), 2) dynamic viscosity (μ_x = 1.862×10^{-5} kg m^{-1} s^{-1}; Rogers and Yau (1989; their Table 7.1)), and 3) thermal conductivity (K_x = 2.63×10^{-2} J m^{-1} s^{-1} $K^{-1;}$ Rogers and Yau (1989; their Table 7.1)).

Operator

$<y>$ Time average of property *y*

References

Albrecht, B., M. Poellot, and S.K. Cox, Pyrgeometer measurements from aircraft, Review of Scientific Instruments, 45, 33-38, 1974

Borkhuu, B., Snowfall at a high-elevation site: Comparisons of six measurement techniques, M.S. Thesis, Department of Atmospheric Science, University of Wyoming, 2009

Boudala, F.S., R.Rasmussen, G.A.Isaac, and B.Scott, Performance of hot plate for measureing solid precipitation in complex terrain during the 2010 Vancouver Winter Olympics, J. Atmos.Oceanic Technol., 31, 437-446, 2014

Brandes, E.A., K. Ikeda, G. Zhang, M. Schonhuber, and R.M. Rasmussen, A statistical and physical description of hydrometeor distributions in Colorado snowstorms using a video disdrometer, J. Appl. Meteor. Climatol., 46, 634- 650, 2007

Brock, F.V., and S.J. Richardson, Meteorological Measurement Systems, Oxford University Press, New York, 304 pp., 2001

Campbell, L.S., W.J. Steenburgh, P.G. Veals, T.W. Letcher, and J.R. Minder, Lake-Effect Mode and Precipitation Enhancement over the Tug Hill Plateau during OWLeS IOP2b, Mon. Wea. Rev., 144, 1729–1748, doi: 10.1175/MWR-D-15-0412.1, 2016

Currie, I., Snow in the rain gauge (photograph), Weather, 53, 100, 1989

Deshler, T., Corrections of surface particle probe measurements for the effects of aspiration, J. Atmos.Oceanic Technol., 5, 547–560, 1988

Goodison, B.E., P. Y. T. Louie, and D. Yang, WMO solid precipitation measurement intercomparison. WMO Tech. Doc. 872, 211 pp., 1998

Hansen, L.G. and B.W. Webb, Air jet impingement heat transfer from modified surfaces, International Journal of Heat and Mass Transfer, 36, 989-997, 1992

Hass, G., Filmed surfaces for reflecting optics, Journal of the Optical Society of America, 45, 945-952, 1955

Havilcek, L.L., and R.D. Crain, *Practical Statistics for the Physical Sciences*, American Chemical Society, 1988

Iribarne, J.V., and W.L.Godson, *Atmospheric Thermodynamics*, 2nd ed., Reidel, 1981

Jevons,W. S., On the deficiency of rain in an elevated rain gauge as caused by wind, London Edinburgh Dublin Philos. Mag., 22, 421–433, 1861

King, W.D., D.A. Parkin, and R.J. Handsworth, A hot-wire liquid water device having fully calculable response characteristics, J. Appl. Meteor., 17, 809-813, 1978

Kobus, C.J. and G.L.Wedekind, An experimental investigation into forced, natural and combined forced and natural convective heat transfer from stationary isothermal circular disks, Int. J. Heat Mass Transfer, 38, 3329-3339, 1995

Lempio, G.E., K. Bumke, and A. Macke, Measurement of solid precipitation with an optical disdrometer, Advances in Geosciences, 10, 91-97, 2007

Locatelli, J.D. and P.V.Hobbs, Fall speeds and masses of solid precipitation particles, J. Geophys. Res., 79, 2185-2197, 1974

Loffler-Mang, M. and J. Joss, An optical disdrometer for measuring size and velocity of hydrometeors, J. Atmos.Oceanic Technol., 17, 130-139, 2000

Lovblad, G., J.W. Erisman, and D. Fowler, Deposition monitoring. Models and Methods for the Quantification of Atmospheric Input to Ecosystems, Chapter 3, The Nordic Council of Ministers, 37-41, 1993

Nespor, V., and B. Servuk, Estimation of wind-induced error of rainfall gauge measurements using a numerical simulation, J. Atmos.Oceanic Technol., 16, 450-464, 1999

Panofsky, H.A. and J.A.Dutton, *Atmospheric Turbulence*, Wiley-Interscience, New York, pp. 397, 1984

Rasmussen, R.M., J. Hallett, R. Purcell, S.D. Landolt, and J. Cole, The hotplate precipitation gauge, J. Atmos.Oceanic Technol., 28, 148-164, 2011

Rasmussen, R., B. Baker, J. Kochendorfer, T. Meyers, S. Landolt, A.P. Fischer, J. Black, J.M. Theriault, P. Kucera, D. Gochis, C. Smith, R. Nitu, M. Hall, K, Ikeda, and E. Gutmann, How well are we measuring snow?, Bull. Amer. Meteor. Soc., 93, 811-829, 2012

Rogers, R.R. and M.K. Yau, *A Short Course in Cloud Physics*, 3rd ed. Permagon Press, 304 pp., 1989

Steenburgh, J., L.Campbell, and P. Veals, North Redfield Snow Study Station, http://data.eol.ucar.edu/datafile/nph-get/382.023/Redfield_met_stn_readme.pdf, 2014

Stickel, J., B.Maloney, C.Pape and D.Burkheimer, Evaluation of the hotplate snow gauge, Center for Transportation Research and Education, Iowa State University, Aurora Project 2004-01, 2005

Thériault, J.M, R.Rasmussen, K.Ikeda, and S.Landolt, Dependence of snow gauge collection efficiency on snowflake characteristics, J. Appl. Meteor. Climatol., 745-762, 2012

Warnick, C.C., Rime ice and snow capping on high altitude precipitation gages, Proceedings of the 25th Annual Western Snow Conference, Santa Barbara, California, Western Snow Conference, 24-34, 1957

Weast, R.C., Ed.,Handbook of Chemistry and Physics, 56th ed, Chemical Rubber Company, 2350 pp., 1975

Wettlaufer, A., A fully compensated algorithm for the hotplate precipitation sensor, M.S. Thesis, Department of Atmospheric Science, University of Wyoming, 2013

Wolfe, J.P., and J.R.Snider, A Relationship between Reflectivity and Snow Rate for a High-Altitude S-Band Radar, J. Appl. Meteor. Climatol., 51, 1111–1128, 2012

~~World Meteorological Organization (WMO), Guide to Meteorological Instruments and Methods of Observation, Geneva, Switzerland, Chapter 6, Part I Measurement of Meteorological Variables, 2008~~

YES, INC., TPS-3100 Total Precipitation Sensor, Installation and User Guide, Version 2.0, Rev M, 43 pp., 2011

Young, H.D., *Statistical Treatment of Experimental Data*, McGraw-Hill Book Company, pp. 172, 1962

Figure 1 – The Yankee Environmental Systems TPS-3100 Total Precipitation Sensor with longwave and shortwave radiation sensors.

Formatted: Indent: First line: 0.5", Space After: 0 pt, Line spacing: Double

~~Figure 1 – The Yankee Environmental Systems TPS-3100 Total Precipitation Sensor with longwave and shortwave radiation sensors.~~

Figure 2~~2~~ – Picture taken during indoor testing showing a hotplate’s precipitation sensor positioned between top and bottom painted-steel sheets.

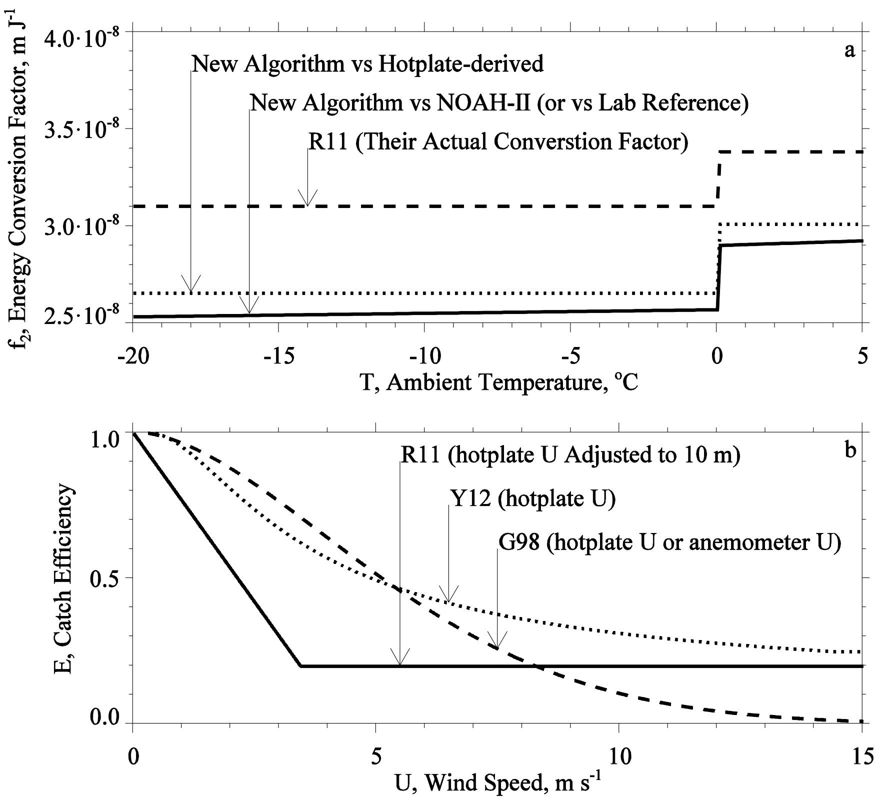

Figure 3 – a) Electrical-to-precipitation conversion factors vs ambient temperature assuming snow at $T < 0$ °C and rain at $T > 0$ °C. See text for details. b) Snow particle catch efficiency vs wind speed using the R11, Y12, and G98 formulations discussed in the text.

Formatted: Indent: First line: 0"

Formatted: j_ind

~~Figure 3 – a) Electrical-to-precipitation conversion factors vs ambient temperature assuming snow at T < 0 °C and rain at T > 0 °C. See text for details. b) Snow particle catch efficiency vs wind speed using the R11, Y12, and G98 formulations discussed in the text.~~

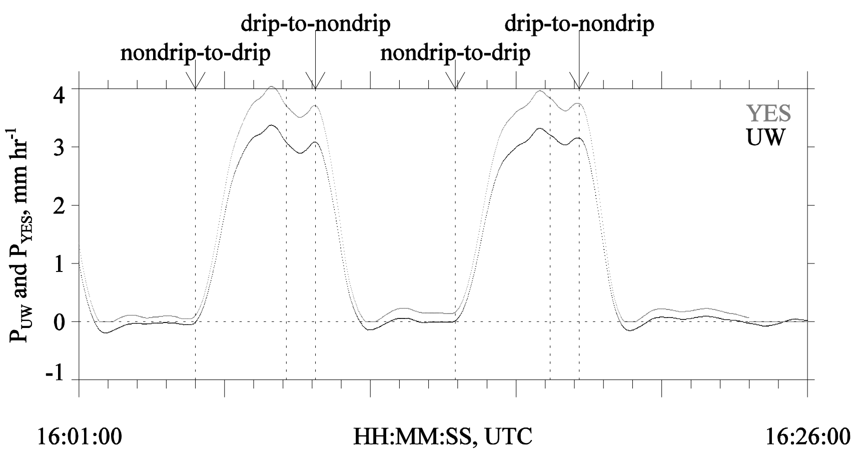

Figure 4 – Precipitation rates, derived using the UW and YES algorithms, plotted vs time. Dashed vertical lines illustrate nondrip-to-drip transitions, drip-to-nondrip transitions, and one-minute precipitation averaging intervals. In this figure, the one-minute averaging intervals are ~ 16:08 to ~ 16:09 UTC and ~ 16:17 to ~ 16:18 UTC. Measurements are from the UW hotplate operating indoors on 20120229. The UW/GLE calibration constants (Table 3) and an f_2 derived with the second of two methods (section 3.8) were applied in the UW algorithm. ~~Figure 4 – Precipitation rates, derived using the UW and YES algorithms, plotted vs time. The figure shows two drip periods (starting at the nondrip-to-drip transitions), both with the reference set at 3.1 mm hr^{-1}, and nondrip periods (starting at the drip-to-nondrip transitions). Dashed vertical lines indicate the transitions and 1-min precipitation averaging intervals. Measurements are from the UW hotplate operating indoors on 20120229. The UW/GLE calibration constants (Table 3) and an f_2 derived with the second of two methods (section 3.7) were applied in the UW algorithm.~~

Formatted: j_ind, Indent: First line: 0", Line spacing: single

Formatted: Font: Italic

Formatted: Font: Italic, Subscript

Formatted: j_ind, Space After: 0 pt, Line spacing: single

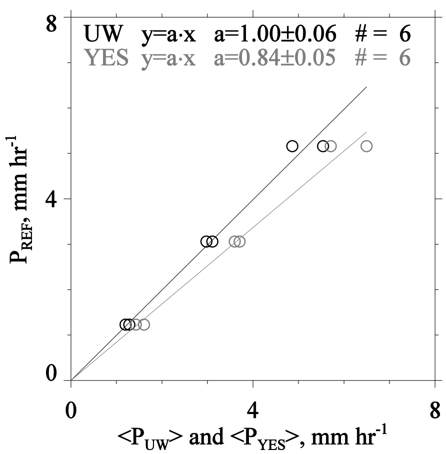

Figure 5 - Reference precipitation rate vs time-averaged P_{UW} and P_{YES}. Measurements are from the UW hotplate operating indoors on 20120229. The UW/GLE calibration constants (Table 3) and an f_2 derived with the second of two methods (section 3.8~~7~~) were applied in the UW algorithm. Regression lines were forced through the origin and *x* deviations (horizontal departures of data from regression line) were used as the basis for the least squares criterion of best fit (Young, 1962). Standard deviations on the fitted ratios (confidence intervals) were derived using Student's t-distribution at the 95% level (Havilcek and Crain, 1988).

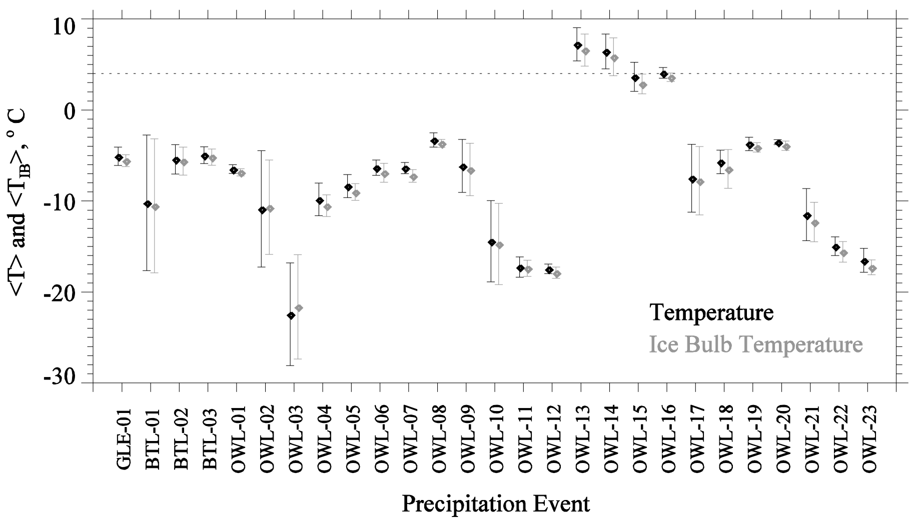

Figure 6 – Event-averaged ambient temperature (<T>) and event-averaged ambient ice bulb temperature (<T_{IB}>). The abscissa shows the 27 precipitation events in the order presented in Table 5. Error bars are ± 2 standard deviations. The dashed horizontal line is drawn at +4 °C.

Formatted: Indent: First line: 0.5"

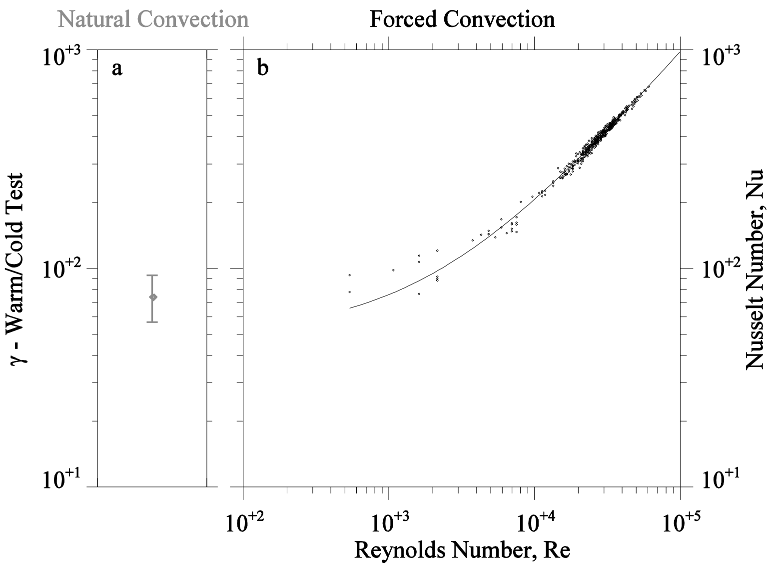

Formatted: Indent: First line: 0"

Figure 7 – a) γ from the warm-cold test summarized in the second row of Table 3. Error limits were derived by perturbing $Q_{top,w}$ (i.e., the value acquired in the warm test) by ± 0.5 W and repeating the analysis based on Eq. 7a - b. b) *Nu* vs *Re* scatterplot and fit curve for the UW hotplate at the GLE site. For clarity, only every fortieth *Nu*-*Re* data pair is plotted. The minimum *Re* plotted (data and fit function) corresponds to the minimum *U* reported in the UHP file (0.1 m s^{-1}). The measurement interval is 20120402 04:00 UTC to 20120402 09:00 UTC at the GLE site. The UW/GLE T_h (Table 3) was applied in the data analysis.

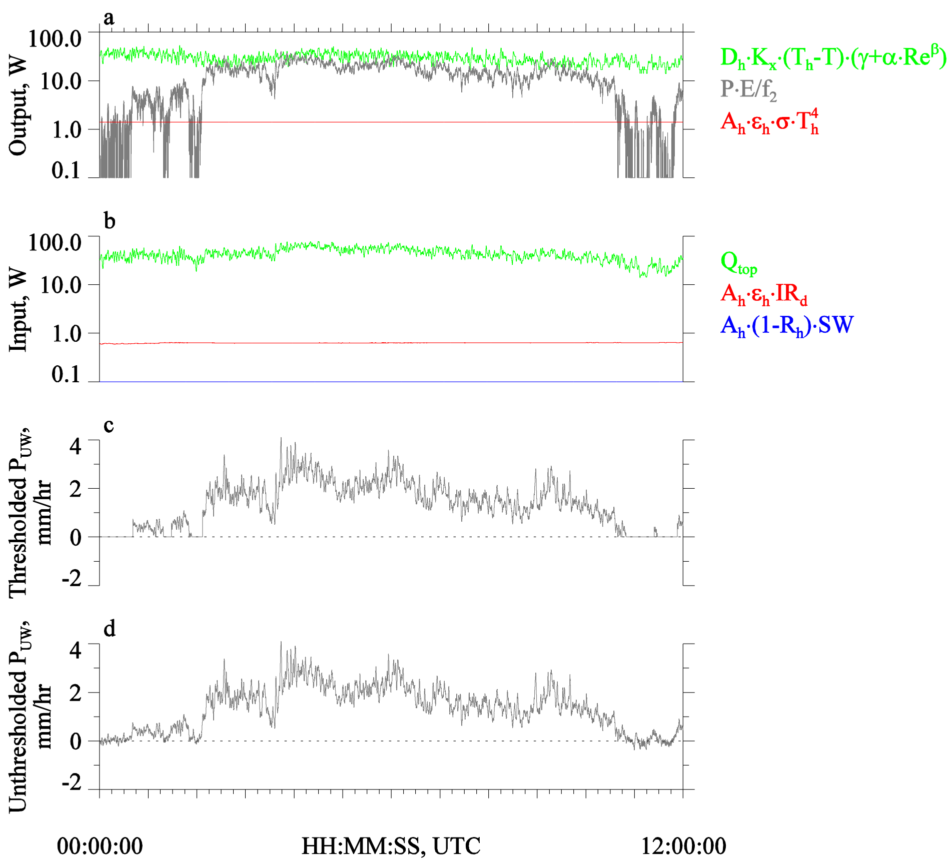

~~Figure 8 – Hotplate properties during rain (event = OWL-15 in Fig. 6 and Table 5). Because this event classifies as rain, *E* = 1 was applied in the UW algorithm. a) Power output terms in the Eq. 3; i.e., the sensible, latent, and upwelling longwave terms. b) Power input terms in the Eq. 3; i.e., the top plate power, downwelling longwave, and shortwave terms. The shortwave term is zero for this nighttime example, but is set to 0.1 W in the plot. c) Thresholded precipitation rate. d) Unthresholded precipitation rate.~~ Figure 8 – Hotplate properties during rain (event = OWL-15). Because this event classifies as rain, *E* = 1 was applied in the UW algorithm.

Formatted: Font: Italic

a) Budget output terms (Eq. 3); i.e., the sensible, latent, and longwave outputs. b) Budget input terms (Eq. 3); i.e., top plate, longwave, and shortwave inputs. The shortwave term is zero for this nighttime example, but is set to 0.1 W in the plot. c) Thresholded precipitation rate. d) Unthresholded precipitation rate.

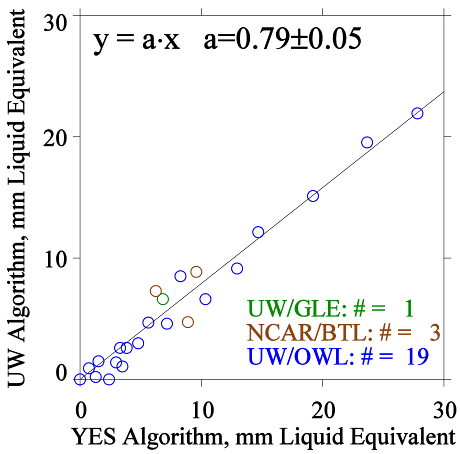

Figure 9 – Snow accumulations derived using the UW algorithm vs snow accumulations derived using the YES algorithm. Both the Y12 catch efficiency function and an f_2 derived with the first of two methods discussed in section 3.8~~7~~ were applied in the UW algorithm. The regression line was forced through the origin and *y* deviations (vertical departures of data from regression line) were used as the basis for the least squares criterion of best fit (Young, 1962). The standard deviation on the fitted ratio (confidence interval) was derived using Student's t-distribution at the 95% level (Havilcek and Crain, 1988).

Formatted: j_ind, Indent: First line: 0", Line spacing: single

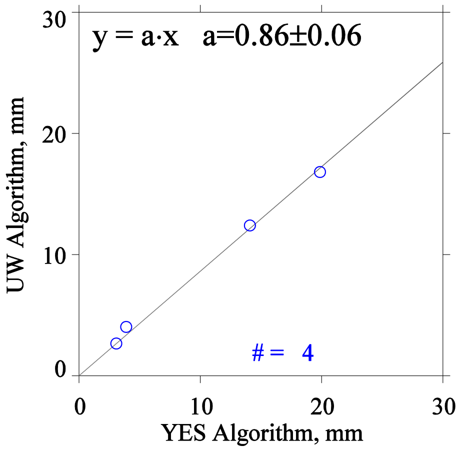

Figure 10 – Rain accumulations derived using the UW algorithm vs rain accumulations derived using the YES algorithm. An f_2 derived with the first of two methods discussed in section 3.8~~7~~ was applied in the UW algorithm. The r~~R~~egression line~~s~~ was~~ere~~ forced through the origin and *y* deviations (vertical departures of data from regression line) were used as the basis for the least squares criterion of best fit (Young, 1962). The standard deviation~~s~~ on the fitted ratio~~s~~ (confidence intervals) was~~were~~ derived using Student's t-distribution at the 95% level (Havilcek and Crain, 1988).

Formatted: j_ind, Indent: First line: 0", Line spacing: single

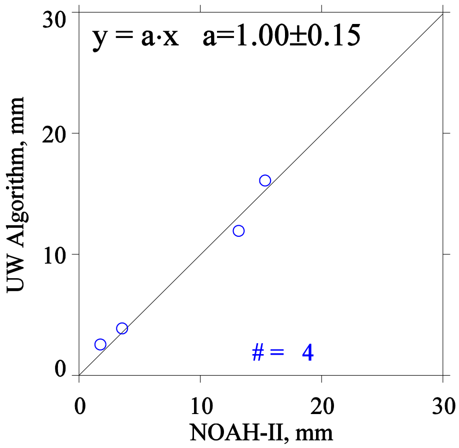

Figure 11 –Rain accumulations derived using the UW algorithm vs rain accumulations from the NOAH-II gauge. An f_2 derived with the second of two methods discussed in section 3.8~~7~~ was applied in the UW algorithm. The regression line was forced through the origin and y deviations (vertical departures of data from regression line) were used as the basis for the least squares criterion of best fit (Young, 1962). The standard deviation on the fitted ratio (confidence intervals) was derived using Student's t-distribution at the 95% level (Havilcek and Crain, 1988). ~~Regression lines were forced through the origin and *y* deviations (vertical departures of data from regression line) were used as the basis for the least squares criterion of best fit (Young, 1962). The standard deviations on the fitted ratios (confidence intervals) were derived using Student's t-distribution at the 95% level (Havilcek and Crain, 1988).~~

Formatted: j_ind, Indent: First line: 0", Line spacing: single

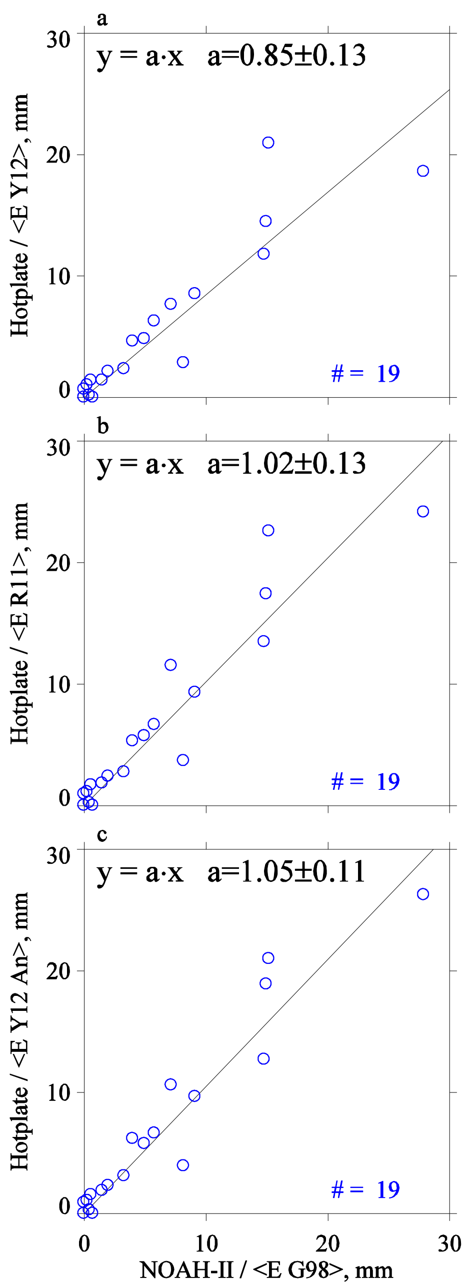
a
y = a·x a=0.85±0.13
# = 19
Hotplate / <E Y12>, mm
b
y = a·x a=1.02±0.13
# = 19
Hotplate / <E R11>, mm
c
y = a·x a=1.05±0.11
# = 19
Hotplate / <E Y12 An>, mm
NOAH-II / <E G98>, mm
0
10
20
30

Figure 12 – UW hotplate and NOAH-II measurements of snow (liquid-equivalent accumulations, not corrected for inefficient catch, divided by an event-averaged snow particle catch efficiency) at OWL. An f_2 derived with the second of two methods discussed in section 3.8~~7~~ was applied in the UW algorithm. Regression lines were forced through the origin and *y* deviations (vertical departures of data from regression line) were used as the basis for the least squares criterion of best fit (Young, 1962). The standard deviations on the fitted ratios (confidence intervals) were derived using Student's t-distribution at the 95% level (Havilcek and Crain, 1988).

Formatted: j_ind

Table 1 – Hotplate Data Files

Recorded Variable [a], units	File UHP	File SHP	Symbol
Unix Time, s	✓	✓	
Liquid-equivalent Precipitation Rate, mm hr^{-1}	✓		P_{YES}
Accumulated Liquid-equivalent Precipitation, mm	✓		
Ambient Temperature, °C	✓	✓	T
Enclosure Temperature, °C	✓	✓	
Wind Speed, m s^{-1}	✓		U
Downwelling Shortwave Flux, W m^{-2}	✓	✓	SW
Longwave Radiation Measurement, W m^{-2}	✓	✓	M_{IR}
Barometric Pressure, hPa	✓	✓	p [b]
Relative Humidity Sensor Temperature, °C	✓	✓	
Relative Humidity, %	✓	✓	RH
Top Plate Voltage, V		✓	
Bottom Plate Voltage, V		✓	
Top Plate Current, A		✓	
Bottom Plate Current, A		✓	
Top Plate Resistance, Ω		✓	
Bottom Plate Resistance, Ω		✓	
Top Plate Power, W		✓	Q_{top}
Bottom Plate Power, W		✓	Q_{bot}
Radiation Sensors' Temperature, °C		✓	

[a] With the exception of Unix time, all recorded variables are 60-s running averages, sampled at 1 Hz (YES, 2011)

[b] Although pressure is a recorded variable, the pressure used in the UW algorithm (p_x; section 3.7 and Appendix) is the standard-atmosphere pressure at the altitude of the measurement

~~Table 1 – Hotplate Data Files~~

Formatted Table

Formatted: Space After: 10 pt, Line spacing: Multiple 1.15 li

Formatted: Font: 11 pt

~~Recorded Variable [a], dimension~~	~~File UHP~~	~~File SHP~~	~~Symbol~~
~~Unix Time, s~~	✓	✓	
~~Precip. Rate, mm hr^{-1}~~	✓		P_{YES}
~~Accumulated Precip., mm~~	✓		
~~Ambient Temp., °C~~	✓	✓	T
~~Enclosure Temp., °C~~	✓	✓	
~~Wind Speed, m s^{-1}~~	✓		U
~~Shortwave Radiation, W m^{-2}~~	✓	✓	SW
~~Net Longwave Radiation, W m^{-2}~~	✓	✓	M_{IR}
~~Barometric Pressure, hPa~~	✓	✓	p [b]
~~RH Sensor Temp., °C~~	✓	✓	
~~RH, %~~	✓	✓	RH
~~Top Plate Voltage, V~~		✓	
~~Bottom Plate Voltage, V~~		✓	
~~Top Plate Current, A~~		✓	
~~Bottom Plate Current, A~~		✓	
~~Top Plate Resistance, Ω~~		✓	
~~Bottom Plate Resistance, Ω~~		✓	
~~Top Plate Power, W~~		✓	Q_{top}
~~Bottom Plate Power, W~~		✓	Q_{bot}
~~Radiation Sensors' Temp., °C~~		✓	

~~Recorded Variable [a], dimension~~	~~File UHP~~	~~File SHP~~	~~Symbol~~
~~Unix Time, s~~	✓	✓	
~~Precip. Rate, mm hr^{-1}~~	✓		P_{YES}
~~Accumulated Precip., mm~~	✓		
~~Ambient Temp., °C~~	✓	✓	T
~~Enclosure Temp., °C~~	✓	✓	
~~Wind Speed, m s^{-1}~~	✓		U
~~Shortwave Radiation, W m^{-2}~~	✓	✓	SW
~~Net Longwave Radiation, W m^{-2}~~	✓	✓	M_{IR}
~~Barometric Pressure, hPa~~	✓	✓	p [b]
~~RH Sensor Temp., °C~~	✓	✓	
~~RH, %~~	✓	✓	RH
~~Top Plate Voltage, V~~		✓	
~~Bottom Plate Voltage, V~~		✓	
~~Top Plate Current, A~~		✓	
~~Bottom Plate Current, A~~		✓	
~~Top Plate Resistance, Ω~~		✓	
~~Bottom Plate Resistance, Ω~~		✓	
~~Top Plate Power, W~~		✓	Q_{top}
~~Bottom Plate Power, W~~		✓	Q_{bot}
~~Radiation Sensors' Temp., °C~~		✓	

~~[a] With the exception of Unix time, all recorded variables are 60-s running averages, sampled at 1 Hz (YES, 2011)~~

~~[b] Although pressure is a recorded variable, the pressure used in the UW algorithm (p_x; section 3.6 and Appendix) is the standard-atmosphere pressure at the altitude of the measurement~~

Table 2 – Field Sites, Site Location, Vegetation at the Site, Gauge Location, Number of Events, and Event Type

Site Abbreviation Site Reference Hotplate	Site Location	Height of Vegetation, m AGL	Gauge Location at Site	Precipitation Events
GLE Wettlaufer (2013) UW	SE Wyoming 106.240 °W 41.3665 °N 3190 m MSL	10 to 20 m	Hotplate: 27 m AGL on top deck of a meteorological tower [a] NOAH-II: 3 m AGL (clearing in conifer forest 80 m SE of tower)	1 Snow
BTL Wettlaufer (2013) NCAR	SE Wyoming 106.975 °W 41.1558 °N 3010 m MSL	10 to 20 m	Clearing in conifer forest Hotplate: 3 m AGL NOAH-II: 3 m AGL	3 Snow
OWL Steenburgh et al. (2014) UW	NW New York 75.8771 °W 43.6245 °N 385 m MSL	2 to 5 m	Clearing in deciduous brush and deciduous trees Hotplate: 1.7 m AGL [b] and 2.5 m AGL [c] NOAH-II: 2.5 m AGL	4 Rain 19 Snow

[a] This is the Brooklyn Lake, Wyoming AmeriFlux Tower; AmeriFlux is a network of sites that measure energy and trace-gas transfers~~fluxes~~.

[b] First 7 of 23 OWL precipitation events (Date < 20131217)

[c] Last 16 of 23 OWL precipitation events (Date > 20131217)

Table 3 – Summary of Warm-cold Tests

Indoor Calibration (Warm-cold Tests)			
Year	Hotplate/Field Site	$T_{h\cancel{p}}$, ^{o}C	γ
2012	NCAR/BTL	42.2 ± 7.4 [a]	106. ± 15.1 [a]
2012 - 2013	UW/GLE	52.2 ± 15.7	74.8 ± 18.1
2013 - 2015	UW/OWL	66.5 ± 7.8	57.8 ± 7.7

[a] Error limits derived by perturbing $Q_{top,w}$ (i.e., the value acquired in the warm test) by ± 0.5 W and repeating the analysis based on Eq. 7a - b.

Table 4 – Summary of Drip Tests

Indoor Calibration (Drip Tests)				
Year	Hotplate/Field Site	P_{REF} vs $\langle P_{UW} \rangle$ ratio [a]	P_{REF} vs $\langle P_{YES} \rangle$ ratio [a]	# [b]
2012	NCAR/BTL	0.99 ± 0.02	0.81 ± 0.03	6
2012 - 2013	UW/GLE	1.00 ± 0.06	0.84 ± 0.05	6
2013 - 2015	UW/OWL	0.97 ± 0.04	0.79 ± 0.03	6

[a] Ratios were derived as the slope of a regression lines forced through the origin. The *x* deviations (horizontal departures of data from regression line) were used as the basis for the least squares criterion of best fit (Young, 1962). Standard deviations on the fitted ratios (confidence intervals) were derived using Student's t-distribution at the 95% level (Havilcek and Crain, 1988).

[b] # = number of tests.

Table 5 – Precipitation Events

Precipitation Event	Start Date, YYYYMMDD UTC	Start Time, HH:MM UTC	End Time HH:MM UTC	<T> [a], °C	<T_{IB}> [b], °C	<U> [c], m s^{-1}	UW [d], mm	YES [d], mm	<E Y12> [e]	<E Y12 An> [f]	<E R11> [g]	NOAH-II [d], mm	<E G98> [h]
GLE-01	20120414	0:00	13:00	-5.1	-5.6	1.8	5.6	6.0	0.84	NA [i]	NAP [j]	7.3	0.89
BTL-01	20120116	11:00	1:00	-10.2	-10.5	2.0	3.8	7.5	0.80	NA	NAP	8.0	0.87
BTL-02	20120119	8:00	18:00	-5.4	-5.6	4.3	3.8	3.4	0.55	NA	NAP	1.0	0.60
BTL-03	20120120	7:00	18:00	-5.0	-5.2	2.4	6.3	7.1	0.75	NA	NAP	8.2	0.83
OWL-01	20131211	18:00	0:00	-6.5	-6.9	1.4	16.9	21.5	0.91	0.64	0.70	20.0	0.72
OWL-02	20131212	0:00	6:00	-10.9	-10.7	0.4	1.0	3.5	0.99	0.94	0.90	0.3	0.96
OWL-03	20131212	6:00	12:00	-22.5	-21.6	0.3	0.0	2.4	1.00	1.00	0.93	0.0	1.00
OWL-04	20131212	18:00	0:00	-9.8	-10.5	1.3	0.2	1.2	0.90	0.53	0.67	0.3	0.57
OWL-05	20131213	6:00	12:00	-8.4	-9.0	0.9	13.9	18.5	0.96	0.73	0.80	12.1	0.81
OWL-06	20131215	19:45	0:00	-6.3	-6.9	0.9	1.3	2.9	0.94	0.85	0.78	0.5	0.88
OWL-07	20131216	0:00	6:00	-6.4	-7.3	0.3	20.9	27.8	1.00	1.00	0.93	15.2	1.00
OWL-08	20131218	18:00	0:00	-3.3	-3.7	1.5	10.4	13.2	0.88	0.82	0.77	12.9	0.87
OWL-09	20140106	18:00	0:00	-6.2	-6.5	3.9	4.5	4.6	0.58	0.42	0.39	2.5	0.35
OWL-10	20140107	0:00	6:00	-14.4	-14.7	3.8	0.4	0.3	0.60	0.44	0.42	0.0	0.38
OWL-11	20140107	6:00	12:00	-17.3	-17.4	3.0	1.9	3.3	0.67	0.49	0.52	4.0	0.49
OWL-12	20140107	18:00	0:00	-17.5	-17.9	3.9	0.0	0.0	0.58	0.42	0.39	0.3	0.35
OWL-13	20140111	15:45	21:00	7.2	6.6	1.1	11.9	14.1	1.00	1.00	1.00	13.2	1.00
OWL-14	20140111	23:00	2:00	6.4	5.8	2.4	3.9	3.9	1.00	1.00	1.00	3.5	1.00
OWL-15	20140114	0:00	12:00	3.7	2.9	0.9	16.1	19.9	1.00	1.00	1.00	15.3	1.00
OWL-16	20140114	12:45	15:45	4.1	3.6	1.2	2.6	3.1	1.00	1.00	1.00	1.8	1.00
OWL-17	20140119	0:00	12:00	-7.5	-7.8	1.3	1.9	3.3	0.91	0.84	0.81	1.8	0.88
OWL-18	20140119	18:00	0:00	-5.7	-6.5	1.9	1.9	2.6	0.81	0.61	0.69	2.3	0.69
OWL-19	20140120	0:00	2:00	-3.7	-4.1	3.1	0.9	1.0	0.67	0.50	0.52	0.8	0.51
OWL-20	20140120	2:00	12:00	-3.5	-3.9	2.1	3.8	4.8	0.78	0.66	0.66	3.5	0.72
OWL-21	20140127	18:00	0:00	-11.5	-12.3	1.7	4.0	6.6	0.86	0.65	0.75	2.8	0.69
OWL-22	20140128	0:00	6:00	-15.0	-15.6	0.4	6.3	10.3	1.00	0.95	0.94	5.6	0.96
OWL-23	20140128	6:00	12:00	-16.5	-17.3	0.9	8.0	12.1	0.94	0.83	0.86	8.1	0.88

[a] Event-averaged ambient temperature
[b] Event-averaged ice bulb temperature
[c] Event-averaged hotplate *U*
[d] Liquid-equivalent precipitation amount not corrected for inefficient catch (UW values are computed with an f_2 derived with the second of two methods discussed in section 3.8~~7~~)
[e] Event-averaged snow particle catch efficiency derived using Y12 and the hotplate *U*
[f] Event-averaged snow particle catch efficiency derived using Y12 and the anemometer *U*
[g] Event-averaged snow particle catch efficiency derived using R11 and hotplate *U* adjusted to 10 m AGL
[h] Event-averaged snow particle catch efficiency derived using G98 and hotplate *U* (GLE and BTL) or anemometer *U* (GLE)
[i] NA = not available
[j] NAP = not applicable

Table 6 – Summary of Fitted *Nu-Re* Coefficients

Field Calibration (*Nu* - *Re* Coefficients)			
Hotplate/Field Site	γ	α	β
NCAR/BTL [a]	86.2	0.126	0.781
UW/GLE [b]	49.1	0.130	0.771
UW/OWL [c]	45.6	0.172	0.713

[a] NCAR hotplate; measurement interval 20120118 23:00 UTC to 20120119 5:00 UTC

[b] UW hotplate; measurement interval 20120402 04:00 UTC to 20120402 09:00 UTC

[c] UW hotplate; measurement interval 20140107 18:00 UTC to 20140108 08:00 UTC